Influence of Transverse Reinforcement on Bridge Column Resistance against Blast Loads

Amir Hossein Kavousifard

A Thesis
in
The Department
of
Building, Civil and Environmental Engineering

Presented in Partial Fulfillment of the Requirements
for the Degree of Master of Applied Science (Civil Engineering) at
Concordia University
Montreal, Quebec, Canada

June 2018

CONCORDIA UNIVERSITY

School of Graduate Studies

This is to certify that the thesis prepared

By: Amir Hossein Kavousifard

Entitled: Influence of Transverse Reinforcement on Bridge Column Resistance against Blast Loads

and submitted in partial fulfillment of the requirements for the degree of

Master of Applied Science (Civil Engineering)

complies with the regulations of the University and meets the accepted standards with respect to originality and quality.

Signed by the final Examining Committee:

_____ Chair

DR. A. M. ZSAKI

_____ Examiner

DR. A. BHOWMICK

_____ Examiner

DR. R. GANESAN

_____ Supervisor

DR. L. LIN

Approved by _____

Chair of Department or Graduate Program Director

June 21, 2018 _____

Dean of Faculty

ABSTRACT

Influence of Transverse Reinforcement on Bridge

Column Resistance against Blast Loads

Amir Hossein Kavousifard

After the terrorist attacks of September 11th, 2001, blast load resistance of infrastructure has been of great concern to structural engineers, and government institutions in the United States have provided guidelines to mitigate these risks. The focus of these guidelines has been on buildings, and measures to protect infrastructure such as bridges have not received similar attention. However, data on terrorist attacks show that bridges are often targeted, and the majority of these attacks are on non-landmark bridges, such as highway bridges.

With the threat of global terrorism, it is required to understand the behavior of bridges in Canada under blast loads. Specifically, bridge columns are often targeted and they represent a critical structural function as their failure can lead to collapse of the entire bridge. Transverse reinforcement is the key element in design of reinforced concrete (RC) bridge columns against blast, and it is also the key element in design for seismic loads. A generic two-span bridge located in Toronto, Ontario; Vancouver, British Columbia; and Victoria, British Columbia, is designed using the Canadian Highway Bridge Design Code (CHBDC). The three cities are chosen to represent low, high, and extremely high seismic hazard levels, respectively. The bridge

columns are designed according to the required seismic detailing of the different hazard levels with a focus on spacing, bar size, and type of transverse reinforcement. The finite element software LS-DYNA is used to model the bridge columns and simulate the application of blast loads at different charge heights for various charge weights and standoff distances.

Analysis of the simulation results concentrates on the performance of columns with respect to concrete failure mechanisms, behavior and stress patterns of steel reinforcement, and displacement curves. The results of this study indicate that for equivalent blast loads, a charge closer to the base of the column is more critical than a charge at mid-height. Moreover, charge weight has more of an impact than standoff distance in a columns ability to resist blast. The results also indicate that seismic detailing is extremely important in blast load resistance of columns. Specifically, columns with smaller spacing of transverse reinforcement, as well as bigger bar size, demonstrate an ability to successfully resist blast and allow a column to carry the required structural loads. Moreover, columns with spiral transverse reinforcement perform better than columns with tied transverse reinforcement.

Acknowledgements

I would like to express my sincere gratitude to my supervisor Dr. Lan Lin. The quality and depth of this study would have suffered had it not been for her dedication and guidance. She offered tremendous personal and professional support during the completion of my degree.

Table of Contents

List of Tables

List of Figures

Chapter 1: Introduction

1.1 Motivation

The structural engineering communities' challenge in protecting infrastructure against attacks has been one that goes back decades. The first major example was the failure of the Alfred P. Murrah Federal Building in Oklahoma City, Oklahoma, due to a bomb explosion at the ground level in April of 1995 (National Research Council, 1995). Safety of government buildings has become a considerable concern after the collapse of the Twin Towers of the World Trade Center on September 11th, 2001. In the past, several design guidelines for protecting structures from accidental explosions, such as military and petrochemical compounds, were available. These include, Structures to Resist the Effects of Accidental Explosions (Department of the Army, 1990) and Design of Blast Resistant Buildings in Petrochemical Facilities (ASCE, 1997; 2010). After the attacks of September 11th, 2001, the United States government released new guidelines in order to improve blast load resistance of structures, e.g., Unified Facilities Criteria: DoD Minimum Antiterrorism Standards for Buildings (Department of Defense, 2002); Reference Manual to Mitigate Potential Terrorist Attacks against Buildings (FEMA, 2003; 2011); and Progressive Collapse Analysis and Design Guidelines for New Federal Office Buildings and Major Modernization Projects (GSA, 2003).

It should be noted that the current guidelines are mainly for buildings. However, it has been reported that infrastructure such as bridges are being targeted more and more by terrorists as the potential site for an attack (FTA, 2001). It is not surprising that landmark bridges are an attractive target for terrorists. For example, the US Federal Bureau of Investigation has thwarted

planned attacks on the Golden Gate Bridge and the Brooklyn Bridge since the beginning of the 21st century. If these incidents would occur, they would have a very negative socioeconomic impact as reported in Mahoney (2007). In addition to landmark bridges, Jenkins and Gersten (2001) reported that based on statistical data between 1980 and 2001, 58% of attacks on bridges were on non-landmark bridges. This indicates that highway bridges might also be at risk.

Explosives can be placed anywhere on a bridge, but the preferred target, and the area that is of the most importance to structural engineers, is columns. In the last decade, research on the effects of blast loads on bridge columns has significantly advanced due to experimental work, which was not previously available, and advancements in finite element modelling for blast loads in software such as LS-DYNA (LSTC, 2016a). The results from experimental tests and analytical studies have clearly shown that blast loads could cause severe damage to bridge columns, which in turn will jeopardize the structural integrity of the entire bridge system. Accordingly, there is an urgent need to prepare guidelines for blast resistance for design of new bridges and retrofitting techniques for old bridges. It is necessary to mention that the majority of research that has been conducted is focused on bridges in the United States, which were designed in accordance with the requirements specified by the American Association of State Highway and Transportation Officials (AASHTO). Considering that terrorist attacks are becoming a global threat, it is important to understand the behaviour of Canadian bridges under blast loads, which will help the code authority to improve the requirements for bridge column design and the emergency-response agencies to prepare for rescue plans.

1.2 Objective and Scope of Study

The main objective of this study is to examine the influence of transverse reinforcement in terms of type (tied or spiral), diameter, and spacing on the blast load resistance of reinforced

concrete columns of typical highway bridges located in different cities in Canada. These cities are selected to represent the seismic hazard from low to extremely high across Canada for the design of bridges against earthquake load as one of the lateral loads. The behaviour of these earthquake-protected columns will help to understand the contribution of seismic detailing to the blast load resistance. This is due to the fact that both earthquake load and blast load are categorized as dynamic load and applied laterally on bridge columns. In this study, both qualitative failure mechanisms and quantitative measurements (e.g., column displacement and strain in the steel bars) with regards to time are examined.

Accordingly, the following tasks are carried out in this study:

- Design a reinforced concrete (RC) column in a two-span continuous bridge according to CHBDC 2006. Three locations are considered, namely Toronto, Ontario; Vancouver, British Columbia; and Victoria, British Columbia, which are used to represent low, high, and extremely high seismic hazard regions in Canada, respectively, for the design of bridges for earthquake loads. In total, eight columns are examined, two (one tied column and one spiral column) in Toronto, two in Vancouver, and four (two tied columns and two spiral columns) in Victoria.
- Model bridge columns subjected to blast loads in LS-DYNA.
- Examine the effects of equivalent scaled standoffs for blast loads to determine the importance of charge weight and standoff distance.
- Compare the behaviour of columns reinforced with two types of transverse reinforcement, i.e., ties and spirals.
- Investigate the effects of charge height on the performance of RC bridge columns.

1.3 Outline of the Thesis

This thesis is organized into the following seven chapters.

Chapter 1 briefs the motivations of the study.

Chapter 2 provides detailed information on blast loads including the definition and classification of blast loads and structural performance due to blast loads. This chapter also summarizes past studies related to the objective of this study, along with their major findings.

Chapter 3 describes the design of columns used in the study. A typical two-span continuous RC highway bridge located in each of the following locations, i.e., Toronto, Vancouver, and Victoria, were designed according to the CHBDC 2006.

Chapter 4 presents details on the techniques for modeling the designed columns in LS-DYNA, such as types of elements used, properties of materials (concrete and steel), and simulation of blast loads.

Chapter 5 and Chapter 6 summarize the qualitative and quantitative results from LS-DYNA. Finally, Chapter 7 presents the main observations and conclusions from the study. Recommendations are also included in this chapter.

Chapter 2: Literature Review

2.1 Introduction

There are several types of explosion categories, each of which is associated with different wave phenomena mechanisms. In addition, several parameters to classify blast loads have been developed based on air blast tests performed in the 20th century, and they have been implemented in finite element analysis software to simulate blast loads. Dynamic characteristics of blast loads are another concern for the assessment of blast load resistance of bridges. Both simplified and advanced methods have been developed as knowledge on blast loads has increased. Specifically, the simplified methods are mainly used to conduct preliminary assessments of blast load resistance of bridges, while the advanced methods are used to evaluate the performance of specific bridges (i.e., important bridges) under blast loads. Due to the lack of guidelines for design of bridges against blast loads, comprehensive research is underway. It is well accepted by the engineering community that the design requirements for blast loads will be based on those for seismic loads, given that both explosions and earthquakes are treated as extreme events that apply lateral loads onto the structure.

2.2 Blast Loads

2.2.1 Blast Loads and Shock Wave Phenomena

A blast, which is often attributed to a bomb explosion, can be classified as a sudden and violent release of energy. More specifically, blast loads are considered as dynamic loads whose impact lasts an extremely short amount of time, usually in milliseconds. However, it can produce very high pressures in the order of hundreds of Megapascal. The waves of pressure expand radially from the charge source, and the pressure decays as distance from the source increases.

As waves travel, they create what is known as a shock front, which is the foremost wave layer to expand away from the source of the charge. When the wave passes through the ambient atmosphere, it compresses the air in its path and creates an overpressure, which is the excess pressure relative to the ambient atmosphere. When the shock front has passed through, the pressure (i.e., positive pressure) then drops below the ambient pressure, and this creates suction pressure (i.e., negative pressure). Figure 2.1 schematically shows the positive and negative pressures *vs* time. It can be seen in the figure that negative pressure is extremely small compared to positive pressure. Therefore, the effect of the negative pressure phase is normally ignored in the analysis as recommended by Williams and Williamson (2011). The area under the time-pressure curve represents impulse, which is the total energy available from the blast.

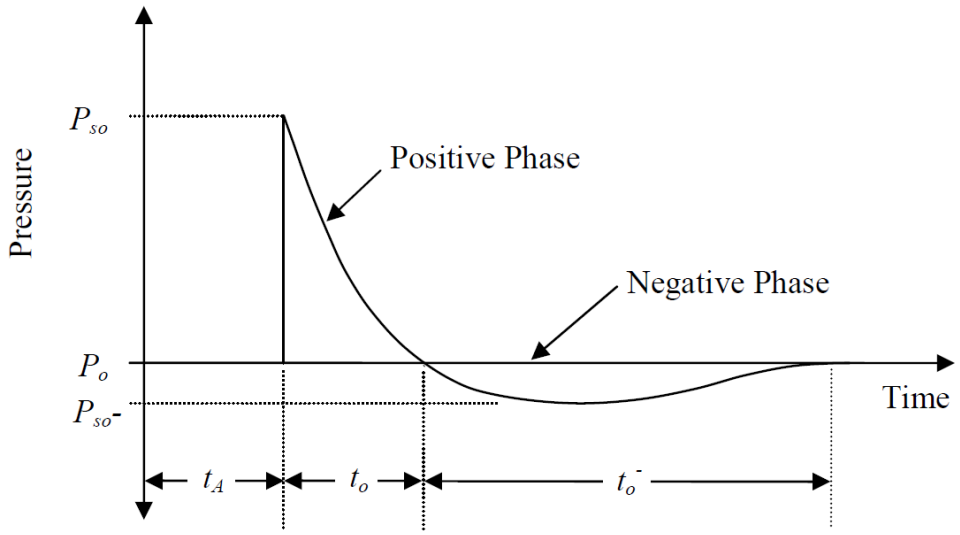

Figure 2.1 Time-pressure curve for free air explosions (Department of the Army, 1990).

Currently, the positive pressure phase is calculated using the Friedlander equation (Baker, 1973), i.e., Equation 2.1, while the impulse is the integration of the pressure as expressed in Equation 2.2. The two equations were used by the US Army Corps of Engineers to develop the

Conventional Weapons (ConWep) code for blast load analysis (US Army Corps of Engineers, 2001). Furthermore, they are adopted by most of the finite element analysis software including LS-DYNA in order to determine pressure due to blast.

$$P(t) = P_{so}\left(1 - \frac{(t-t_A)}{t_o}\right)e^{\left(\frac{-b(t-t_A)}{t_o}\right)} \quad (2.1)$$

$$I(t) = \int_{t_A}^{t_A+t_o} P_s(t)\,dt = \frac{P_{so}t_o}{b^2}(b - 1 + e^{-b}) \quad (2.2)$$

Where,

Ps_0 = Peak overpressure from shock front,

t_A = Arrival time of shock front,

t_0 = Duration of positive pressure phase,

b = Rate of pressure decay coefficient.

2.2.2 Types of Explosions and Effect on Waves

The Department of the Army (1990) classifies explosions based on whether the explosion is confined or unconfined. Confined explosions occur in enclosed areas such as buildings while unconfined explosions occur in open space areas. Blast loads on bridge columns due to bombs fall into the category of unconfined explosions. Unconfined blasts are divided into three categories, such as free air burst, air burst, and surface burst, as presented in Fig. 2.2. For the free air burst and the air burst, the center of the charge is located above ground, and for the surface burst, the charge is located on the ground. The major difference for a charge above ground (Figs. 2.2a and 2.2b) is that the shock front from a free air burst reaches the target unimpeded, whereas the shock front from an air burst reaches the ground first and is then reflected upwards to reach the structure (dashed lines in Fig 2.2b). When these waves bounce off the ground, they then move through the hot compressed air left behind by the shock front and catch up to the incident

wave, which will be the first wave layer to reach the structure. This creates a super positioning of waves, known as the Mach front, and it drastically amplifies the effect of the blast and can cause severe damage (Winget et al., 2005a). With respect to the surface burst, since the charge is placed on the ground, the waves propagate upwards as they cannot reflect off the ground.

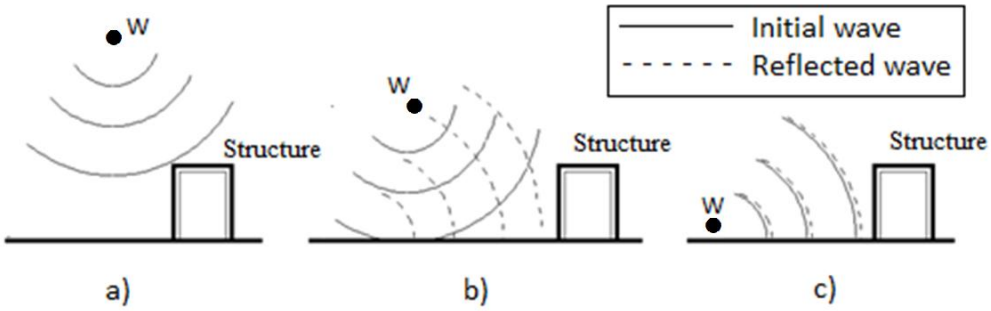

Figure 2.2 Components of blast loads: (a) free air burst, (b) air burst, and (c) surface burst, adopted from Karlos and Solomos (2013).

2.3 Classification of Blast Loads

There are several categories to classify explosions based on factors such as charge weight and charge location. Furthermore, experimental work has been conducted in order to identify major parameters for blast load classifications. It should be noted that the immediate and resulting pressures on a structural member depend greatly on the explosion category.

In the past decades, the US Department of the Army conducted hundreds of tests to study the parameters that would affect the positive pressure phase of blast loads. Based on observations from the test results, several parameters were identified and were correlated to the positive pressure phase of the blast. As show in Fig. 2.3, the Department of the Army (1990) reported that the parameters that can be correlated empirically with each other from the positive pressure phase are peak incident pressure (P_{so}), reflected pressure (P_r), incident impulse (i_s), reflected impulse (i_r), time of arrival of peak incident pressure (t_a), duration of positive pressure phase (t_o),

shock front velocity (U), and scaled wavelength of positive pressure phase (L_W). These parameters follow the Hopkinson-Cranz scaling law, which was developed in the beginning of

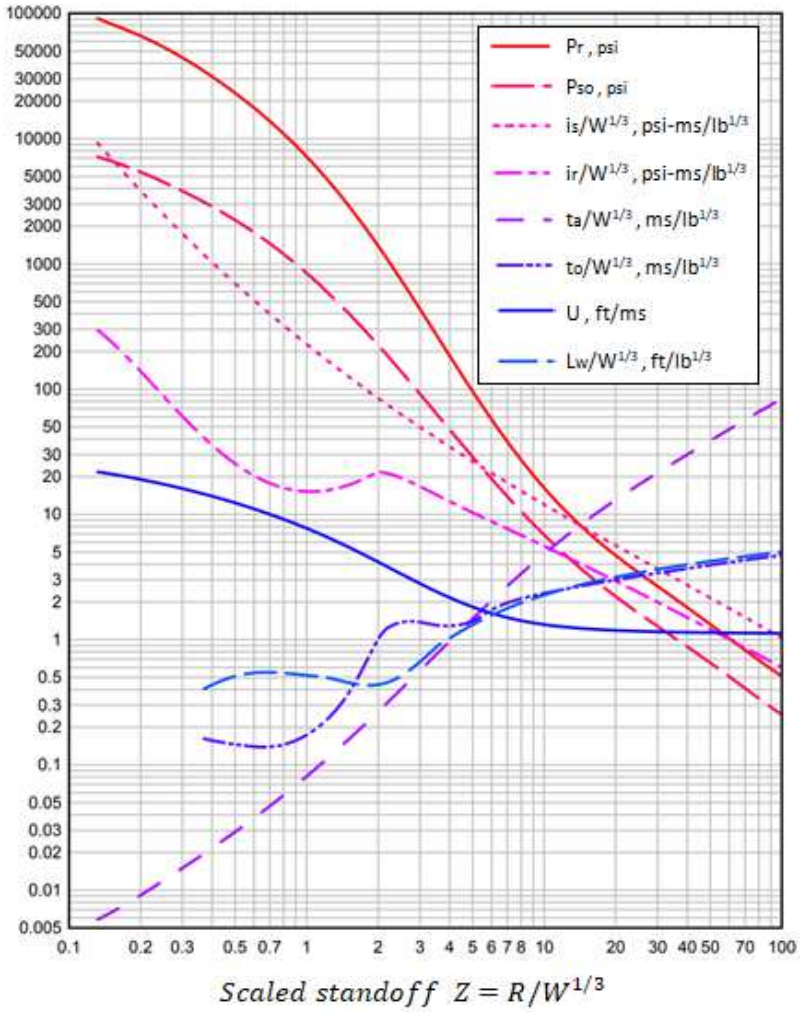

Figure 2.3 Blast wave parameters during the positive phase of blast (Department of the Army, 1990).

the 20th century and is defined by scaled standoff (Z), charge weight (W), and distance from charge to the target (R). Figure 2.3 shows the value of these parameters (vertical axis) vs scaled standoff (horizontal axis). Scaled standoff (Z) can be calculated using Equation 2.3, and as reported in Conrath et al. (1999), the same blast effect can be created with different charge weights and standoff distances. In addition, Equation 2.3 has been coded into finite element

analysis software like LS-DYNA through the ConWep code (US Army Corps of Engineers, 2001) to quantify the effects of the positive pressure phase. It is necessary to mention that the scaled standoff *Z*, its corresponding reflected pressure, and impulse are crucial to the level of column damage regardless of column properties such as mass or stiffness (Shi et al., 2007). Given this, scaled standoff Z is used as a major parameter in this study.

$$Z = \frac{R}{W^{1/3}} \tag{2.3}$$

Where,

Z = Scaled standoff ($m/kg^{1/3}$)

R = Standoff distance (m), measured from the center of the charge to the target structure

W = Equivalent weight of TNT charge (kg)

TNT had been the explosive of choice for hundreds of experimental tests, and it was used to validate Equation 2.3, which is also referred to as the Hopkinson-Cranz scaling law or cube root scaling law. But terrorist attacks have shown that TNT is not always the explosive of choice. Table 2.1 lists typical explosives along with the pressure and impulse of each as compared to the equivalent pressure and impulse of TNT.

Due to the fact that the ConWep code in finite element analysis software such as LS-DYNA is based on scaled standoff (i.e., parameter Z in Equation 2.3), equivalent mass factors were created for different types of explosives. All explosives other than TNT can be converted to an equivalent mass of TNT, and can then be used in Equation 2.3. Table 2.2 presents these equivalent mass factors with a range between 0.50 and 1.42.

Table 2.1 Equivalent TNT pressure and impulse for various explosives (Department of the Army, 1990).

Explosive	Pressure	Impulse
Comp. A-3	1.09	1.08
Comp. B	1.11	0.98
Comp. C-4	1.37	1.19
Cyclotol (70/30)	1.14	1.09
HBX-1	1.17	1.16
HBX-3	1.14	0.97
H-6	1.38	1.15
Minol-2	1.20	0.11
PETN	1.27	-
Pentolite	1.42	1.00
Picrotol	0.90	0.93
Tetryl	1.07	-
TNETB	1.36	1.10
TNT	1.00	1.00
TRITONAL	1.07	0.96
ANFO	0.82	-

Table 2.2 Equivalent TNT mass factor for various explosives (Dusenberry, 2010).

Name of explosive	TNT equivalent mass factor
TNT	1.00
C4	1.37
RDX	1.10
PETN	1.27
PENTOLITE 50/50	1.42
NITROGLYCRIN	1.00
NITROMETHANE	1.00
NITROCELLULOSE	0.50
AMON./NIT (ANFO)	0.87

2.4 Dynamic Structural Response to Blast Loads

Figure 2.4 presents the methods that are used for blast load analysis. It can be seen in the figure that the methods are divided into two primary categories, i.e, uncoupled analysis and coupled analysis. Uncoupled analysis describes the case where wave propagation from the blast and the structural response are analyzed separately. More specifically, the blast load is first

calculated and is then applied onto the structural member. In this case, the entire load is being applied onto the member at once. Given the very short duration of blast loads, energy dissipation from structural failure cannot be accounted for as reported in Williamson (2010). Therefore, this method tends to overestimate structural damage. The coupled analysis method describes the case where wave propagation from the blast and the structural response are considered together as they interact over time. Although these results are more realistic compared to the results from uncoupled analysis, this method requires advanced knowledge of dynamic analysis and finite element modeling. Furthermore, this method significantly increases computational time. Due to uncertainties in the characteristics of blast loads such as charge weight, shape of charge, position of charge, etc., the effort and complexity required for this method is not always warranted (Biggs, 1964).

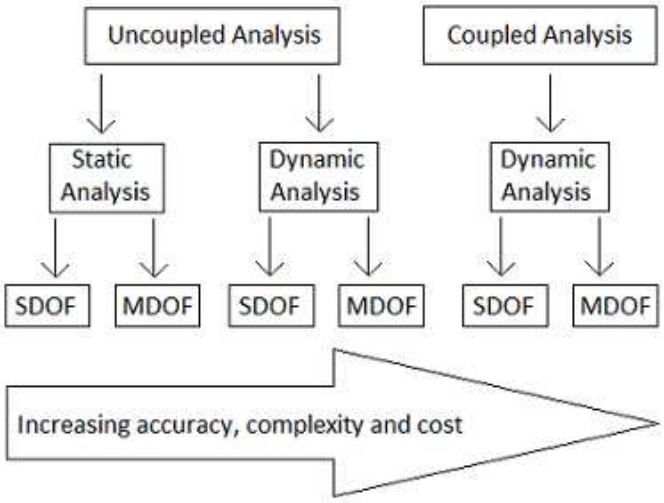

Figure 2.4 Typical blast loads analysis methods adopted from Winget (2003).

Like wind and earthquake loads, blast loads can also be considered as an equivalent static load for design purpose. However, this might lead to tremendously inaccurate results. Blast loads are unpredictable, and there is no verifiable historical data for the virtually unlimited scenarios

that can occur (Bounds, 1998). As a result, there are no applicable equations to find an equivalent static load. Given these facts, dynamic analysis is the most common method presently used for blast loads analysis.

It is well known that an equivalent single degree of freedom system (SDOF) can be used instead of a multiple degree of freedom system (MDOF) to estimate some parameters of building response (e.g., roof displacement) due to earthquake loads (Fajfar, 2000). However, this method has not been validated for blast loads. Before the 1990's, analysis was conducted using the uncoupled static SDOF method. With ground-breaking advancements in programming codes that can accurately simulate complex blast loads, the coupled dynamic method with MDOF analysis has been adopted in the most powerful blast load analysis software such as LS-DYNA.

Damping is usually ignored when dealing with blast loads as velocity damping is extremely small compared to the energy dissipated through plastic hinging (Williams, 2009). Material strain rate due to blast is another factor that will affect structural response. Ngo et al. (2007) reported that blasts produce the highest strain rate in materials such as concrete and steel, ranging from 10^2 s^{-1} to 10^4 s^{-1}, as compared to other types of loads including earthquake (Fig. 2.5). The experimental work on both concrete and steel has shown that these materials can

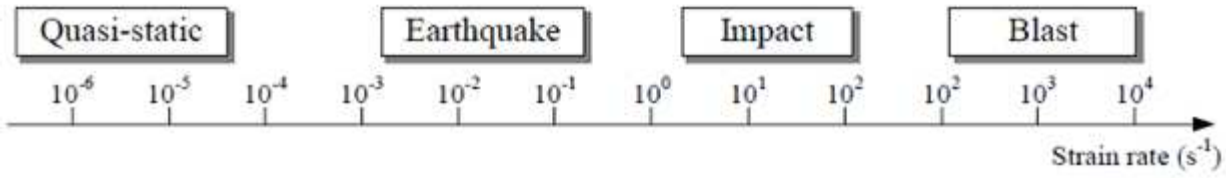

Figure 2.5 Range of strain rates for various types of loadings (Ngo et al., 2007).

experience an increase in strength due to blast. This is because the rate of loading from a blast is so rapid that these materials cannot respond quickly and show deformation (Tedesco et al.,

1999). For example, blast loading would increase concrete compressive strength for flexure by approximately 25% and approximately 10% for shear as compared to static loading. The yield strength of steel bars during blast tests was increased by about 23% in flexure and 10% in shear as compared to static loading (Department of the Army, 1990). This perceived increase in strength has been quantified from experimental testing and is given by Dynamic Increase Factor (DIF) values, which represent the ratio of material strength during dynamic loading to that during static loading. Some studies have reported that concrete in compression could obtain a DIF as high as 4 (Grote et al., 2001).

2.5 Previous Studies

After the attack of September 11th, 2001, terrorist attacks on infrastructure became a serious concern and bridges were no exception. During that year, the Conventional Weapons (ConWep) code was developed by the US Army Corps of Engineers and allowed for basic simulation of blast loads on bridges. Ray et al. (2003) investigated the effects of blast loads on a highway bridge due to a bomb placed below its deck. This study was focussed on assessing the difference between programming codes available for blast load simulations, such as ConWep, Blast-X (Britt et al., 1998), and SHAMRC (Crepeau, 2001), with respect to pressure and impulse. Baylot et al. (2003) listed some issues about blast load analysis on bridges for military and civilian purposes. For example, regarding the effect of charge, the military tends to focus on missiles and the charge shape is modelled as a cylinder. However, for civilian analysis the concern is hand placed and vehicle delivered bombs; therefore, the charge shape is spherical. Moreover, the military focuses on above deck explosions while civilian research focuses on underneath deck explosions. In addition, Baylot and his fellows modelled and examined the effects of blast on I-beams and found the importance of web thickness and beam depth in

preventing failure. Their beams were further examined by Islam and Yazdani (2008). They reported that below deck explosions could cause girder failure due to pressure build-up in confined areas between girders, which, in turn, led to large negative moment, crushing and shearing after the uplifting and dropping down of the deck. They also concluded that girder failure was mainly due to shear not flexure. Winget et al. (2005a) examined a two-span bridge with AASHTO girders and a three-column bent. They assumed a vehicle delivered bomb and modelled the resulting blast at different locations of the bridge. Results from their study showed that below deck explosions are more severe than above deck explosions. The main failure mechanisms for the columns observed in the study are crushing, spalling, and shear at the base. In addition, recommendations were made in Winget et al. (2005b) on how to better protect highway bridges against blast loads. This includes physical security and layout measures such as barriers around columns to increase standoff, and elimination of vegetation that could be used for hiding. They also found that circular columns had better performance than square columns. Pressure waves can go around circular geometries but not square geometries that have flat surfaces. As such, pressure can accumulate on the front face of square columns and the energy is not able to dissipate. Furthermore, the results showed that columns that are pinned at the top had satisfactory performance with regards to shear resistance. A pinned boundary condition allows rotation which can decrease shear failure. Fujikura et al. (2008) tested the performance of quarter-scale concrete filled steel tube (CFST) columns with fixed-pined boundary conditions. Their work showed that steel tubes could prevent spalling and breaching of the concrete core. Ductile failure was observed during the tests. Very recently, Wang et al. (2017) tested CFST columns under blast loads and found that, although mid-height deflection of columns was reduced by 67%, the columns could still carry 60% of the required axial load. Fujikura and

Bruneau (2010) investigated the benefits of using steel jacketing, which is commonly used to retrofit columns for seismic loads, against blast loads. The concept of steel jacketing is the same as that of CFST columns, except steel jacketing is discontinuous at the top and bottom of the column. It was found that the performance of a steel-jacketed column was very similar to that of a CFST column. However, the steel-jacketed columns experienced brittle failure from shear due to the discontinuity of the steel jacket at the top and bottom boundaries.

Williamson et al. (2011a) conducted a very comprehensive experimental study on bridge columns subjected to blast loads. In total, ten half-scale circular and square columns with different cross sectional dimensions were tested. These columns were designed according to the seismic provision specified in AASHTO LRFD (2007) and design manuals in eleven states issued by their respective Department of Transportation in the United States. The goal of the study was to evaluate the effects of column characteristics, such as shape of the cross section, type of the transverse reinforcement (i.e., ties and spirals), reinforcement ratio, and the location of lap splices. Their results showed that circular columns had better wave clearance, especially at the base, compared to square columns. More specifically, it was noticed that significant pressure was accumulated at the front face of square columns as the waves could not clear the free edges, while this is not the case for circular columns. Accordingly, larger impulse was developed at the front of the square columns. They also found that spiral reinforcement was better than ties to resist blast loads even though ties are preferred in practice due to ease of construction. For the same column-blast scenario, spirals experienced extensive damage but no brittle failure was observed in the tests. With respect to the ties, the test results showed that the minimum hook length required by both AASHTO LRFD (2007) and CHBDC (2006) was not sufficient for blast load resistance. The hooks open up and the tie reinforcement is pulled out. Similar observations

were reported in Bae and Bayrak (2008). Another point of interest was reinforcement ratio, and results showed that by increasing volumetric reinforcement by one-and-a-half times the requirement, columns performed much better. In terms of lap splicing, mechanical splicing was preferred in order to avoid the separation of longitudinal reinforcement. Based on the test results mentioned above, several recommendations were made in Williamson et al. (2011b). For example, three categories were developed for scaled standoffs. For each category, the preferred type of transverse reinforcement and location of lap splices were recommended. The failure mechanism of spalling of concrete side cover was also highlighted in Williamson et al. (2011b). Side spalling of circular columns, in addition to spalling at the back of the columns, was observed. It should be noted that side spalling of concrete cover was not considered as a failure mechanism in the requirements for blast load analysis issued by the Department of Defense (2002, 2008). This failure mechanism occurs when blast waves penetrate the front face of the column and travel to the back face, which causes contraction in the cross section. While these waves hit the back face and travel back towards the front face, the cross section experiences expansion. This expansion then causes spalling on the side of the column. Side spalling will reduce the cross section of a column, which will in turn decrease its load-carrying capacity. When analyzing bridges with regard to failure mechanisms from blast and seismic loads, there are a total of fourteen possible failure modes, and nine of them are common to both seismic and blast loads as reported by Yi et al. (2013a). The failure modes that do not occur from an earthquake but do occur from blast are related to the characteristics of the external loads. Seismic loads only act laterally and vertically, whereas blast loads are radially distributed. In general, both seismic and blast loads can cause failure modes related to erosion, shearing, rebar breakage, plastic hinging, and breakage of the column.

In parallel with the advancement of numerical and experimental work, modelling and simulation of blast loads in structural analysis software have tremendously improved these days. Although the ConWep code was developed in 2001, it is still used as a primary tool to examine the effects of blast. Recently, improved methods such as the **M**ulti-**M**aterial **A**rbitrary **L**agrangian **E**ulerian (MM-ALE) method were introduced. According to MM-ALE, the charge is explicitly modeled with an explosive burn equation, which can vary between programs, and the air domain between the charge and the structure is modelled as Eulerian elements. It has been noted that the MM-ALE method significantly increases the accuracy of the results. However, MM-ALE requires advanced knowledge of finite element modelling and extremely long computation times (Slavik, 2010). Yi et al. (2013b) proposed a hybrid method to couple the ConWep code and MM-ALE in order to use it in the commercial software LS-DYNA, which is the most popular program for structural analysis of blast loads on bridges. According to Yi et. al. (2013b), the blast pressure is modelled using empirical equations embedded in the ConWep code, i.e., the charge is not explicitly modelled, while the Eulerian air domain is modelled around the vicinity of the structural member under examination. Furthermore, the air domain does not span from the center of the charge to the structure, it only surrounds the immediate area around the structure. Yi et al. (2013a) reported that this hybrid combination could save tremendous computation time and effort while keeping accuracy of the results. Liu et al. (2015) compared the failure mechanisms of a typical three-column bent based on ConWep, MM-ALE, and the coupling of ConWep and MM-ALE. They found that ConWep alone did not represent all wave reflections, and it could not demonstrate extreme failure mechanisms unless relatively heavier charges were used in the modelling. In addition, they suggested that the air domain should be modelled explicitly in order to include the effects of wave reflection and confinement for decks,

bents, girders, and abutments. It is necessary to mention that the latest ConWep code in LS-DYNA can account for wave reflection on the ground and can be used for analysis of unobstructed columns.

Currently, LS-DYNA is the most popular software for modelling blast loads on bridges and has been used in numerous studies, including those mentioned above. More specifically, the major advantages of LS-DYNA are:

- Modelling techniques for applying blast pressure have been validated.
- Material models and program codes have been created specifically for blast load analysis of bridges.
- Providing detailed information from output files, including concrete failure, reinforcement stress, and displacement of columns.

Chapter 3: Design of Bridge Column

3.1 Bridge Description

For the purpose of this study, a generic bridge (Fig. 3.1) located in each of the following cities was designed, i.e., Toronto, Vancouver, and Victoria. These locations were selected to represent the low, high, and extremely high seismic hazard zones in Canada.

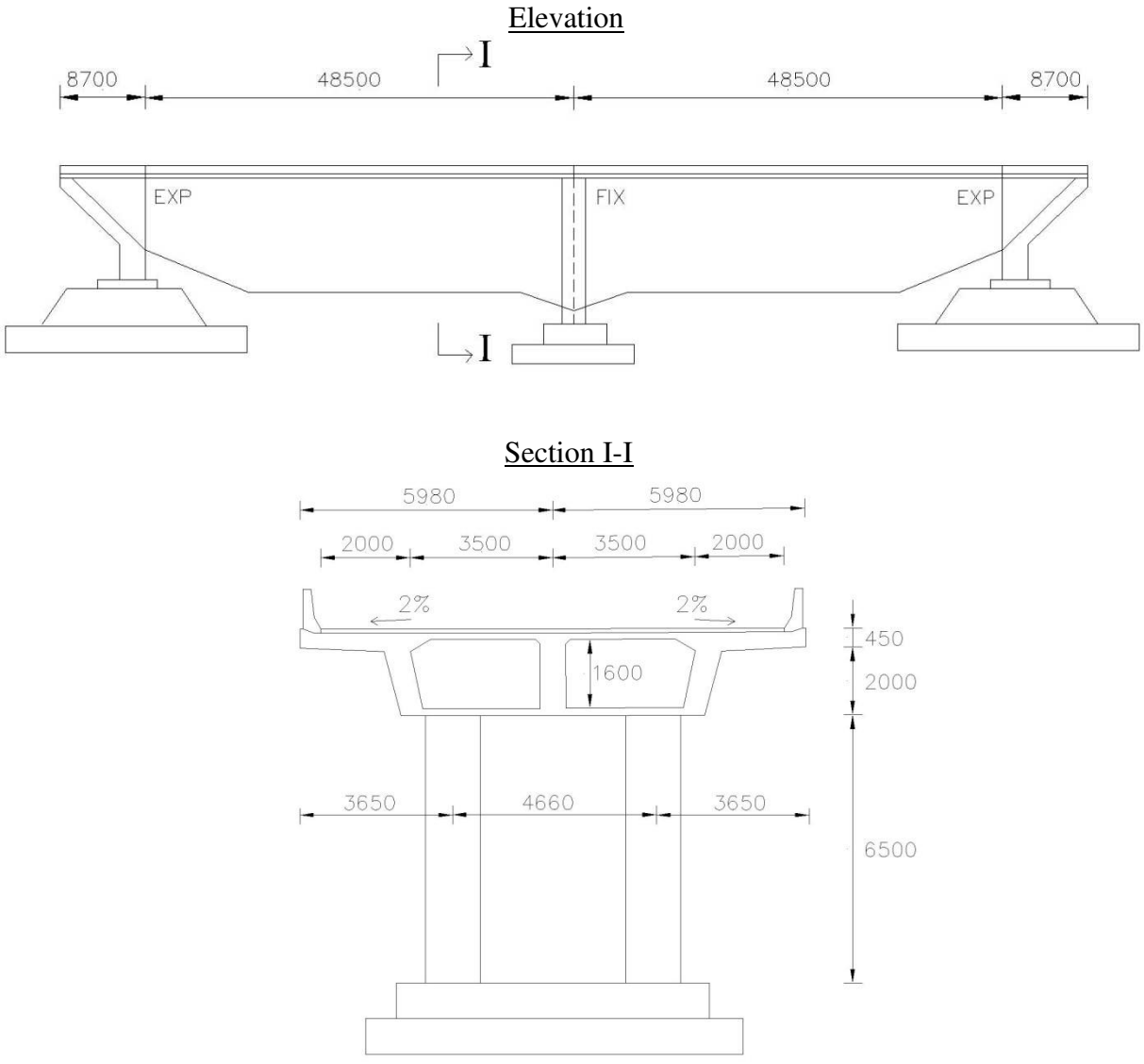

Figure 3.1 Geometric configuration of the bridge (units: mm).

It is a two-span continuous reinforced concrete bridge with each span of 48.5 m. The length of the wing wall on the east and west abutments is 8.7 m. The total width of the deck is 11.96 m. The wearing surface is 90 mm. The superstructure consists of a two-cell post tensioned cast-in-place concrete box girder with an overall thickness of 2.0 m, in which the depths of the top and the bottom flange are 175 mm and 225 mm, respectively. The box girder is supported by two columns, and each column has a diameter of 1.3 m and a height of 6.5 m. A shallow foundation is used for the pier and the abutments. Expansion bearings are used on the abutments, and fixed bearings are used on the pier. It is necessary to mention that the geometry of the bridge is the same for all three cities.

3.2 Bridge Column Design

The three-dimensional bridge model was developed using the commercial software CSI Bridge (CSI, 2015a), as illustrated in Fig. 3.2. More specifically, the superstructure was modelled as an area object while the columns were modelled as beam elements. The abutment at each end was simplified as a roller according to the recommendation made by Aviram et al. (2008). The foundation was considered fully rigid, i.e., all six degrees (three rotations and three translations) were restrained. Reduction factors for the flexural moment of inertia of slabs and columns were 0.70 and 0.35, respectively, while no reduction was made to other properties including torsional moment of inertia, shear area, axial stiffness, etc. (Caltrans, 2004).

The traffic load applied on the bridge deck is the CL-625 loading defined in CHBDC. The number of design lanes specified in the modelling was three with a multilane loading factor of 0.8 applied to both truck and lane loads. The seismic responses were determined by conducting response spectrum analysis.

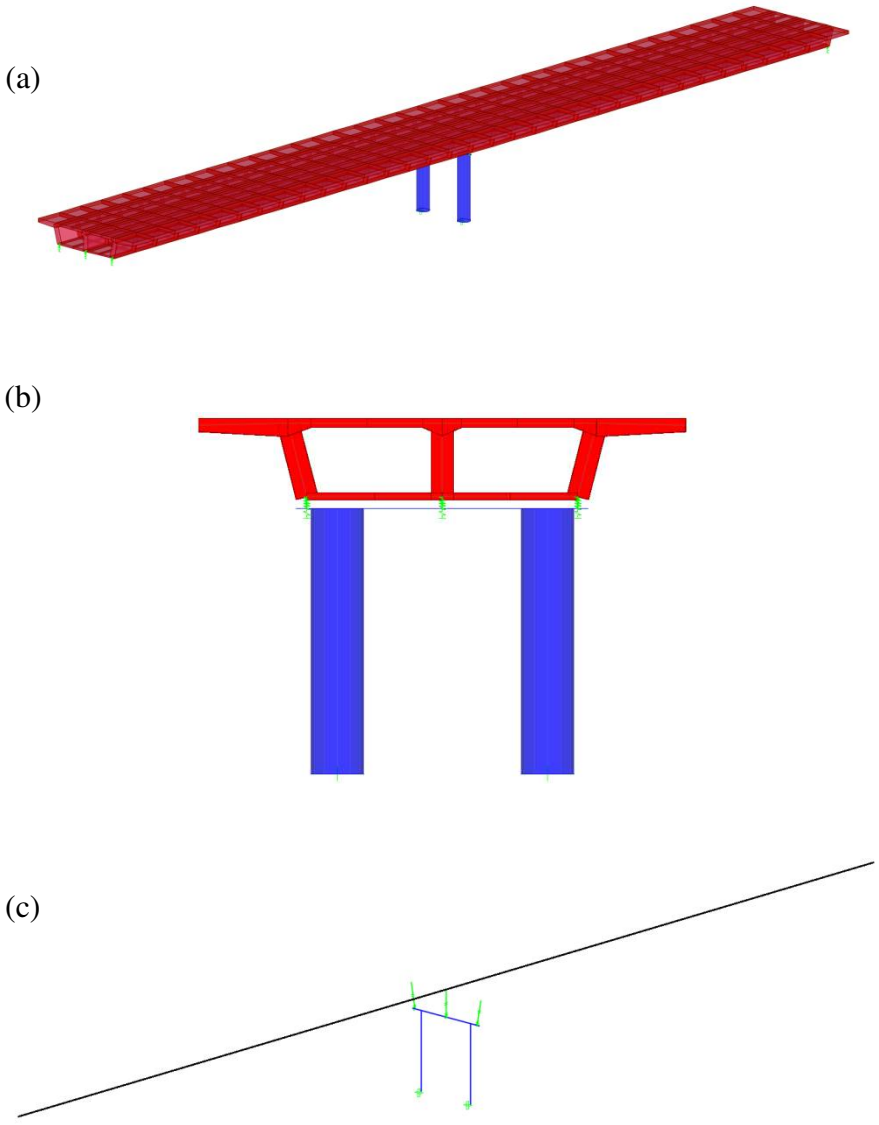

Figure 3.2 Finite element model of the bridge: (a) 3D extruded view, (b) cross section at pier, (c) line model.

Figure 3.3 shows the design spectra for Toronto, Vancouver, and Victoria for the probability of exceedance of 10% in 50 years for soil type I (stiff soil) according to CHBDC (2006). It is necessary to mention that the 2006 edition of CHBDC was used instead of the latest 2014 edition as the objective of this research is to evaluate the performance of existing bridges.

Table 3.1 summarizes the design forces used for the design of columns in each location, including axial force, shear force, and bending moment.

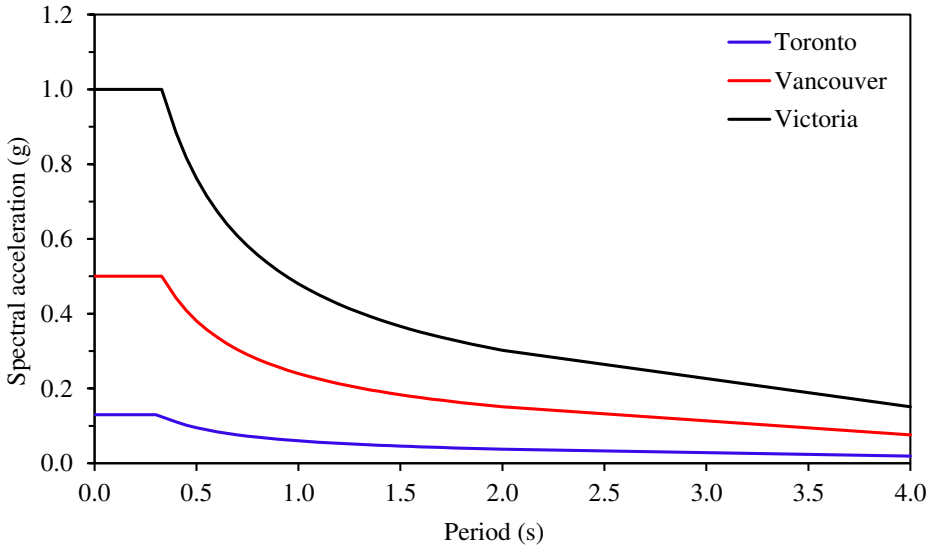

Figure 3.3 Seismic design spectra for Toronto, Vanouver, Victoria, 5% damping, 10%/50years, soil type I.

Table 3.1 Summary of column design forces.

Design forces	Toronto	Vancouver	Victoria
P_f (kN)	9717	9717	9717
V_f (kN)	808	3222	6463
M_f (kN·m)	551	1992	4406

Column design was conducted to satisfy the requirements specified in Section 4 (Seismic Design) and Section 8 (Concrete Structures) of CHBDC. In total, eight columns were designed in the study. More specifically, there is one tied column and one spiral column designed for Toronto and Vancouver, giving a total of four columns in these two cities. A total of four columns (two are tied, two are spiral) were designed for Victoria. The difference between the two designs of columns for Victoria is the bar size for the transverse reinforcement and its

spacing, i.e., smaller bar diameter and smaller spacing *vs* larger bar diameter and larger spacing. The tied and spiral columns that have smaller bar diameter and smaller spacing are named as the Set 1 design, and the tied and spiral columns that have larger bar diameter and larger spacing are named as the Set 2 design. Note that for all of the eight columns, the plastic hinge length is the same (i.e., 1.3 m). Table 3.2 presents information on the reinforcement of the eight columns that were designed. For illustration, Fig 3.5 shows the reinforcement in the Vancouver tied column. Detailed reinforcement design of all the columns is given in Appendix A.

Table 3.2 Summary of column reinforcement design.

Location	Column	Longitudinal reinforcement	Transverse reinforcement	
			Plastic hinge	Non-plastic hinge
Toronto	tied	27 - 25M @ 132 mm	15M @ 150 mm	15M @ 200 mm
	spiral	27 - 25M @ 132 mm	20M @ 150 mm	20M @ 150 mm
Vancouver	tied	27 - 25M @ 132 mm	25M @ 100 mm	25M @ 200mm
	spiral	27 - 25M @ 132 mm	25M @ 150 mm	25M @ 150 mm
Victoria	Set 1, tied	27 - 25M @ 132 mm	25M @ 80 mm	25M @ 80 mm
	Set 1, spiral	27 - 25M @ 132 mm	25M @ 80 mm	25M @ 80 mm
	Set 2, tied	27 - 25M @ 132 mm	30M @ 100 mm	30M @ 100 mm
	Set 2, spiral	27 - 25M @ 132 mm	30M @ 125 mm	30M @ 125 mm

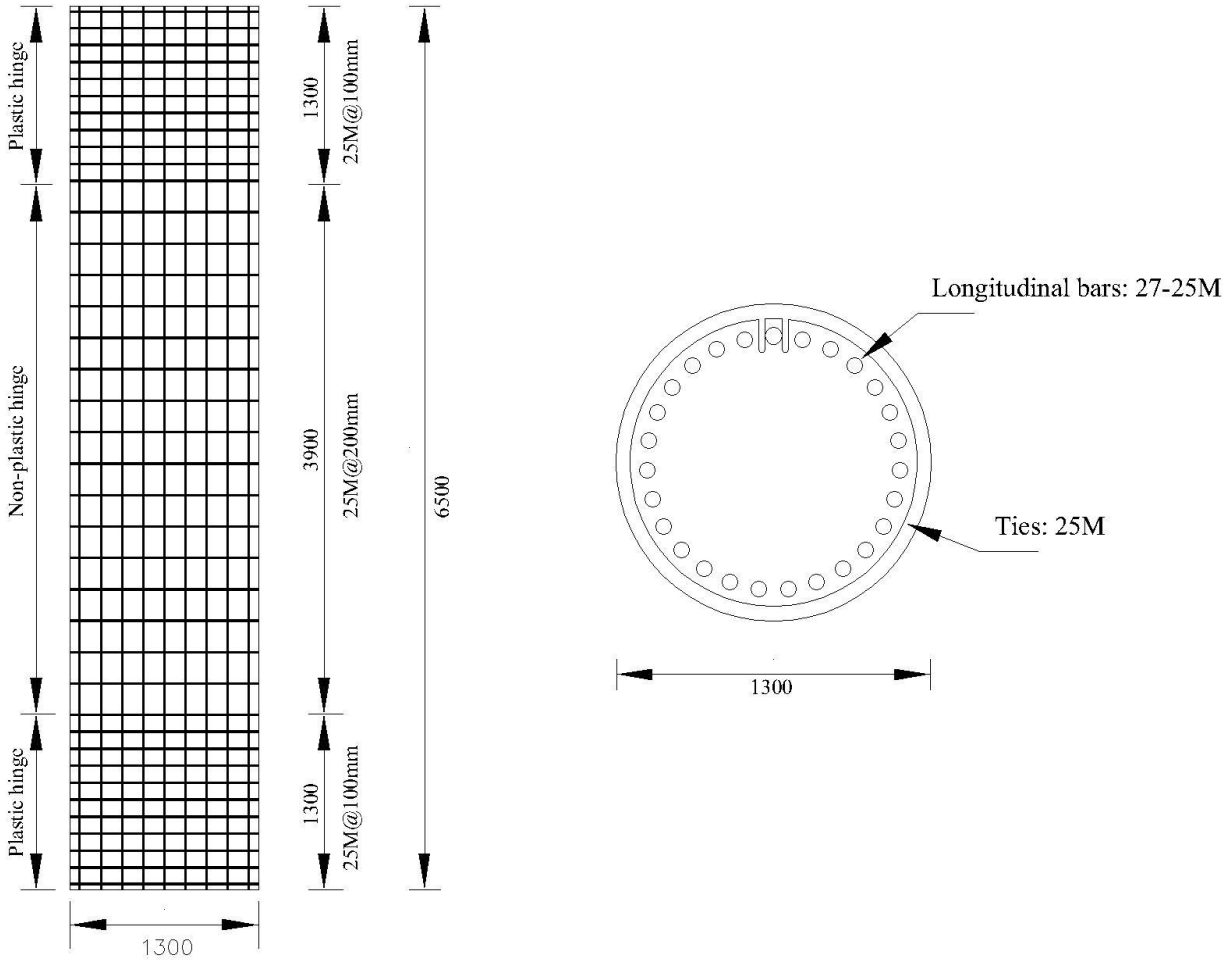

Figure 3.4 Reinforcement details for the Vancouver tied column (units: mm).

Chapter 4: Finite Element Modelling of Blasts in LS-DYNA

4.1 Introduction

The major steps for finite element modelling of blast loads in LS-DYNA in this study are as follows:

- Define materials: this includes selecting the type of elements and the constitutive model used for concrete and steel.
- Model reinforcement: transverse and longitudinal steel bars are modelled.
- Model concrete: concrete mesh is created to represent the bridge column.
- Couple concrete and steel reinforcement: this is to assure the two materials act together.
- Define boundary conditions: some of the nodes on the top and bottom of the column need to be restrained to represent the initial condition of the column at both ends.
- Apply blast loads: the blast loads need to be defined and applied to the appropriate elements of the column.

4.2 Element Types Used in Modelling Concrete and Steel

Solid elements in LS-DYNA can be used to model different shapes, such as hexahedrons, tetrahedrons, and pentahedrons. In this study, concrete is modelled as 8-node hexahedron elements. There are two choices for defining these elements depending on whether the elements are integrated or not integrated, i.e., element form 1 (ELFORM 1, LS-DYNA notation) and element form 2 (ELFORM 2). As illustrated in Fig. 4.1, ELFORM 1 is a single point un-

integrated element in which there is a single point located at the center of the element to measure stress and the corresponding strain. This can lead to a major shortcoming when using ELFORM 1. In LS-DYNA, when an element is experiencing stress, the resulting strain will be recorded. However, if the stress has not reached the single point in the center of the element, the software could interpret that no strain occurred. This case is referred to as the hourglass effect and is reported in LSTC (2006). Furthermore, Erhart (2011) addressed that hourglass stabilization was required and attention should be given on choosing an appropriate hourglass method if ELFORM 1 is used. In addition, the double precision solver might be required to create stability instead of the standard single precision solver, and this tremendously increases computational time (LSTC, 2016b). To overcome the disadvantages of ELFORM 1, the integrated ELFORM 2 was introduced and has more than one integration point within a single element, as illustrated in Fig. 4.1b. In scenarios where the elements have poor aspect ratios, integrated elements can become too stiff, which is known as volumetric locking (LSTC, 2006). In this study, poor aspect ratios are not concerning since the elements are uniform and optimized for size. Even though computational time for ELFORM 2 is greater than for ELFORM 1, the former is chosen in the study to avoid the hourglass effect.

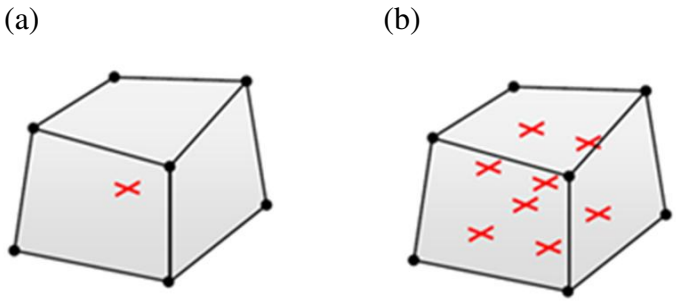

Figure 4.1 Solid elements in LS-DYNA (Erhart, 2011): (a) ELFORM 1, (b) ELFORM 2.

Steel reinforcement was modelled as beam elements with three options available, namely the Belytschko beam, the Hughes-Liu beam, and the Warped beam. Among these three types of beams, the Hughes-Liu beam was the first model implemented in LS-DYNA and is the primary beam model used for steel reinforcement in blast load analysis on columns. This model is well accepted as it is effective and requires less computational time (Schwer, 2014). More specifically, the beam is modelled as an 8-node hexahedron solid element with a single integration point (i.e., ELFORM 1) as there is no hourglass effect for this beam element according to LSTC (2006).

4.3 Material Models

4.3.1 Constitutive Concrete Model

There are several models available in LS-DYNA to simulate the behaviour of concrete. Four of them can be used to represent nonlinearity of concrete due to blast loads, and they are:

- Material 72: The MAT_CONCRETE_DAMAGE model, known as the Karagozian and Case model (KCC), has three shear failure surfaces. It was originally developed to model buried reinforced concrete elements subjected to impulsive loadings. Recently, the third revision of this model (MAR_CONCRETE_DAMAGE_REL3) became available.
- Material 84: The MAT_WINFRITH_CONCRETE model, known as the Winfrith concrete model, is a smeared crack and smeared rebar model developed by Broadhouse and Neilson in 1987. It should be noted that this model uses a single integration point; therefore, double precision is required to reduce instability.
- Material 111: The MAT_JOHNSON_HOLMQUIST_CONCRETE model, known as the Holmquist-Johnson-Cook model (HJC), was designed to simulate concrete that

experiences large strain under high pressure and the model takes permanent crushing into account.

- Material 159: The MAT_CSCM_CONCRETE model, known as the Continuous Surface Cap Concrete model (CSCM), has a smooth surface and is mainly used for solid elements. In this model, the failure criterion can be modified.

Among the four models described above, the two that can be considered for this study are the KCC and CSCM models for the following reasons:

(i) The KCC model has extensive options for user inputs to include different variables such as pressure hardening coefficients, damage scaling factors, and hardening modulus. Before releasing the third version of this model, all of these user inputs were required and some of them must be validated with experimental data. However, this process has been simplified significantly in the third version that requires more general inputs such as concrete compressive strength. On the other hand, the CSCM model, which was developed for the US Federal Highway Administration, is able to properly simulate impact loads on reinforced concrete structures (FHWA, 2007a; 2007b). In addition, it requires fewer and more basic user inputs as compared to the KCC model.

(ii) The KCC and CSCM models are the only two models that allow for failure criteria. One of the differences between the two models is that the KKC model requires a separate keyword to assign the appropriate failure criterion, while the CSCM model has a built-in failure criterion in the form of concrete element erosion. In addition, the KCC model requires an equation of state that is necessary to accurately determine the

hydrostatic behavior of the material based on density and energy. The CSCM model does not require an equation of state and calculates behavior based only on the volumetric strain of the material.

(iii) The KCC and CSCM models are the only two models that account for strain rate sensitivity and a Dynamic Increase Factor (DIF), which was described in Chapter 2. It was reported by Wu et al. (2012) that the KCC model performed better than the CSCM model in situations where confinement could have significant impact on failure since its strain rate effects were better calibrated. The KCC model requires the user to define a property curve that accounts for the DIF, which can be obtained from experimental tests or literature. However, the CSCM model has an option to activate and include strain rate effects that is already implemented in the program, i.e., no user-defined curve is required, and strain rate effects are automatically calculated based on properties such as concrete compressive strength.

By considering the advantages and disadvantages of the two models, the CSCM model was chosen to represent the material model for concrete. It is isotropic and demonstrates elastic behaviour of concrete before cracking. Once concrete enters plasticity, its yielding is defined by a three dimensional surface, as illustrated in Fig. 4.2. More specifically, if the stress on the element is below the yielding surface, the material is in an elastic state. Otherwise, it is in the plastic stage. In addition, the model has a damage predictor criterion in which the base value is 1 and represents the onset of cracking. Any value larger than 1 indicates that the element is eroded and it will be deleted from the simulation (Murray et al., 2007). With respect to the strain rate effects, LS-DYNA uses the CEB-FIP model to take the Dynamic Increase Factor (DIF) into

account for both compression and tension (Euro-International Committee for Concrete, 1990; Brannon and Leelavanichkul, 2009).

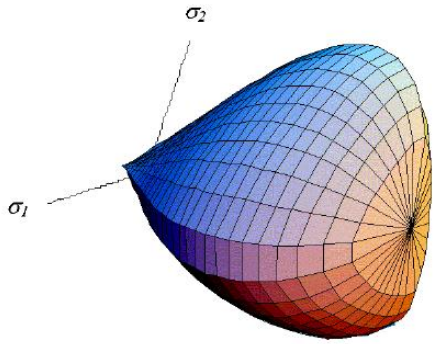

Figure 4.2 Schematic illustration of concrete yielding surface (FHWA, 2007a).

4.3.2 Constitutive Steel Model

The most commonly used model for steel reinforcement in LS-DYNA is Material Type 24, denoted as MAT_PIECEWISE_LINEAR_PLASTICITY, which has been validated with experimental work from blasts. It is an elasto-plastic model and considers plastic deformation, strain rate effects, and member failure (LSTC, 2016b). The required user inputs for the model are material density, Poissoin ratio, modulus of elasticity, tangent modulus, and yield stress. It is necessary to mention that the DIF for this model must be defined manually with steel stress-strain property as suggested by Schwer (2014).

4.4 Modelling of Reinforced Concrete Column

The modelling is carried out following the steps outlined below,

Step 1: Modelling of Reinforcement

Two sets of reinforcements are modelled separately in this study in which one set is for the transverse reinforcement and the other set is for the longitudinal reinforcement. As an

example, Figure 4.3 illustrates the LS-DYNA model for the reinforcement of the Vancouver tied column before and after element generation. The element generator is then used to create elements for each set. Finally, the keyword SET_PART_LIST is applied to combine the transverse and longitudinal reinforcement into a single part in order for them to act together.

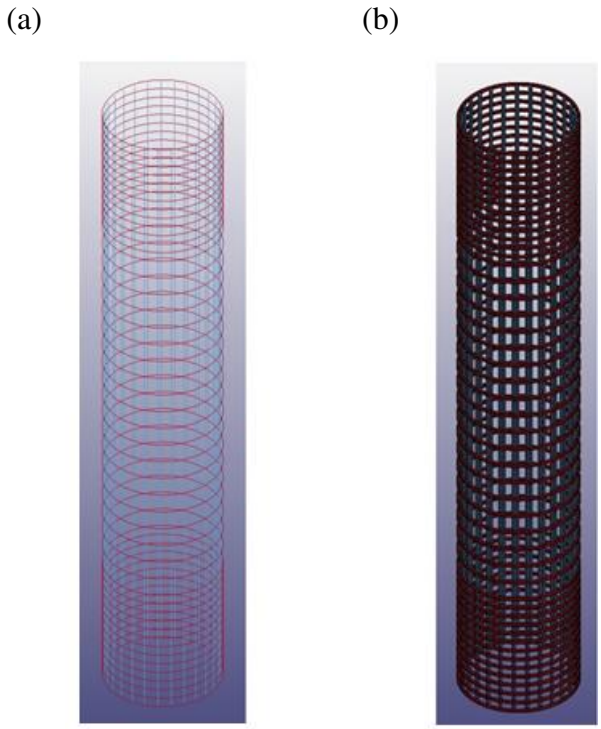

Figure 4.3 Model of reinforcement in the Vancouver tied column:
(a) before element generation, (b) after element generation.

Step 2: Modelling of Concrete

The concrete mesh used for the circular column is based on a cylinder with solid elements where the radius and height of the column are defined. In order to create elements, LS-DYNA assigns the number of elements along the circumferential direction and along the height of the column based on the selected mesh size, followed by the application of element

generation. For illustration, Fig. 4.4 shows the LS-DYNA model generating concrete in the Victoria Set 1 tied column.

(a) (b)

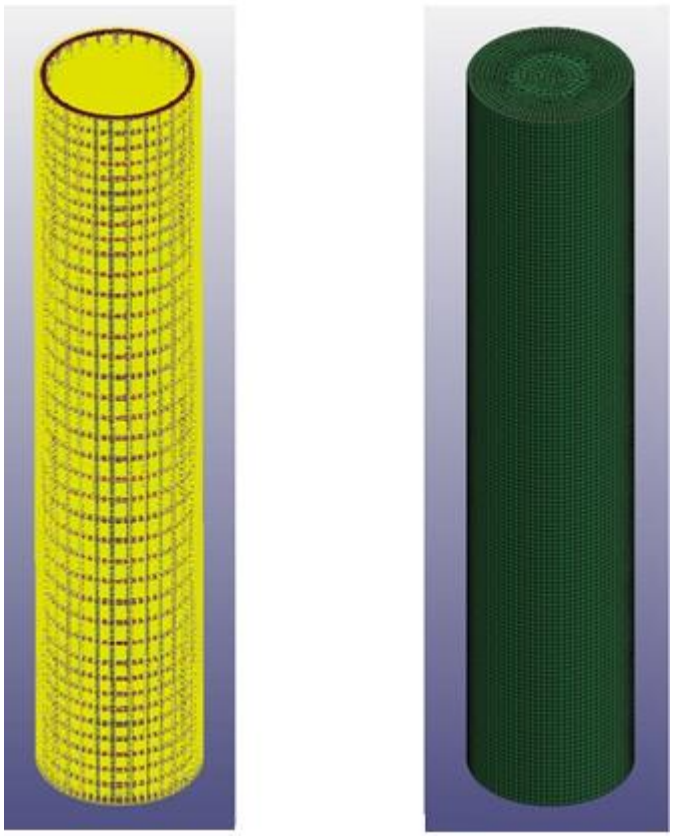

Figure 4.4 Model of concrete in the Victoria Set 1 tied column:
(a) before element generation, (b) after element generation.

Step 3: Application of Sections and Materials

After the elements for reinforcement and concrete are created, the next step is to assign the section and material properties for each element. For reinforcement, SECTION_BEAM is used to assign beam properties. The diameter of the transverse and longitudinal reinforcement is also specified. Finally, the keyword MAT_PIECEWISE_LINEAR_PLASTICITY is applied to define the properties of steel. For concrete, SECTION_SOLID is used to identify the concrete mesh as solid elements, and the ELFORM 2 option is selected to assign element form 2

properties. The keyword MAT_CSCM_CONCRETE is used to define the concrete material. It is necessary to mention that an erosion parameter was assigned with a value greater than 1, and strain rate effects from DIF are activated from the IRATE key card. Lastly, the keyword PART is used to combine the elements and materials to both concrete and reinforcement.

Step 4: Coupling of Concrete and Steel Reinforcement

Steel reinforcement needs to be merged to the concrete in order for them to work simultaneously. Two methods are available in LS-DYNA to achieve this goal, which are the smeared method and the explicit method.

For the smeared method, the total volume of reinforcement is divided by the total volume of concrete, which gives a volume fraction coefficient. This fraction is used to give a weight to the properties of concrete and steel. Accordingly, a composite material property is created (Schwer, 2014). This method works well within the elastic range, but it is not a good option for elements that could undergo significant plastic deformation, as is the case for blast loads (LSTC, 2006). For the explicit method, there are two options: the shared nodes and constraint methods. The shared nodes method involves connecting the common nodes of concrete and reinforcement (Tavarez, 2001). This can be extremely long and tedious, especially as element size decreases. Therefore, the preferred method is the constraint method in which the concrete mesh and reinforcement elements are modelled separately in LS-DYNA and a system is automatically developed to restrain the motion of the two based on relative geometry (Schwer, 2014). The keyword that applies this concept is CONSTRAINED_LAGRANGE_IN_SOLID, where the concrete mesh is considered as the master and the reinforcement is treated as the slave.

Step 5: Boundary Conditions

In both experimental and modelling work, boundary conditions of highway RC bridge columns are assumed to be fixed to the footing and pinned at the top, which is a critical case for blast load analysis and the configuration of the bridge in this study. In the modelling, a set of nodes is created for the nodes at the top and another set is created for nodes at the bottom of the column using the command SET_NODE. Then, the translational and rotational constraints that are applied to the set of nodes are defined through the BOUNDARY_SPC_SET keyword. For illustration, Fig. 4.5 shows the constrained nodes at the top of the Toronto spiral column.

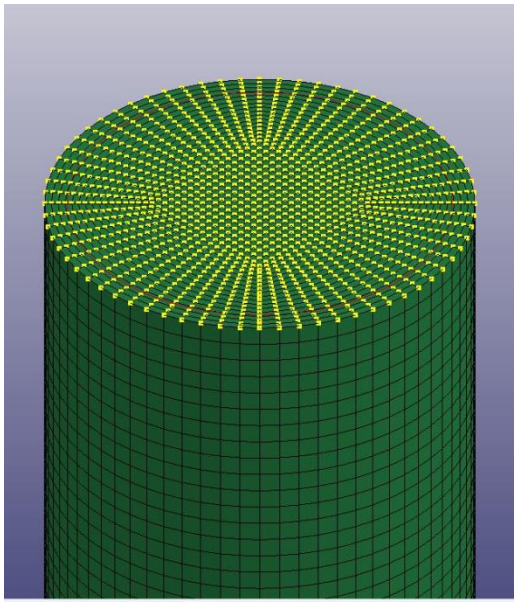

Figure 4.5 Constrained nodes at the top of the Toronto spiral column.

4.5 Mesh Size and Sensitivity Analysis

The two critical parameters for meshing of circular columns considered in this study are the number of elements along the circumferential direction and along the height of the column. For the purpose of sensitivity analysis, the Toronto tied column was taken under examination as

it is expected to be the worst performing column of this study. In this study, simulations for the blast will run for 80 milliseconds (ms) in order to observe all major failure mechanisms. Based on LS-DYNA's internal conversion of bytes to words of memory and the computer core used for this analysis, it is found that the maximum memory for running an input file is 900 million words of memory. As illustrated in Table 4.1, the 887 million words of memory from a concrete mesh size of 30 mm is very close to the maximum memory that is available. Accordingly, this is used as a minimum mesh size in the sensitivity analysis. It should be noted that the solver removes deleted nodes and elements that have failed from the simulation. This process increases computational time and the real time that is required to run simulations is drastically longer than the approximate time given by LS-DYNA's solver at the beginning when it reads the input file. As an example, when testing the 55 mm mesh, the approximated simulation time given by the solver was 8,060 seconds (about 2.2 hours). The actual time that was required for completion of the simulation was 19,908 seconds (about 6 hours), which represents an incredible increase of about 250% from the original estimate due to significant erosion that occurred during simulation. The results in Table 4.1 indicate that convergence and optimization occur for a mesh size of 55 millimeters.

Table 4.1 Mesh sensitivity analysis results of the Toronto tied column for 80 ms simulation.

Mesh size (mm)	Number of elements	Memory words required (million)	Approximate simulation run time (seconds/hours)
70	39093	32	1774/0.5
60	155073	110	14651/4.1
55	99194	54	8060/2.2
50	98527	70	11379/3.2
45	131781	94	14113/3.9
30	1231105	887	265237/7.4

Figure 4.6 illustrates the mesh sizes of the six examined cases, ranging from 30 mm to 70 mm. It can be seen clearly in the figure that the shapes of the cross sectional elements vary along the radial direction since LS-DYNA automatically configures the elements along the radial length, such that the column's transverse reinforcement would fall within the first element that is at the exterior surface of the column. LS-DYNA optimizes the number of elements in the radial direction based on the number of elements along the circumferential direction and along the height of the column. Given this, the 55 mm mesh was chosen because there is a clear element at the exterior surface of the column and transverse reinforcement is embedded into the second element that is moving away from the surface of the column. This will better emulate the concrete clear cover that a real column has, and accordingly this provides better simulation results. Furthermore, 20 mm elements for both transverse and longitudinal reinforcement are selected based on observations by Williams (2009). Therefore, the concrete mesh size is chosen as 55 mm elements and reinforcements are chosen as 20 mm elements.

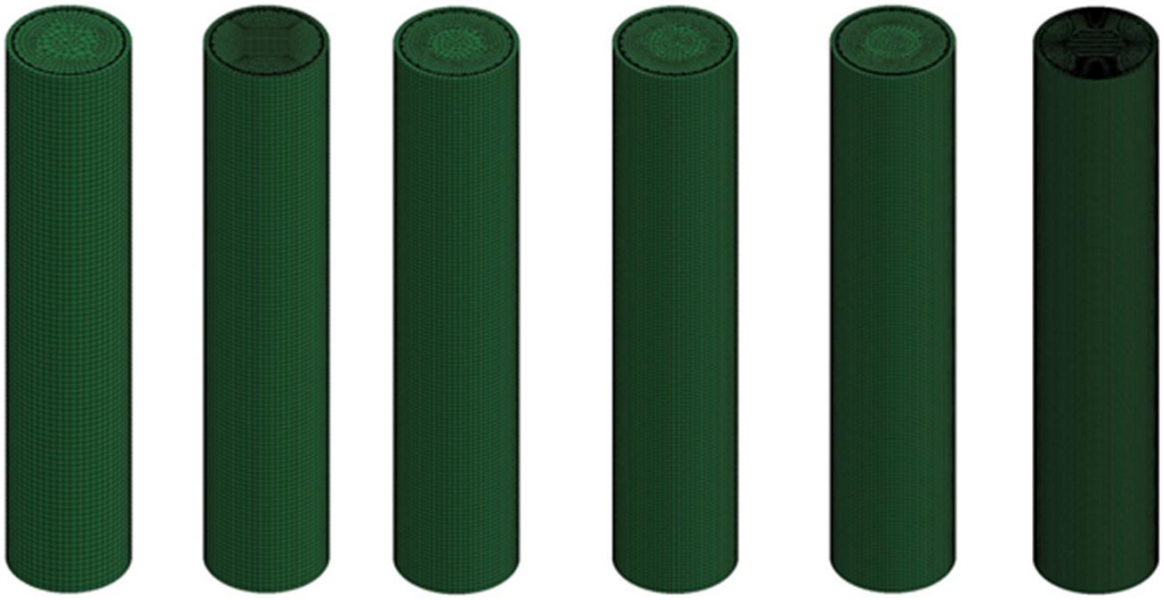

Figure 4.6 Visual representation of mesh sizes of the six examined cases.

4.6 Modelling of Blast Loads

There are three methods used to model blasts in LS-DYNA, which are the Conventional Weapons (ConWep) method, the Multi-Material Arbitrary Lagrangian Eulerian (MM-ALE) method, and a hybrid coupling method that combines the two above-mentioned methods.

The ConWep code was developed by the U.S. Army Corps of Engineers in 2001 based on data from hundreds of air blast tests to create empirical equations. This method applies pressure from the positive phase of the blast onto the structural element. The air between the charge and the structural element is not modelled explicitly in this method. Therefore, when the pressure from the shock front reaches the structural element, it only propagates through the element if there are solid elements in its path. As a result, if elements become eroded, the pressure disappears along with those elements. Furthermore, since the air domain is not explicitly modelled, wave reflections are not accounted for and accordingly, the effects of confinement are ignored (Schwer, 2010).

The MM-ALE method is more accurate than the ConWep method as both the explosive charge and air domain are explicitly modelled, and this overcomes the drawbacks of the ConWep method. However, this method requires tremendous expertise and computational effort. For example, for the same simulation parameters, the time for the MM-ALE method is about 340 times greater than that of the ConWep method, as reported by Slavik (2010). In order to reduce computational time and keep the accuracy of MM-ALE modelling, attempts have been made to modify the Eulerian air domain. Traditionally, the air between the charge and the structure is modelled as a single Eulerian domain that works well for building structures with multiple stories in the vertical direction. Since bridges span horizontally, they do not require a large

vertical domain like buildings. One of the improvements that have been made to MM-ALE modeling for bridges is that the one big Eulerian air domain is replaced by several small domains, such that a specific domain is deleted when the pressure from the blast leaves that domain. By using this approach, it has been found that the computational time could be reduced by 40%-60% as compared to having one big domain (Pan, 2012).

The hybrid coupling method that combines ConWep and MM-ALE has drawn attention over the last few years due to its high efficiency in keeping the accuracy of the results and decreasing computational time. In this method, the blast pressure is based on the ConWep code, and the charge is not explicitly modelled with a burn equation like it is with the MM-ALE method. The burn equation is a user-defined function that controls explosive behavior, including density and rate of explosion. Moreover, the Eulerian air domain does not cover the entire area between the charge and the structure. Instead, the air domain only covers the immediate area surrounding the structure in question. Therefore, both wave reflection and confinement around the structure are taken into consideration while the computational time is reduced as an air domain is not needed between the charge and areas that do not immediately surround the structure. It was reported by Schwer (2010) that computational time for the coupling method could be less than half than that of the MM-ALE method.

Generally, the ConWep method is not appropriate for scenarios involving pier-bents and larger scale models (e.g., modeling of an entire bridge) since wave reflection and confinement will have significant effects on failure (Yi et. al, 2013a). However, Liu et al. (2015) recently showed that the ConWep method can still be used if the weight of the charge is increased in order to compensate for the lack of wave reflection and still allow for severe failure mechanisms to occur. Moreover, in this study where only a column is modelled, the charge has a clear and

unobstructed view of the column. Therefore, the only reflections that will occur are from the waves that hit the ground and bounce up to join the incident wave, which in turn creates a Mach front. A Mach front is created when there is a super positioning of waves due to reflection, and this creates a powerful wave that can significantly increase damage. For this study, these reflections can be considered using the keyword LOAD_BLAST_ENHANCED in LS-DYNA, in which the user has to input values for equivalent charge weight of TNT, distance of the charge from the column, and height of the charge above ground. In order to activate the ground wave amplification factor and account for the Mach front, a node residing on the ground is identified using the DEFINE_VECTOR keyword, where a vector perpendicular to the ground is created. This allows the LOAD_BLAST_ENHANCED function to know where the ground resides. Once the blast load has been created, the segments of column elements that will receive the positive phase pressure are identified using LOAD_BLAST_SEGMENT_SET. These segment element sets are those that have a clear view of the blast and will absorb the initial pressure (LSTC, 2016b). With regards to the coupling method, there are a number of uncertainties for the air domain (e.g., thickness of the Eulerian air domain mesh, wavelength, initial density of the air, etc.) that would affect the results, as explained in Schwer (2010), Marburg (2002), Han and Liu (2015). Given that this study focuses solely on columns (i.e., not a large scale model) and wave reflections can be accounted for, the ConWep method was selected for modelling in this study.

4.7 Validation of LS-DYNA Modelling

As reported in Williams (2009), the maximum displacement of columns from Single Degree of Freedom (SDOF) analysis is commonly used to validate LS-DYNA modelling. Following this practice, in this study, the software RCBlast (Jacques, 2014) is selected to determine the maximum displacement of a column as a SDOF. It is necessary to mention that

RCBlast is designed specifically for modelling of singular columns against blast loads and has been validated with experimental work at the Shock Tube Test Facility at the University of Ottawa (Jacques, 2012).

For the purpose of validation of the LS-DYNA models developed in the present study, the Vancouver tied column, whose reinforcement detailing is illustrated in Fig. 3.4 (Chapter 3), is chosen for comparison of maximum displacement. The SDOF analysis is performed for Case I, which is one of three blast load cases examined in this study, and the blast is placed at mid-height of the column. Figure 4.7 illustrates the Graphic User Interface for SDOF analysis of the examined column in RCBlast along with some typical results such as the pressure *vs* time curve and the displacement-time history.

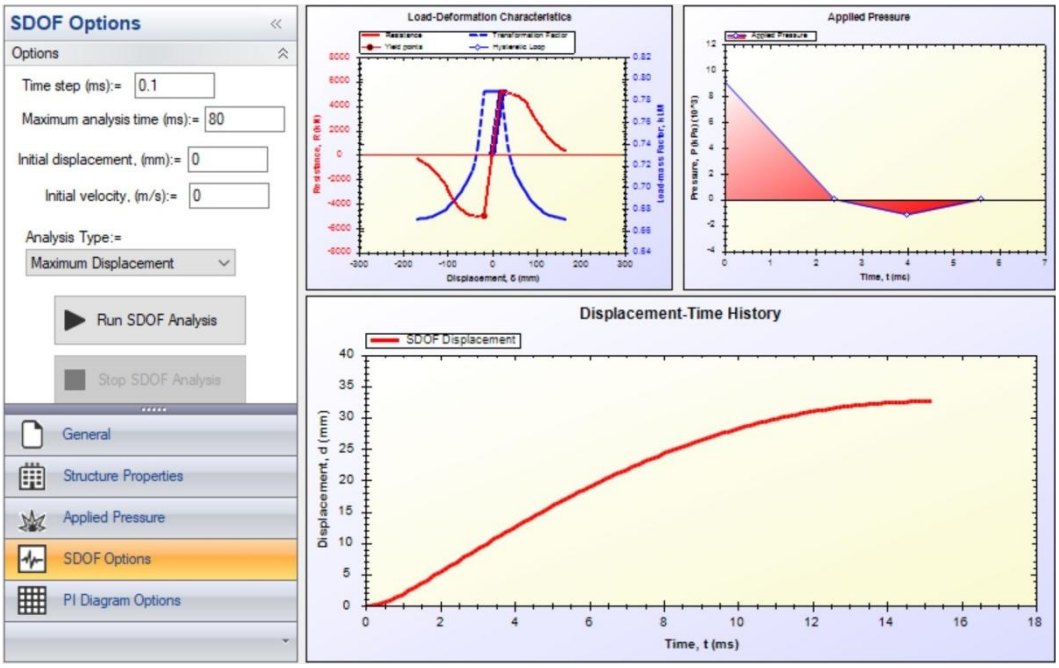

Figure 4.7 Graphic User Interface of SDOF results for the Vancouver tied column in RCBlast.

The curve of the maximum displacement given in RCBlast is then compared to the one in LS-DYNA (Fig. 4.8). It can be seen in the figure that both curves follow almost the same trend. The maximum displacements obtained in SDOF and LS-DYNA are 32.50 mm and 35.62 mm, respectively, which represents a difference of about 9%. This observation is consistent with the one reported in Kyei (2014). More specifically, Kyei conducted experimental testing of RC columns subjected to blast loads as part of a research project undertaken at Carleton University. The data collected in the tests was then applied in numerical analysis using LS-DYNA. During his study, he also compared the values of the maximum displacement of columns in a SDOF system with those obtained in a more complex finite modelling in LS-DYNA. It was concluded that difference in maximum displacements was about 8%-14% for the given scaled standoff considered in Kyei (2014), which is equivalent to the one considered in the current study (i.e., parameter Z in Equation 2.3, Chapter 2). It should be noted that the LS-DYNA modelling techniques in this study are adopted from Kyei (2014). Therefore, the above-mentioned finding is not a surprise.

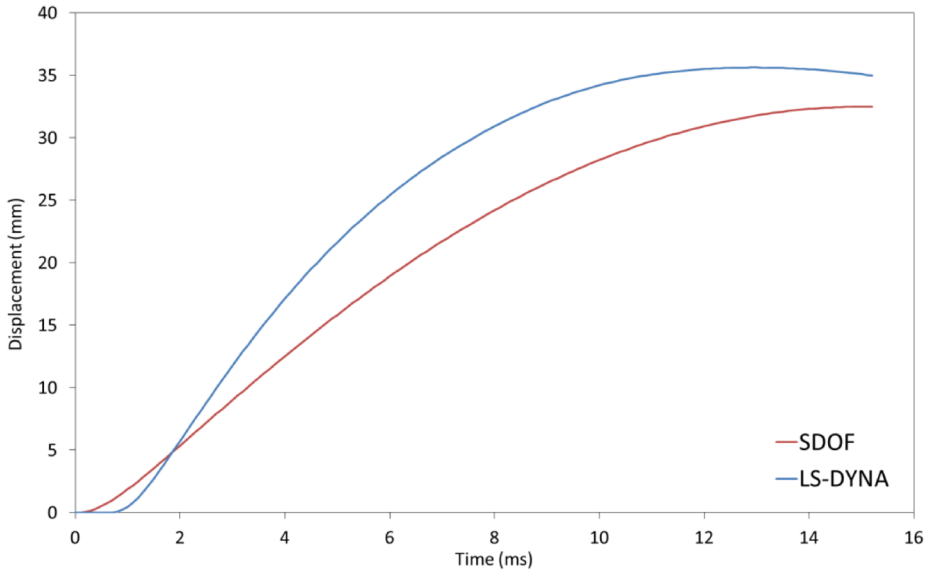

Figure 4.8 Comparison of results between RCBlast and LS-DYNA.

Chapter 5: Analysis and Results – Charge Height X1

5.1 Introduction

Due to the sensitive nature of blast loads on public infrastructure, specific details of the simulations including charge weight, charge height, and standoff distance will not be revealed in this thesis. The eight columns located in Toronto, Vancouver, and Victoria, as described in Chapter 3, are examined for two charge heights (X1 and X2). They represent the cases where a charge is located at mid-height of the column (X1) and close to the base of the column (X2), respectively. Charge height X2 is within range of the target location for hand placed or vehicle delivered bombs recommended by the Department of Defense. However, the exact location will not be revealed. For each charge height, three cases, namely Case I, Case II, and Case III, are tested. The results from Case I, with a specific charge weight and standoff distance, are considered as a reference for the purpose of comparison. In Case II, the charge weight is increased by 12% as compared to Case I, while in Case III the standoff distance is 12% closer to the column than in Case I. The factor of 12% was chosen as experimental work has shown that it is within a range of factors that can lead to significant impact on structural performance (Williamson et al., 2011a). It is necessary to mention that the scaled standoff for Case I, Case II, and Case III are the same in order to assess the effect of charge weight and standoff distance on the performance of the column, i.e., which parameter dominates the behaviour of the column. In total, 48 simulations (= 8 columns x 3 cases x 2 column heights) are performed in this study.

For a better understanding of the results, both qualitative and quantitative results are recorded from LS-DYNA for each set of simulations. Qualitative results include concrete failure mechanisms such as concrete crushing and spalling, while quantitative results include parameters such as when the steel bars yield and when the column reaches maximum displacement.

5.2 Analysis of Results for Charge Height X1 (mid-height)

5.2.1 Case I (reference case)

5.2.1.1 Toronto columns

Concrete failure mechanisms

Figure 5.1 illustrates the effective plastic strain in concrete in the Toronto columns at 5 ms, 15 ms, and 30 ms. Effective plastic strain is the total plastic strain acting on the surface of an element and indicates that the element is actively yielding, and the element fails when the scalar value of plastic strain reaches 1 (LSTC, 2006). As expected, the results in Fig 5.1 show that tension is developed on the columns back surface when the shock front makes contact with the column. It can also be seen in Fig. 5.1a that the tied column has already experienced breakage by the 15 ms mark, and more core concrete is eroded around mid-height as time goes on. More importantly, attention should be given to the pattern of erosion at the boundaries of the column, which can be used to explain the effects of boundary conditions on blast load resistance. The results in Fig. 5.1a clearly show that as the simulation progresses, erosion at the boundaries of the column slightly increases. In addition, the erosion at the top boundary mainly occurs outside of the concrete core, i.e., there is little penetration into the core of the concrete. However, at the base, erosion occurs on the entire circumference of the column, and it has penetrated into the concrete core. This pattern is due to the fixed-pinned boundary condition at the ends of the

column. Pinning the column at the top reduces shear but allows for larger flexural deformation, as reported in Winget et al. (2005b).

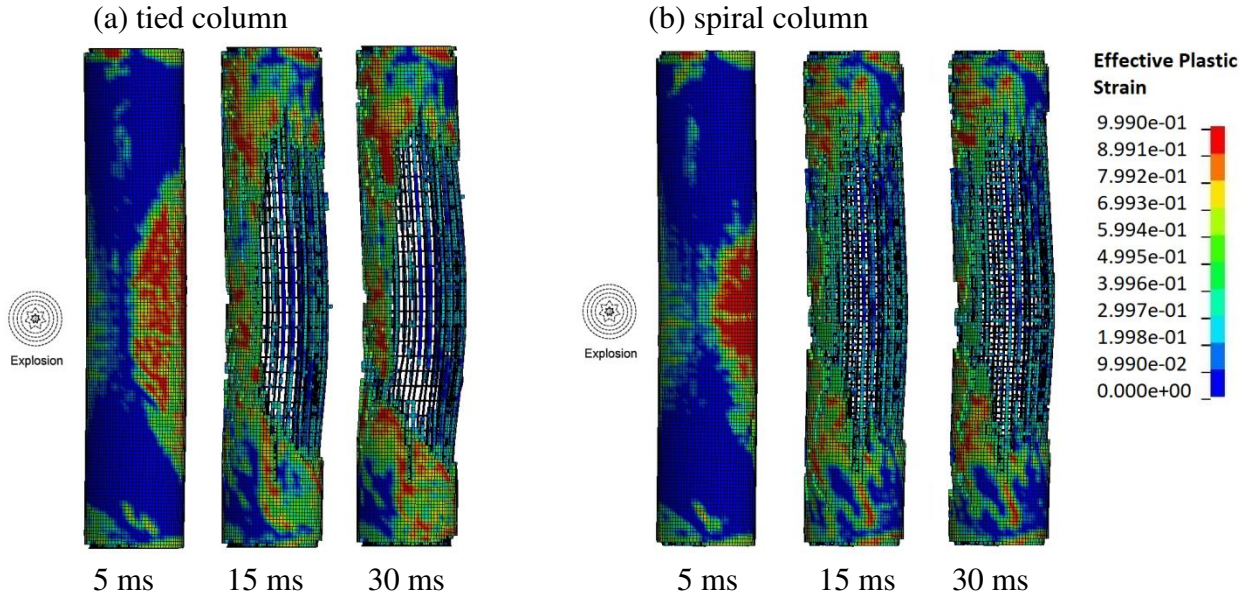

Figure 5.1 Contour of the effective plastic strain in Toronto columns, Case I, X1.

The boundary conditions also affect crack propagation patterns. For example, in the plastic hinge region at the top of the column (pinned connection), cracks propagate in a horizontal manner due to flexure, while at the bottom of the column (fixed connection), the crack line propagates at 45 degrees, which is indicative of shear cracking. By comparing the results between the tied column (Fig. 5.1a) and spiral column (Fig. 5.1b), it is found that the spiral column performs better in terms of concrete erosion. Strain occupies a large area on the back of the tied column, which causes significant erosion. The strain is concentrated in a smaller area for the spiral column and it experiences less erosion overall. The spiral column experiences more erosion at the boundaries compared to the tied column because the spiral column is better at resisting flexural deformation, and as a result the boundaries experience greater erosion. Both the tied and spiral columns experience breakage.

Reinforcement stress and behaviour

Reinforcement stresses of 400 MPa, 450 MPa, and 500 MPa are used to examine the nonlinearity of the steel bars during the simulation, in which 400 MPa represents the yielding stress, 500 MPa represents the maximum stress, and 450 MPa represents the average. Severe reinforcement deformation is defined as the state where the reinforcement has experienced plastic deformation which has led to permanent curvature of the bar even after the positive pressure phase has ended.

The effects of the blast on the reinforcement are assessed from the following aspects: (i) yielding of the transverse and longitudinal reinforcement; (ii) failure mechanisms in the reinforcement. For the tied column, the ties around mid-height never surpass yield stress as the concrete absorbs the majority of deformation through erosion, while the ties near the boundaries do reach yield stress. Moreover, there is pullout of several ties near the point of maximum displacement. This finding is very similar to the one reported in Williamson et al. (2011a) through their experimental work. With respect to the longitudinal reinforcement, the bars reach yield stress and surpass 450 MPa, but this only occurs after breakage of the column. During the positive pressure phase, the highest stress levels for the longitudinal bars are on the back of the column, which is experiencing tension. Furthermore, the longitudinal reinforcement around mid-height experiences severe deformation at the time of column breakage, as illustrated in Fig. 5.2.

Figure 5.2 Deformation of longitudinal bars in the Toronto tied column, Case I, X1.

For the spiral column, it was found that the spirals around mid-height yield almost instantly after the shock front makes impact. Most importantly, almost all the spirals throughout the height of the column, both on the front and back sides, have surpassed yield stress right before breakage of the column. On the other hand, the longitudinal reinforcement surpasses yield stress after breakage of the column. The highest level of stress in the reinforcement is on the tension side of the column. As deflection starts to occur, the stress on the tension side of the column starts to shift towards the top, and at the top, the stress on the front side of the column starts to shift down. This can clearly be seen in Fig. 5.3, showing axial force on longitudinal bars at three time marks at 9.29 ms, 9.89 ms, and 11.29 ms. For example, at 9.29 ms, the highest axial force, which is directly proportional to stress, is on the tension side of the column around mid-height. At 9.89 ms, the stress on the tension side has slighted shifted up and the stress on the front has shifted down; at this point, they have converged to the same area. At 11.29 ms, the stress on the tension side shifts further up, and as time goes by it reaches the top of the column. This mechanism does not occur at the bottom of the column where the boundary is fixed and it only occurs at the top boundary, which is pinned, and allows for greater rotation.

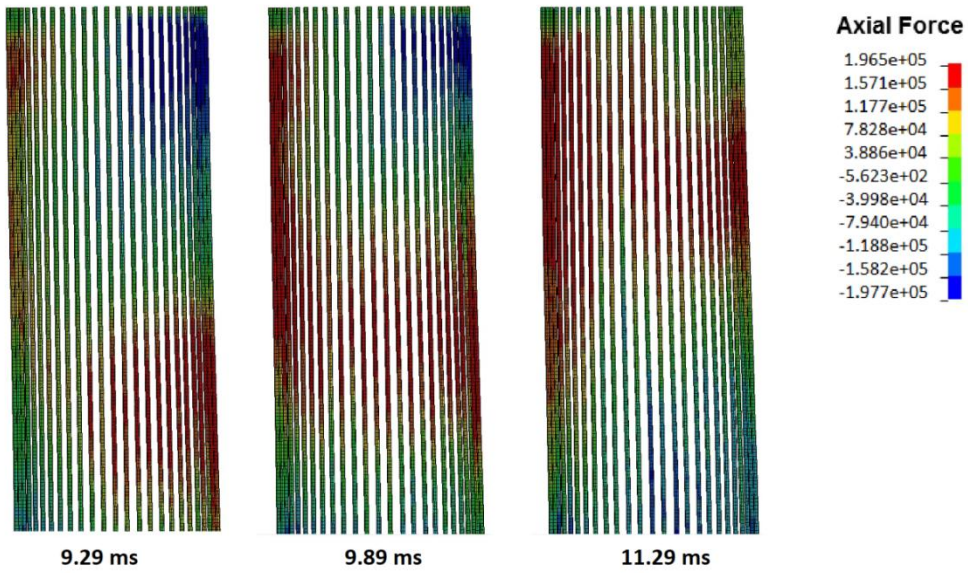

Figure 5.3 Axial force on longitudinal bars for the Toronto spiral column, Case I, X1.

Displacement curves

The displacement curves for the Toronto tied and spiral columns are presented in Fig. 5.4a and 5.4b, respectively. For ease of understanding, the failure mechanisms observed in the simulation are marked on the curve with regards to time of occurrence and the corresponding lateral displacement of the column. It can be seen in Fig. 5.4 that both columns experience the following 4 failure modes: erosion at boundaries (outside/inside core), crushing (outside/inside core), spalling (outside/inside core), and breakage of column. Additionally, the tied column experiences severe rebar deformation (deformation which has led to permanent curvature of the bars). Maximum displacement, steel stress of 400 MPa (i.e., yielding stress) and 450 MPa (i.e., average stress after yielding) are also shown. Based on the results, it can be concluded that both the tied and spiral columns fail to resist the blast. There are two parameters on the displacement curves which show that the spiral column better resisted the blast compared to the tied column. The first parameter is yield stress, and when comparing the two columns, it is noted that the reinforcement of the spiral column experienced yield stress approximately 12 ms sooner than the

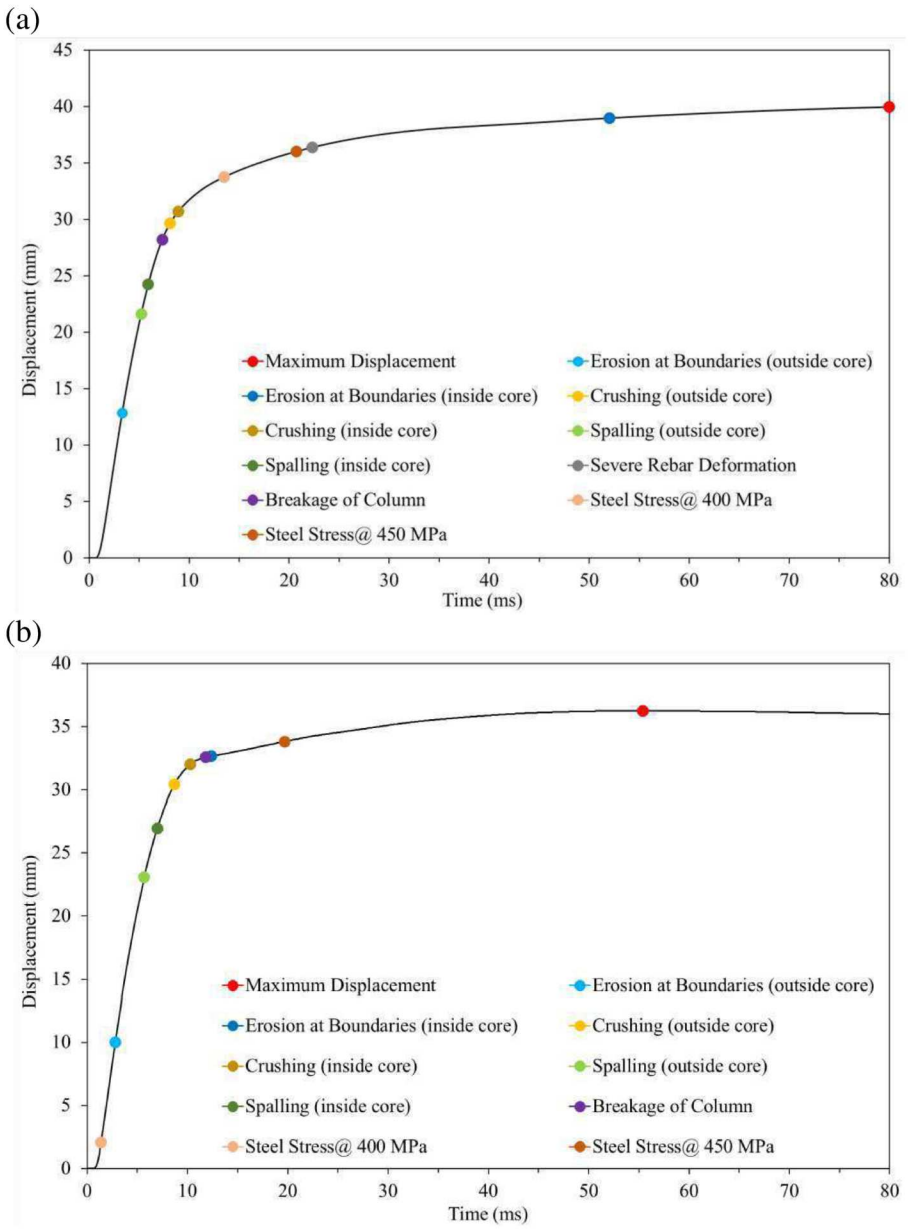

Figure 5.4 Displacement curves for Toronto columns, Case I, X1: (a) tied column, (b) spiral column.

tied column. The second parameter is concrete crushing, and the spiral column experiences crushing before column breakage, whereas the tied column experiences crushing after breakage. Concrete crushing at the front of the column is more preferable than concrete spalling at the back of the column. The more crushing there is at the front of the column, the less spalling occurs at

the back as the front has dissipated the energy. The back of the column is critical as it experiences tension and can cause column failure, and there is rarely any column failure due to crushing. Therefore, the spiral column is more adequate than the tied column in its ability to resist blast. Moreover, the slight difference in the shape of the displacement curves between the columns is a result of reinforcement yielding in the spiral column. The tied column reaches maximum displacement at the end of the 80 ms simulation, whereas greater reinforcement yielding in the spiral column allows it to reach its maximum displacement earlier in the simulation time.

5.2.1.2 Vancouver columns

Concrete failure mechanisms

As discussed in the previous section, Toronto columns experienced severe breakage. However, this failure mode was not observed in the Vancouver columns. Even though the tied column would not be able to support the required axial load, full breakage does not occur. Figures 5.5a and 5.5b illustrate the effective plastic strain distribution in concrete at the time of 5 ms, 15 ms, and 30 ms for the Vancouver tied and spiral columns. The different reaction of the two columns to the blast load can clearly be seen in the two figures. For example, for the tied column, the majority of the concrete core on the back face has been eroded.

For the spiral column (Fig. 5.5b), the concrete core around mid-height remains mostly intact at 30 ms and there is not a significant increase in damage at the end of the simulation. Crushing at the face of the column does not penetrate the core, and on the back face spalling only slightly penetrates the core. Moreover, there is almost no crushing or spalling of concrete in the plastic hinge zones. When erosion of concrete occurs in the plastic hinge zones, there is limited

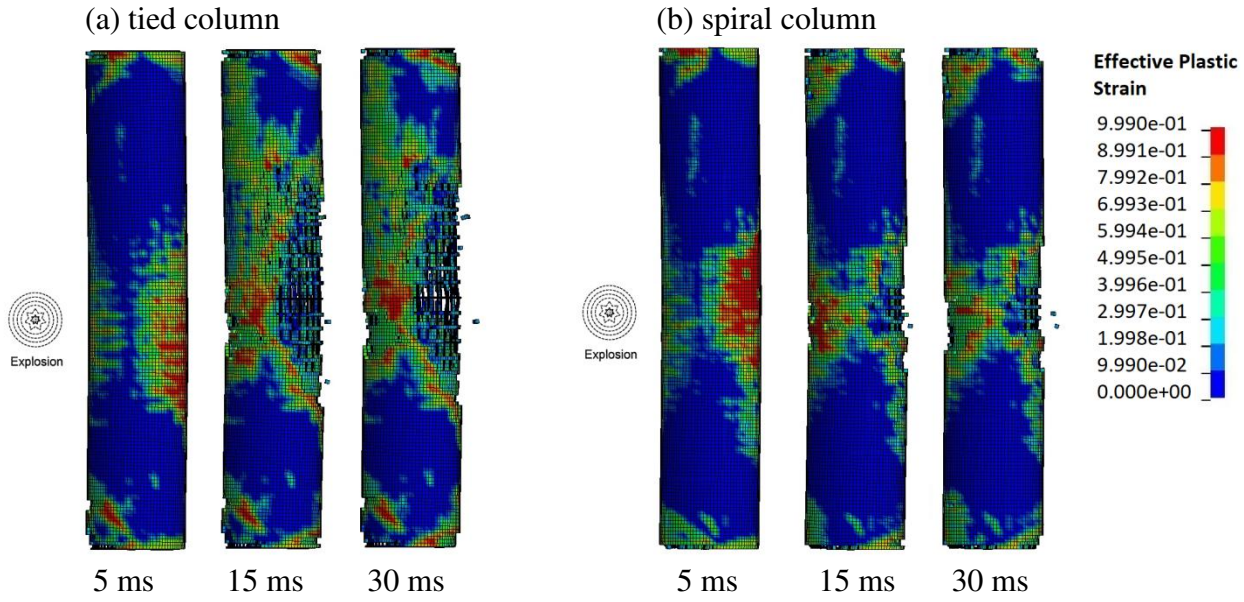

Figure 5.5 Contour of the effective plastic strain in Vancouver columns, Case I, X1.

penetration inside the core. It is also interesting to compare the Toronto spiral column with the Vancouver spiral column. Both columns have the same transverse reinforcement spacing of 150 mm along the entire height of the column, but the Vancouver column uses 25M spirals and the Toronto column uses 20M spirals. Therefore, the bar size of the spirals has had an impact on concrete erosion as the Toronto column breaks but the Vancouver column successfully resists the blast.

Reinforcement stress and behaviour

The results from the Vancouver columns show that reinforcement has significant effects on blast load resistance. For the tied column, the ties (both on the tension and compression side) have surpassed yield stress before maximum displacement has occurred, and some ties exceed stresses of 500 MPa after maximum displacement. The pattern of stress distribution starts at charge height and then stress occurs in the plastic hinge regions. Longitudinal reinforcement also surpasses yield stress right before maximum displacement has occurred. In addition, some bars

sustained severe deformation near mid-height of the column on the tension side. For the spiral column, the spirals surpass yield stress before maximum displacement and exceed stresses of 450 MPa after maximum displacement. Longitudinal reinforcement also yields before maximum displacement, and a distinct comparison can be made with other columns.

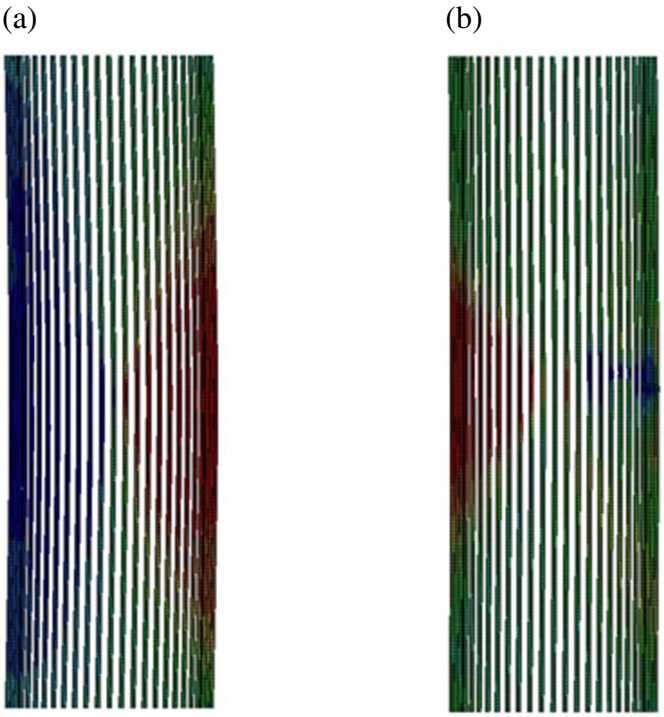

Figure 5.6 Stress distribution on longitudinal bars of the Vancouver spiral column, Case I, X1: (a) at the maximum displacement, (b) at the first rebounding peak.

For Toronto columns, the stress on longitudinal reinforcement shifted from mid-height to the top of the column, and stress from the top of the column shifted down (Fig. 5.3). For the two Vancouver columns, the stress accumulates at mid-height and shifts sideways instead of shifting up and down. This mechanism, where stress on the reinforcement shifts between the back and front of the column, is due to the rebounding phenomena. Rebounding occurs in all columns that demonstrate some ability to resist blast. After maximum displacement has occurred, a column will slightly move back towards its initial position. The column can then move back the other way towards maximum displacement, which creates rebounding as the column moves back and

forth. From the results of this study, it is concluded that the more a column rebounds after its maximum displacement, the greater its ability to resist blast. Figure 5.6 is an example of this mechanism as it happens for the Vancouver spiral column. The column starts its deflection until the point of maximum displacement and stress is at mid-height on the back side. The column rebounds and moves back the other way towards its original position, and stress gets shifted to the front of the column and maximum stress occurs at the first rebounding peak.

Displacement curves

As mentioned in the previous section, rebounding creates a pendulum effect where the column moves back and forth after maximum displacement. The shape of the displacement curve will function like a wave that eventually reaches steady state. Rebounding can cause additional failure, especially concrete erosion, after the positive pressure phase. When the column reaches maximum displacement and rebounds, the front face of the column that was originally experiencing compression is now suddenly experiencing tension. The results of this study indicate that failures that occur as a result of rebounding are extremely minor as the majority of failure occurs during the positive pressure phase before the column reaches maximum displacement.

The Vancouver tied and spiral column both experience rebounding during this simulation. As an example, it can be seen in Fig. 5.7 that both columns (tied and spiral) experienced crushing that penetrated the core after maximum displacement, and this is attributed to rebounding. Compared to the tied column, the spiral column experiences a higher degree of rebounding. It can also be noticed that the spiral column does not experience severe rebar deformation, which occurred for the tied column. Both tied columns in Toronto and Vancouver experience severe rebar deformation, but the spiral columns for both cities do not.

(a)

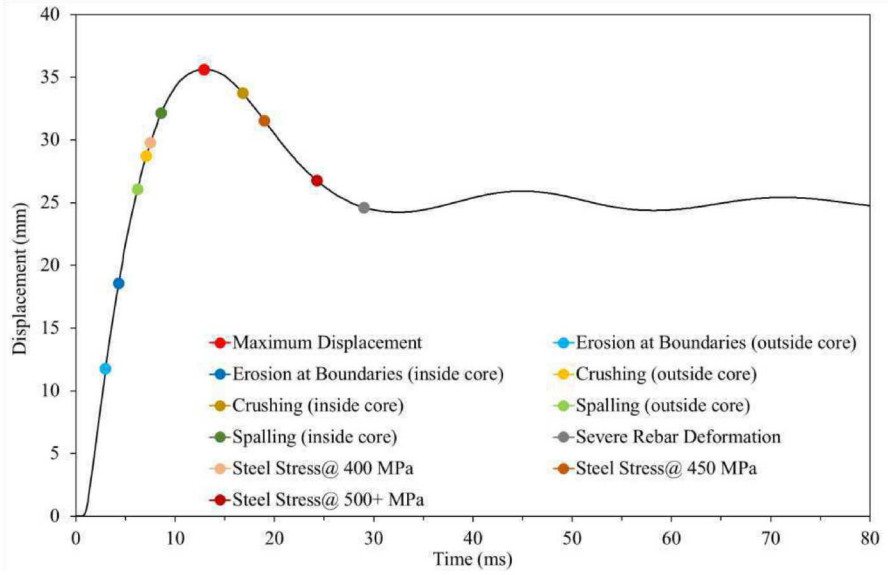

(b)

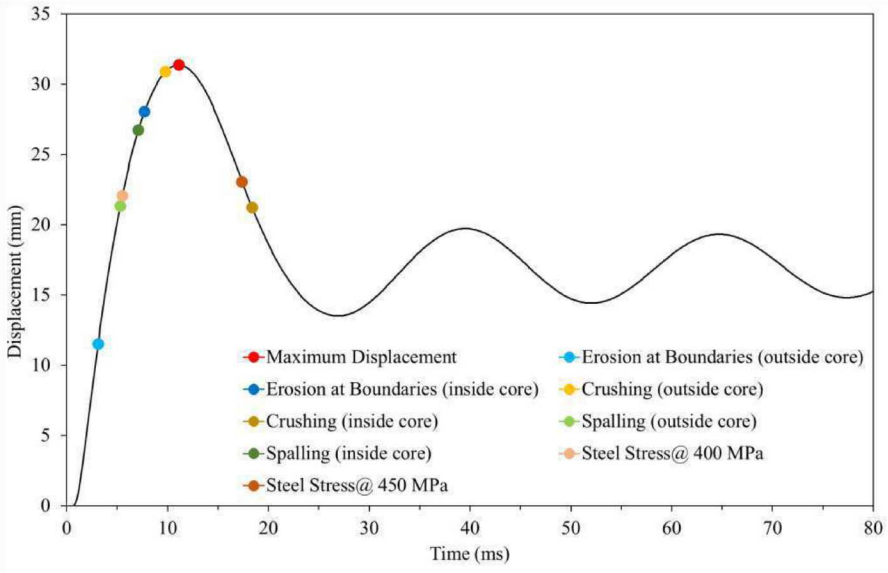

Figure 5.7 Displacement curves for Vancouver columns, Case I, X1: (a) tied column, (b) spiral column.

5.2.1.3 Victoria columns

Concrete failure mechanisms

The Victoria columns performed noticeably better than the columns for Toronto and Vancouver. Figures 5.8a and 5.8b present the effective plastic strain in concrete at 5 ms, 15 ms, and 30 ms for the Victoria Set 1 columns (Transverse reinf. 25M@80 mm) and Fig. 5.9a and 5.9b present the effective plastic strain in concrete at 5ms, 15ms, and 30ms for Set 2 columns (30M@100 mm for tied, 125 mm for spiral). The design for Set 1 has smaller transverse reinforcement bar size and smaller spacing of transverse reinforcement, while the design for Set 2 has bigger transverse reinforcement bar size and larger spacing of transverse reinforcement. As mentioned in Chapter 3, the two sets of column designs for Victoria were considered in order to investigate the effects of spacing and diameter of transverse reinforcement on blast load resistance. The results in Fig 5.8 and Fig. 5.9 show that all four columns performed extremely well in resisting erosion of core concrete. They also performed well with regards to crushing and spalling of concrete outside the core. Generally speaking, crushing of the front face is more desirable than spalling at the back (i.e., tension side) since concrete is stronger in its ability to resist compression compared to tension. Therefore, the crushing failure mechanism, especially when it does not penetrate the core, is preferred. It is also noticed that after maximum displacement, rebounding caused some erosion in the columns. However, this is not a major concern since the majority of erosion on the front face occurred before the column reaches its maximum displacement.

As illustrated in the figures, for the tied columns, the Set 1 design has more erosion at the base while the column of Set 2 has more erosion at the top. Furthermore, Set 1 has less core penetration from spalling than Set 2, and this penetration is due to rebounding and occurs after

the column reaches maximum displacement. Although the difference is minor, due to the fact that crushing is preferred compared to spalling, the advantage is given to the Set 1 design as it experiences less concrete erosion from spalling. Overall, the tied column of Set 1 was better able to resist blast during the positive pressure phase than that of Set 2.

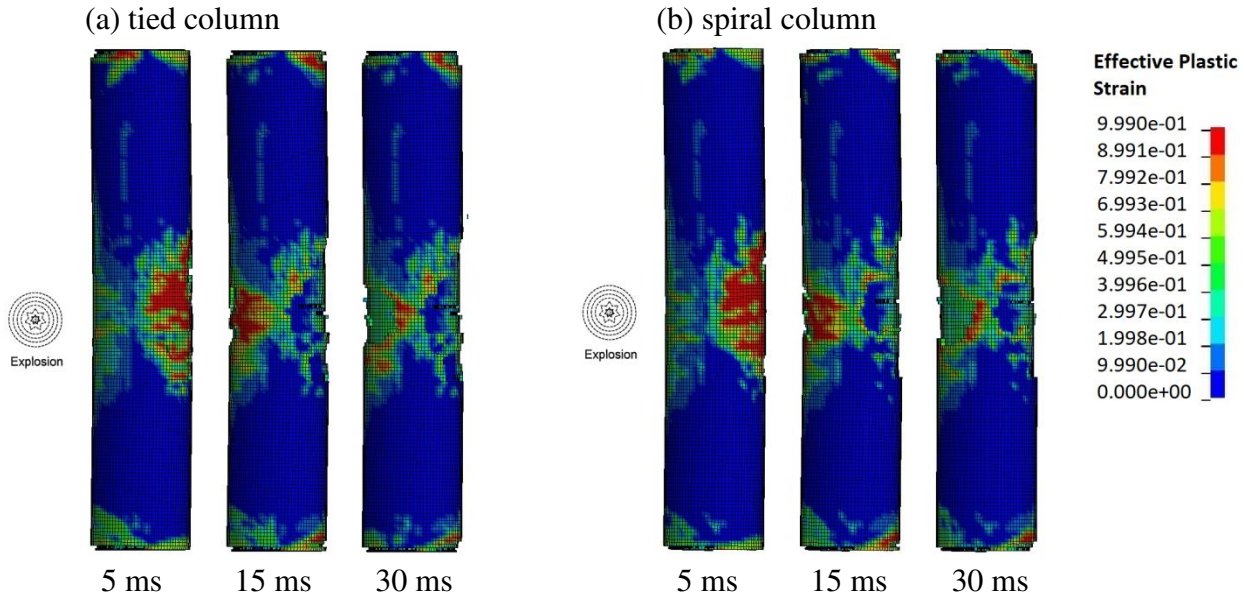

Figure 5.8 Contour of the effective plastic strain in Victoria columns, Set 1 design, Case I, X1.

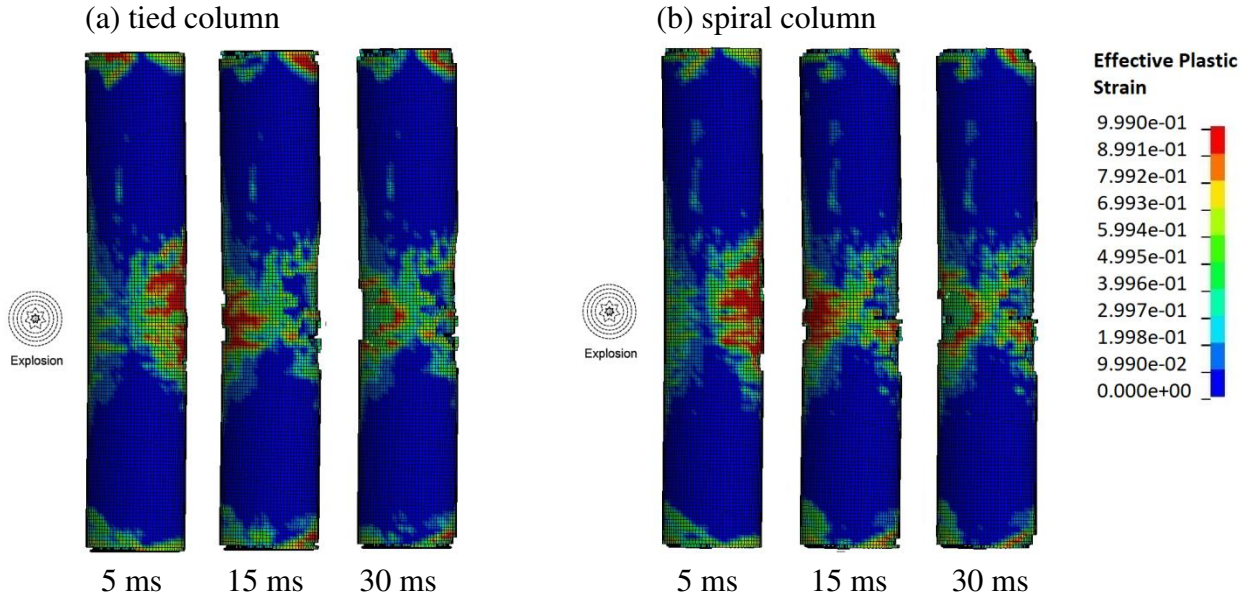

Figure 5.9 Contour of the effective plastic strain in Victoria columns, Set 2 design, Case I, X1.

With respect to the spiral columns, it can be seen in the figures that the spiral column of Set 2 experiences more spalling and core erosion at the boundaries than that of the Set 1 column. This indicates that the Set 1 spiral design was superior, but both columns are able to resist the blast load for Case I. The results demonstrate that once the seismic design requirements for the transverse reinforcement are satisfied, the two types of columns would both survive the blast, and there is no significant advantage between the different designs, i.e., smaller spacing *vs* larger spacing, and smaller bar size *vs* larger bar size for shear reinforcement. Given the detailing of design with respect to the seismic loads, the columns in Victoria did not experience major failure modes like those observed in columns for Toronto and Vancouver. Moreover, breaching of the core from crushing does not occur for any of the Victoria columns, while it occurred for all of the Toronto and Vancouver columns.

Reinforcement stress and behaviour

In general, the behaviour of reinforcement for the two Victoria tied columns is similar to the Vancouver tied column. The ties go to the plastic stage before the column reaches its maximum displacement. Furthermore, the stress in the Set 1 ties exceeded 450 MPa before the first rebound occurred. The stress due to the blast load was primarily in the mid-height region, as well as on the tension side near the boundaries. The stress at the base of the columns on the front side reached the yield stage since the boundary condition is fixed. The performance of the two Victoria spiral columns is similar with regards to the time where they reach yield stress and their stress distribution pattern. The only difference is that yield stress exceeds 450 MPa in the Set 1 column a few milliseconds earlier than in the Set 2 column.

Displacement curves

Figures 5.10 and 5.11 present the displacement curves for the Victoria columns for Set 1 and Set 2, respectively. The results in Fig. 5.10 show that for Set 1, the spiral column experiences failures slightly earlier than the tied column, but the difference is not significant. Furthermore, the reinforcement of the spiral column reaches yield stress much quicker than the tied column.

The displacement curves for the Set 2 columns are very similar to Set 1 columns. Moreover, the spiral column for Set 2 experiences failure mechanisms at a quicker rate, and this includes the reaching of yield stress. The spiral column of Set 2 reaches yield stress of 450 MPa at the same time as when the column reaches the peak of the first rebounding cycle, which occurs on the front side of the column. Although the front was originally in compression, it is now in tension as the column is inching closer to its original position. In addition, none of the Victoria columns experienced severe rebar deformation.

(a)

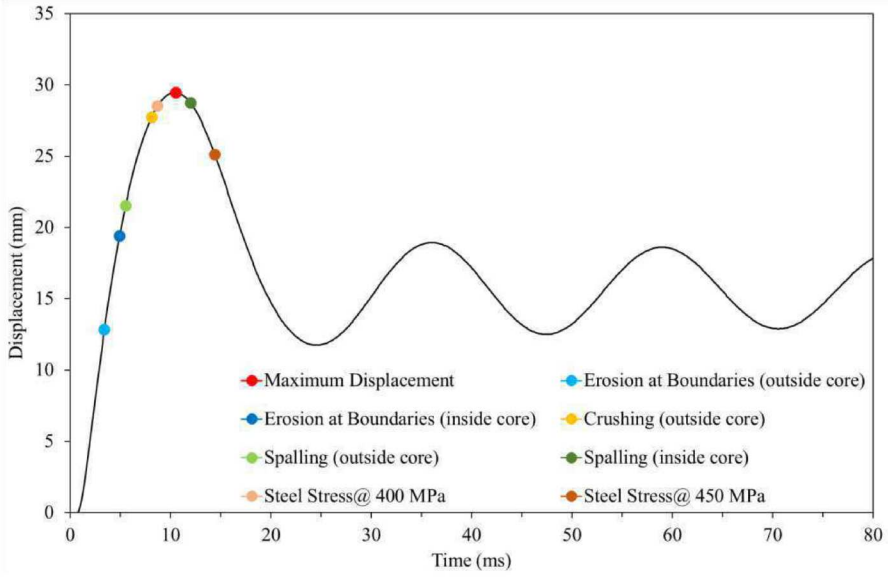

(b)

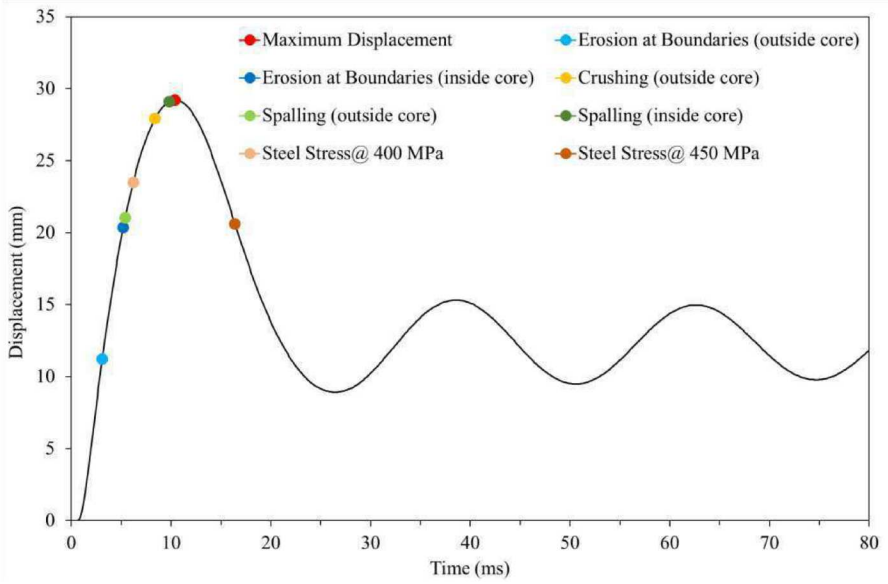

Figure 5.10 Displacement curves for Victoria columns, Set 1 design, Case I, X1: (a) tied column, (b) spiral column.

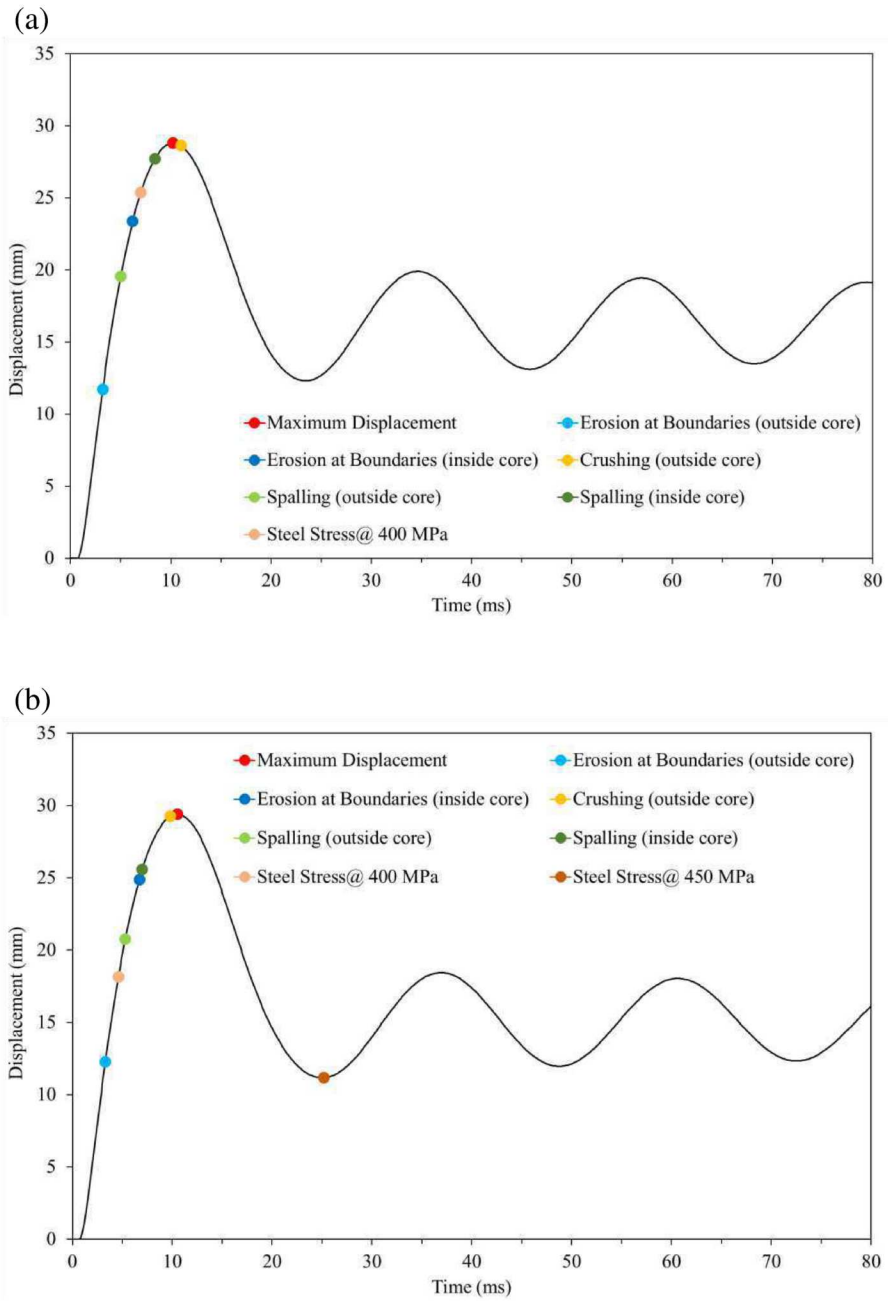

Figure 5.11Displacement curves for Victoria columns, Set 2 design, Case I, X1: (a) tied column, (b) spiral column.

5.2.1.4 Comparison of results for all the columns of Case I

Qualitative comparison

In order to give a comprehensive qualitative summary, all columns are assessed for the failure mechanisms that occurred and when these failures occurred as compared to points in time that are of interest. For concrete, the failure mechanisms that are observed are erosion at the boundaries, crushing, spalling, and breakage of column. For the reinforcement, the mechanisms that are observed are stresses of 400 MPa, 450 MPa, 500 MPa, and severe reinforcement deformation.

Table 5.1 Summary of failure mechanisms for all columns, Case I, X1.

Failure mechanism		Toronto		Vancouver		Victoria			
		Tied	Spiral	Tied	Spiral	Set 1,Tied	Set 2, Tied	Set 1, Spiral	Set 2, Spiral
Erosion at boundaries	outside core	Yes	Yes	Yes	Yes	Yes	Yes	Yes	Yes
	inside core	High	Low	Medium	Medium	Medium	Medium	Low	Medium
Crushing	outside core	Yes	Yes	Yes	Yes	Yes	Yes	Yes	Yes
	inside core	High	High	Low	Low	No	No	No	No
Spalling	outside core	Yes	Yes	Yes	Yes	Yes	Yes	Yes	Yes
	inside core	High	High	High	Medium	Low	Low	Low	Low
Severe rebar deformation		Yes	No	Yes	No	No	No	No	No
Breakage of column		Yes	Yes	No	No	No	No	No	No
Steel Stress	400 Mpa	After	Before	Before	Before	Before	Before	Before	Before
	450 Mpa	After	After	After	After	After	No	After	After
	500 Mpa	No	No	After	No	No	No	No	No

Erosion at the base, crushing, and spalling are first judged based on whether they occurred or not, and the occurrence is based on being outside of the core. If these mechanisms penetrate inside the core, they will be judged based on the level of severity, which includes low, medium, and high. For severe reinforcement deformation and column breakage, it will simply be described as having occurred or not having occurred. For steel reinforcement, occurrence of the three different stress levels (i.e., 400 MPa, 450 MPa, and 500 MPa) will first be based on whether or not they occurred. If they did occur, the two time points of interest are maximum

displacement and/or breakage of the column. The stresses will be marked as having occurred before or after maximum displacement and/or breakage of the column, whichever occurs first. The results are summarized in Table 5.1, and it can be noticed that the Toronto columns experienced severe failure, including very high crushing inside the core, severe spalling, and erosion at the base. The Vancouver columns are the first columns to show ability in resisting the blast for Case I, and they are important as a baseline for comparison. The Vancouver columns had success due to the spacing of transverse reinforcement. For Toronto columns, spacing requirements govern for transverse reinforcement design, but for the Vancouver columns, confinement and the amount of transverse reinforcement in the plastic hinge regions governs for design. All Victoria columns perform extremely well and have low levels of spalling inside the core. Notably, the Set 1 spiral column experiences the least amount of boundary erosion inside the core.

Comparison of maximum displacements

Table 5.2 provides the maximum column displacement observed during the simulation. In the literature, the absolute value for maximum displacement is commonly used in studies related to blast load on bridge columns to determine their ability to successfully resist blast. However, comparison of the Vancouver tied column and the Toronto spiral column shows that peak displacement is not always a governing factor in determining whether or not a column successfully resisted blast. The difference in maximum displacement between these two columns is only about 0.6 mm, but the transverse reinforcement in the Vancouver tied column allowed for rebounding to occur and prevented breakage of the column. It is also noted that the Vancouver spirals column obtains a maximum displacement that is very similar to the well performing Victoria columns.

Table 5.2 Maximum displacement for all columns, Case I, X1.

Location	Column	Maximum displacement (mm)
Toronto	tied	39.9
	spiral	36.3
Vancouver	tied	35.6
	spiral	31.4
Victoria	Set 1, tied	29.5
	Set 2, tied	28.8
	Set 1, spiral	29.2
	Set 2, spiral	29.4

Comparison of displacement curves

Figure 5.12 shows the displacement curves for all 8 columns examined. The Toronto tied and spiral columns both fail and never rebound. Rebounding occurs in columns that have successfully resisted blast to a certain degree. Rebounding does not guarantee that a column successfully resists blast but it is usually a strong indication. With respect to the Toronto spiral column, a few bars start yielding as soon as the shock front hits the front surface, but the majority of bars experience yielding right before column breakage. Although breakage of the column occurs, the overall resultant displacement is limited by the fact that yielding occurred before breakage. For the Toronto tied column, the majority of yielding only occurs after the column breaks, and this is allows it to obtain greater displacement than the Toronto spirals column.

As illustrated in Fig. 5.12, the displacement curve of the Vancouver spiral column is very close to those of the Victoria columns. Moreover, the displacements attained for valley peaks during rebounding for the Vancouver spiral column are approximately the same as the two Victoria tied columns. In conclusion, spiral columns perform much better than tied columns in resisting blast loads.

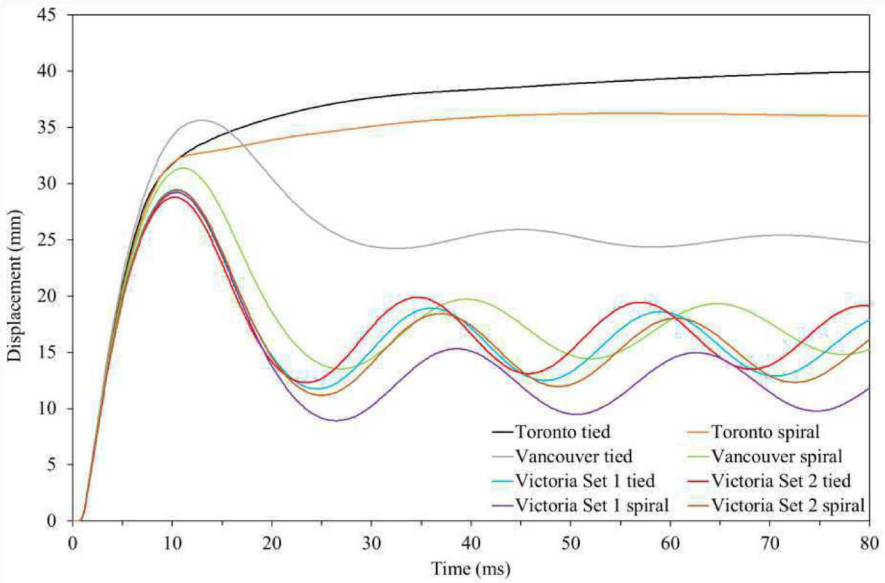

Figure 5.12 Displacement curves for all columns, Case I, X1.

For the Victoria columns, there is a very minor difference between the tied and the spiral columns regarding rebounding time and rebounding displacement. Moreover, the tied columns rebound faster after maximum displacement than the spiral columns; but, the displacement between rebounding peaks is less for the spiral columns. It is necessary to mention that the displacement between the rebounding peaks is more important as it is the actual displacement that causes residual failure. For example, when the column rebounds back and forth, tension shifts back and forth between the front and back of the column. This can cause additional spalling after maximum displacement, which was observed in the Victoria Set 1 tied column. It should be noted that since almost all failure mechanisms occur before the maximum displacement, the two response parameters mentioned above (rebounding time and rebounding displacement) have very minor effects on the blast resistance ability of the columns. The results confirmed that for both tied and spiral columns, the performance of the Set 1 column is slightly better than the Set 2 column; however, the difference is very minor.

5.2.2 Case II (Charge weight is 12% heavier than Case I)

5.2.2.1 Toronto columns

Concrete failure mechanisms

The charge weight of Case II is 12% heavier than that of Case I, and the impact of using a heavier charge in ConWep modelling of blast loads becomes apparent as the damage is significantly worse than Case I. Figure 5.13 shows the effective plastic strain in concrete at 5 ms, 15 ms, and 30 ms for the Toronto tied and spiral columns.

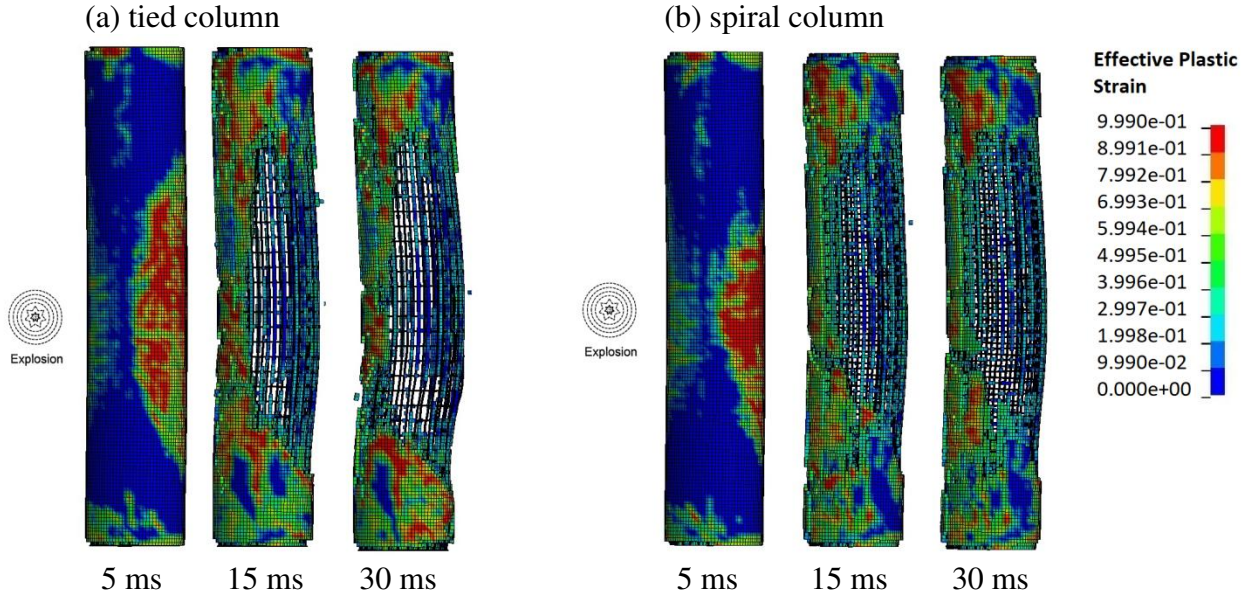

Figure 5.13 Contour of the effective plastic strain in Toronto columns, Case II, X1.

For the Toronto tied column concrete failure mechanisms occur much quicker than they did for Case I. Moreover, although there was severe erosion at the base for Case I, the base did not completely shear off. However, in this case, the severe blast caused complete shearing of the base, as can be seen Fig. 5.14. The Toronto spiral column also experiences erosion and breakage much faster than it did in Case I. Similar to Case I, the yielding of reinforcement allowed this column to obtain maximum displacement within the 80ms time frame.

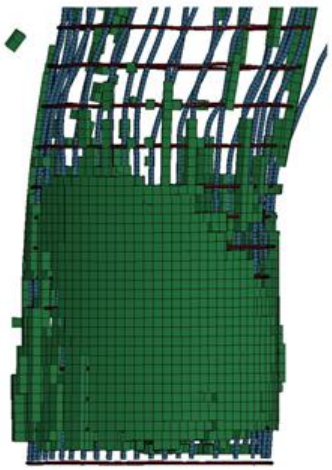

Figure 5.14 Complete erosion of concrete the base of the Toronto tied column, Case II, X1.

Reinforcement stress and behaviour

The Toronto tied column experiences tie pullout and severe deformation of transverse reinforcement. In addition, severe deformation of longitudinal reinforcement is observed at both the front and the back of the column (Fig. 5.15). For the spiral column, severe deformation of

Figure 5.15 Deformation of longitudinal bars for the Toronto tied column, Case II, X1.

longitudinal bars is also observed, which was not seen in Case I. However, the pattern of the stress distribution for Case II is the same as that of Case I.

Displacement curves

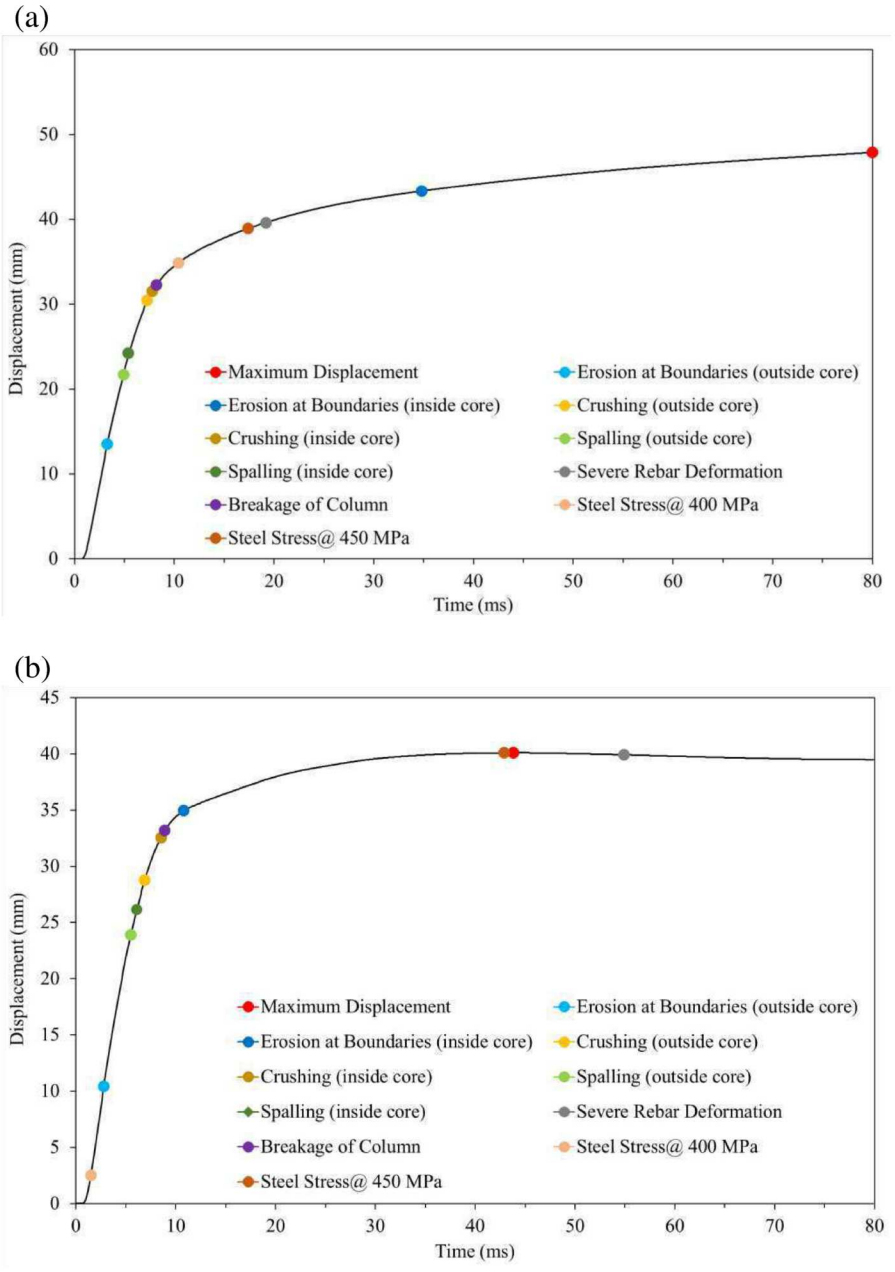

Figure 5.16 Displacement curves for Toronto columns, Case II, X1: (a) tied column, (b) spiral column.

Figure 5.16 shows the displacement curves for the Toronto tied and spiral columns. It is noted that concrete failure mechanisms occur faster and are more severe in Case II than in Case I, while yielding of steel reinforcement occurred later in Case II than in Case I. For example, in Case I, the reinforcement of the tied column surpassed 450 MPa around 19 ms, whereas in Case II it happened around 43 ms. Since the Case II blast is more severe in than the Case I blast, both transverse and longitudinal reinforcement were not as effective in resisting the blast. Although breakage of the column occurred in both cases, yielding of steel reinforcement prevented further damage to the column.

5.2.2.2 Vancouver columns

Concrete failure mechanisms

Both Vancouver columns experienced greater concrete failure in Case II as compared to Case I. In the Case II simulation, the severe blast causes an amplification of the rebounding effect, and this will affect concrete failure mechanisms after maximum displacement has occurred. Figure 5.17 shows the effective plastic strain in concrete at 5 ms, 15 ms, and 30 ms for the tied and spiral columns. It is seen clearly that the tied column experienced crushing of concrete on the front face near the base. This is due to the fact that out of all the columns, the Vancouver tied column has the largest difference in spacing between the plastic and non-plastic hinge regions. Given that the base boundary is fixed, the reinforcement allows for more crushing due to compression rather than spalling. The most important observation regarding the Vancouver tied column is that for Case II, the column experienced breakage, while this did not occur in Case I. With respect to the spiral column, although there is an increase in concrete erosion and maximum displacement, but the blast is still not severe enough to cause breakage of the column (Fig. 5.17b).

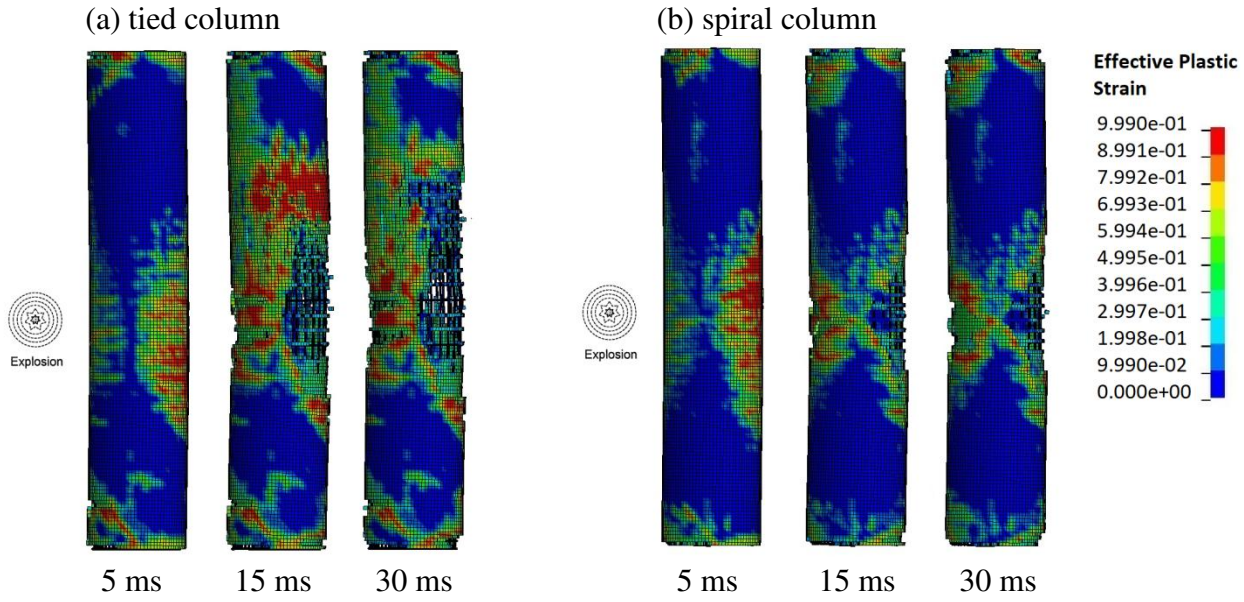

Figure 5.17 Contour of the effective plastic strain in Vancouver columns, Case II, X1.

Reinforcement stress and behaviour

The pattern of stress distribution for both longitudinal and transverse reinforcement of the two Vancouver columns is the same as the pattern obtained for Case I. In Case II, the tied column experiences severe deformation of longitudinal reinforcement, but this does not occur for the spiral column. In this study, it has been found that the spirals in the plastic hinge regions reach yield stress at a much faster pace than the ties. The transverse reinforcement of the spiral column reaches yield stress faster than the tied column, and yielding in the spirals occurs in both the front and back of the column.

Displacement curves

It is necessary to point out that the displacement curve (Fig. 5.19a) of the Vancouver tied column clearly shows a minor form of rebounding. For Case I, rebounding occurred if there was no breakage of the column. However, for Case II, breakage of the Vancouver tied column occurs after the column has reached its maximum displacement and the reinforcement has achieved

stress greater than 500 MPa. Theoretically, this would imply that the concrete core remained mostly intact before the column reached maximum displacement, and rebounding caused the remaining concrete to fail. This phenomenon has been approved in the results shown in Fig. 5.18. Furthermore, rebounding caused more erosion to occur at the back boundaries of the column. Rebounding for the Vancouver tied column had more of an impact for Case II than it did for Case I. In Case I, penetration of the concrete core during the positive pressure phase was limited. Therefore, there was enough core concrete remaining that the impact of rebounding was minimal. In Case II however, rebounding caused the remaining core concrete to erode since there had already been a significant enough breach of the core during the positive pressure phase. Given this, rebounding can have a noticeable impact if there has been significant core concrete damage that has occurred during the positive pressure phase.

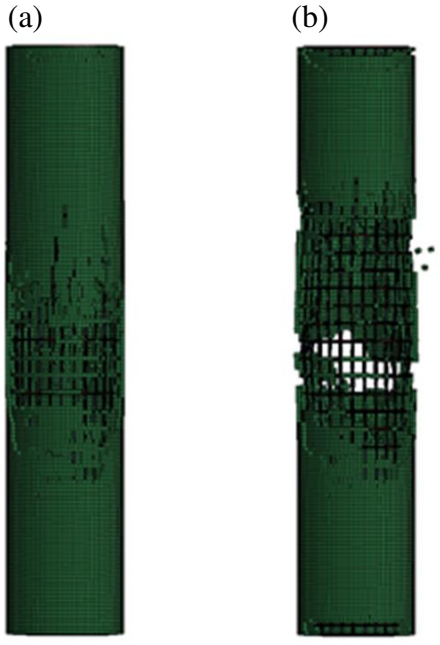

Figure 5.18 Back view of the Vancouver tied column, Case II, X1:
(a) at maximum displacement, (b) at the first rebounding peak.

(a)

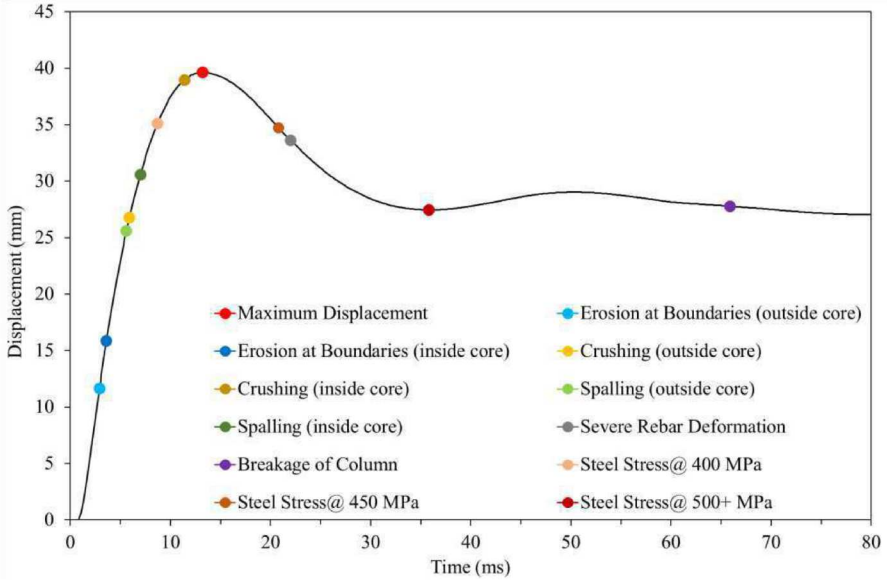

(b)

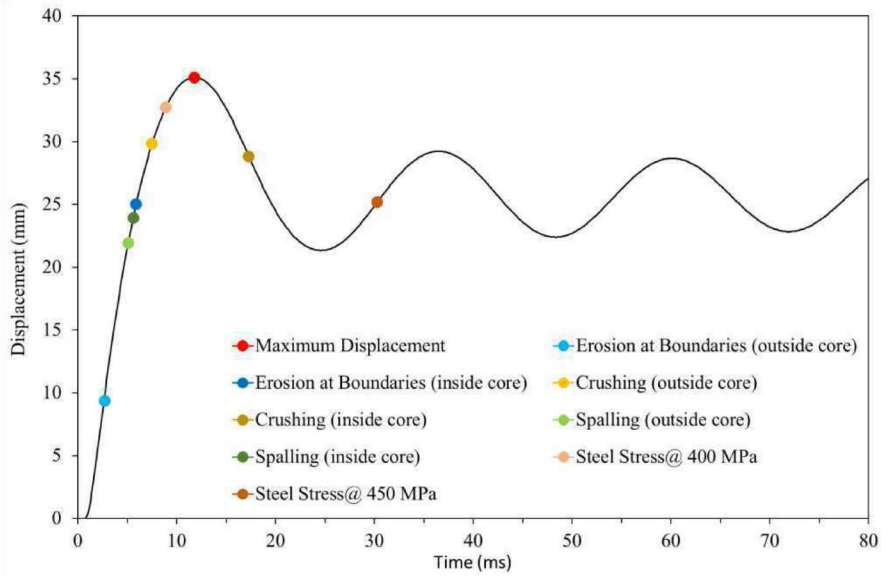

Figure 5.19 Displacement curves for Vancouver columns, Case II, X1: (a) tied column, (b) spiral column.

The displacement curve for the Vancouver spiral column for Case II (Fig. 5.19b) is very similar to that for Case I. Like the findings for the Toronto columns, concrete failure occurred faster in Case II than in Case I for the Vancouver spirals column, and yielding of steel reinforcement occurred later for Case II than for Case I. However, the difference is very minor as

sufficient transverse reinforcement was used in the Vancouver spirals column. The Vancouver spiral column has successfully resisted the blast in Case II.

5.2.2.3 Victoria columns

Concrete failure mechanisms

As a general remark, all of the Victoria columns, including both tied and spiral columns, perform extremely well and have successfully resisted the blast in Case II. Similar to Case I, the discussion will focus on the effects of the two sets of designs on blast load resistance. Figures 5.20 and 5.21 show the effective plastic strain in concrete at 5 ms, 15 ms, and 30 ms for the columns of Set 1 (Transverse reinf. 25M@80 mm) and Set 2 (30M@100 mm for tied, 125 mm for spiral), respectively. It is found that there is more concrete failure in the Case II columns as compared to the Case I columns, but the damage is very limited. In addition, the overall performance of the columns in the two cases is almost the same. The results show that the Set 1 tied column perform better than the Set 2 tied column with regards to concrete erosion. Furthermore, the spiral column of Set 2 shows more erosion and core penetration from spalling than that of the Set 1 scolumn. Therefore, it can be concluded that the design of Set 1 is better than that of Set 2.

It is also interesting to compare the performance of the tied columns and the spiral columns. This comparison is conducted with respect to concrete erosion. As illustrated in Fig. 5.20, both tied and spiral columns experience the same erosion patterns; however, the two spiral columns sustain less concrete erosion before they reach their maximum displacement. The results also show that the spiral columns experience a bigger rebounding distance than the tied columns. Generally speaking, the spiral columns better resist blast during the positive pressure phase and there is minor damage due to rebounding.

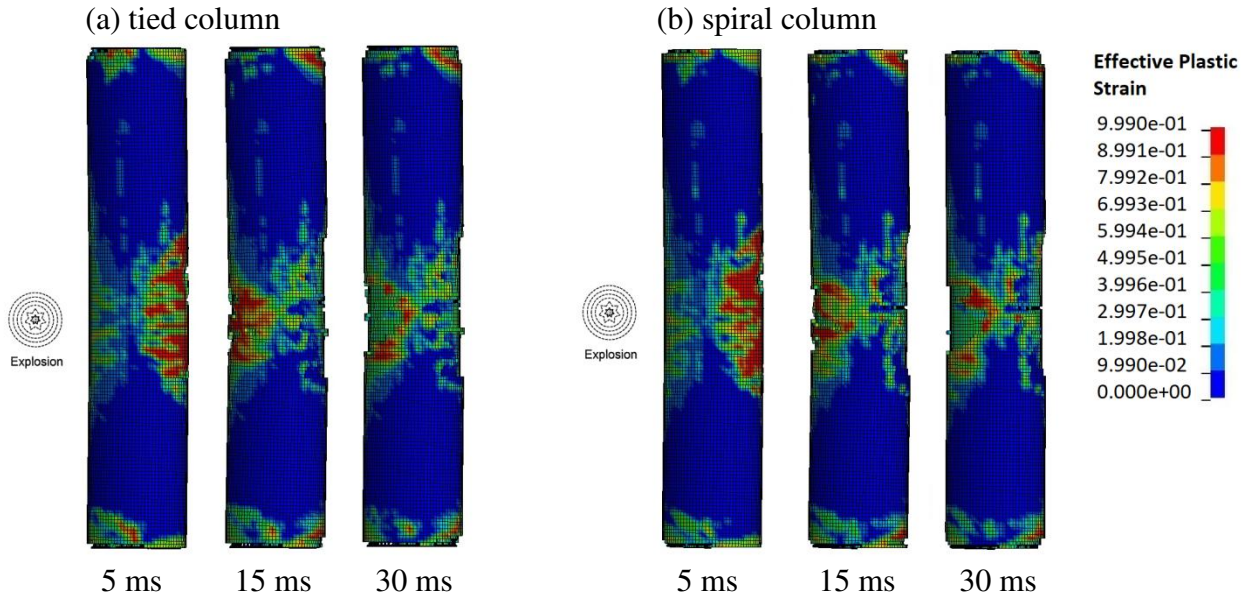

Figure 5.20 Contour of the effective plastic strain in Victoria columns, Set 1 design, Case II, X1.

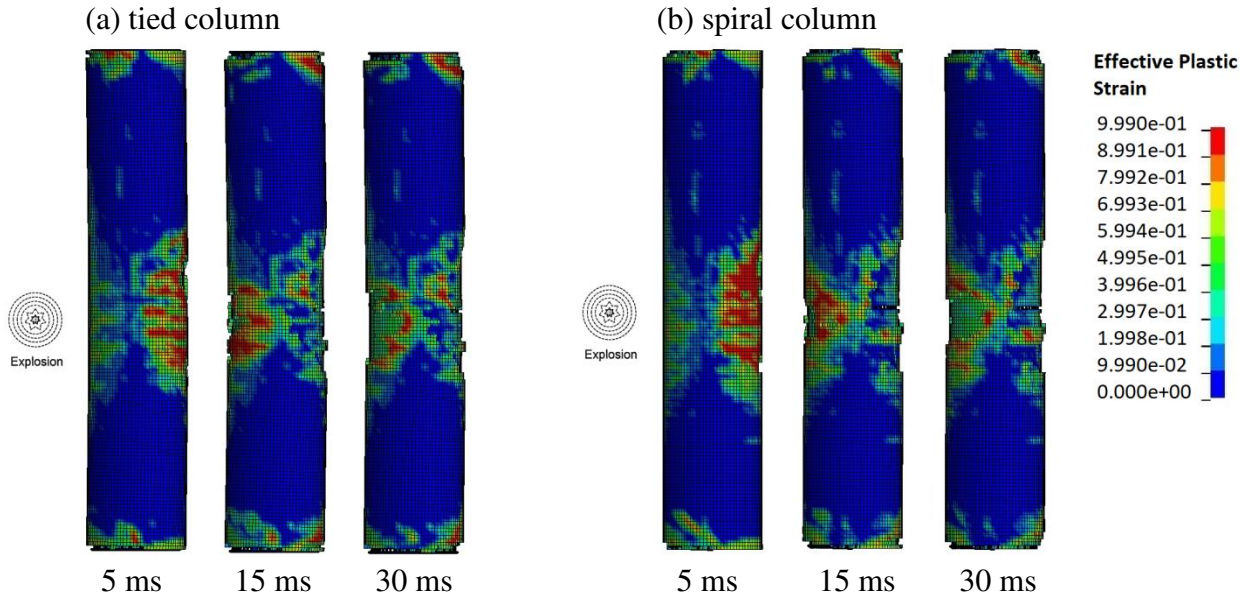

Figure 5.21 Contour of the effective plastic strain in Victoria columns, Set 2 design, Case II, X1.

Reinforcement stress and behaviour

The stress distribution in the reinforcement in Case II is consistent with Case I. However, the transverse and longitudinal reinforcement of the Victoria columns do experience higher

stresses in Case II than in Case I. As an example, the reinforcement of the Set 1 tied column experiences stresses above 500 MPa, while it did not occur in Case I. More importantly, the positive effect of transverse reinforcement can be seen in the timing of reinforcement yielding. For the Toronto and Vancouver columns, the reinforcement in Case II yielded later than in Case I and caused greater energy dissipation through concrete erosion. In this case, the reinforcement of the Victoria columns yielded at approximately the same time as it did in Case I, and this ensured that concrete erosion was not significantly greater in Case II as compared to Case I.

Displacement curves

The displacement curve for the Victoria Set 1 tied column is shown in Fig. 5.22a. It was found that the failure mechanisms occurred faster in Case II than in Case I, but the difference was very minor compared to the scenarios for the Toronto and Vancouver columns. It is necessary to mention that the stress in the reinforcement exceeds 500MPa due to the larger blast load applied in Case II.

When comparing the displacement curve for the Set 1 spiral column (Fig. 5.22b) to Case I, it is noted that the column experiences slightly faster concrete failure mechanisms and higher reinforcement stress in Case II, which is also observed in the Set 2 spiral column. In addition, the reinforcement of the Victoria Set 1 spiral column reaches stresses of 450MPa after the second rebounding, while this occurred before the first rebounding cycle in Case I. This is not concerning as the columns are adequately reinforced.

(a)

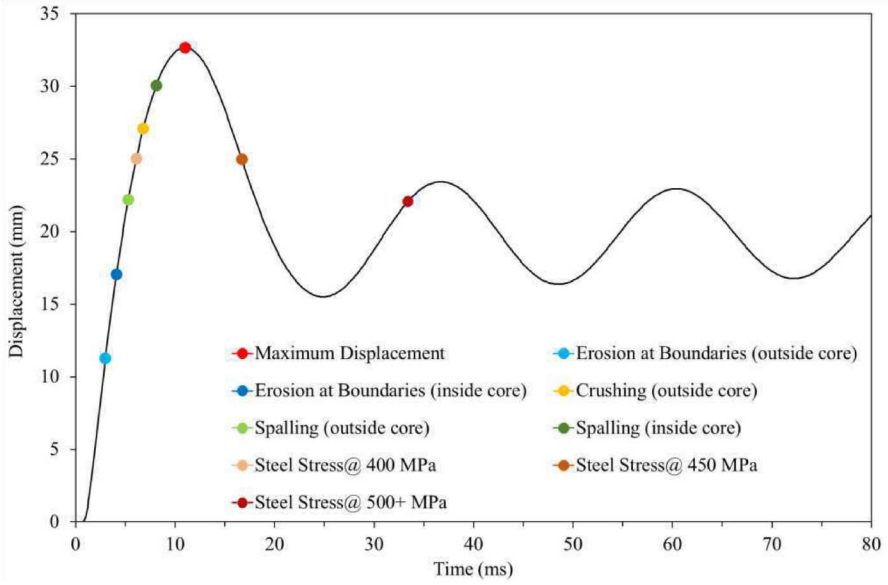

(b)

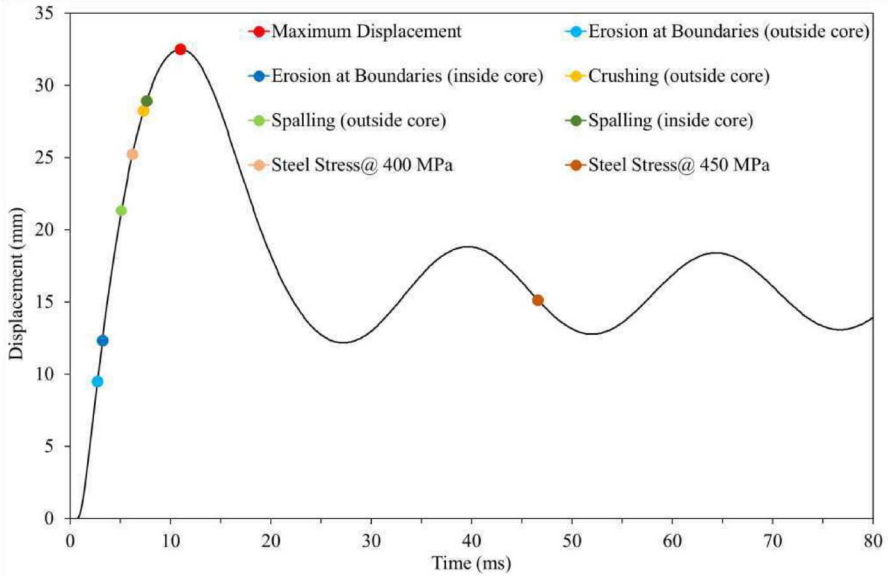

Figure 5.22 Displacement curves for Victoria columns, Set 1 design, Case II, X1: (a) tied column, (b) spiral column.

.

(a)

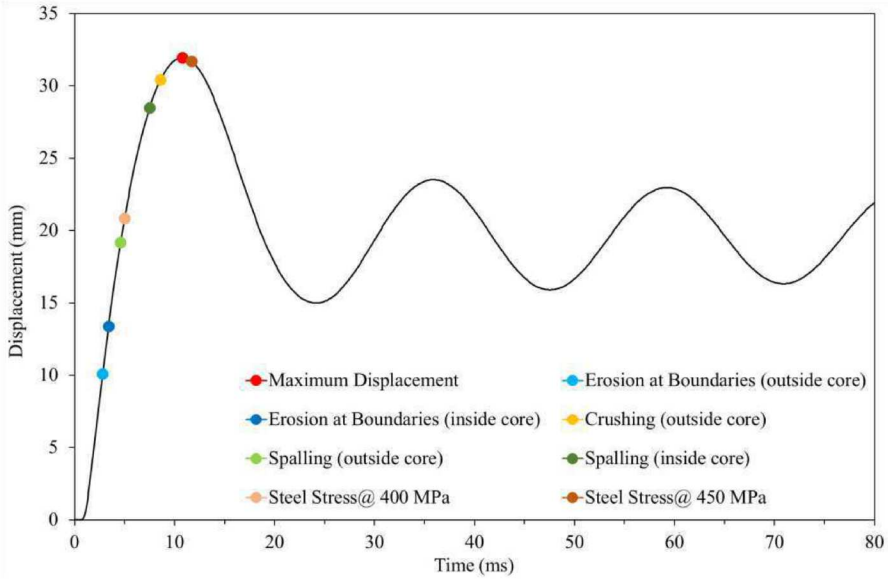

(b)

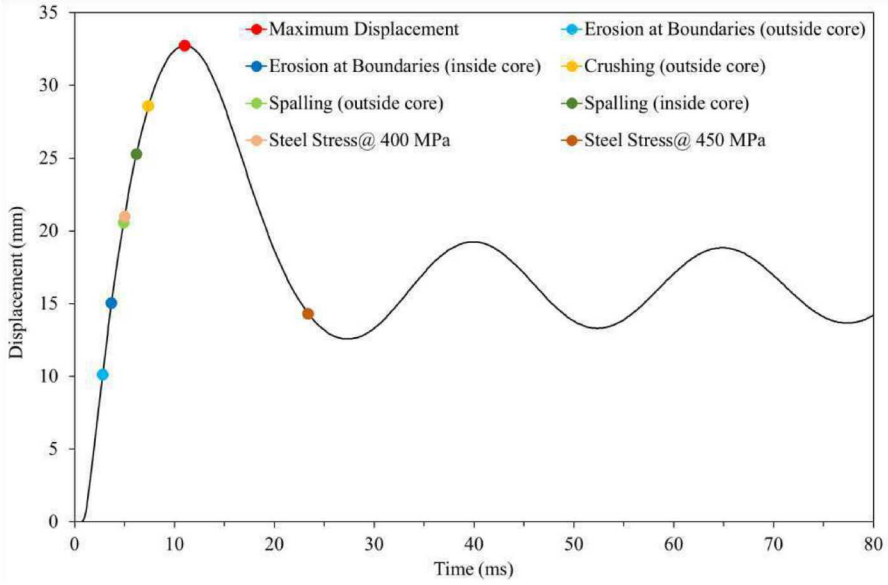

Figure 5.23 Displacement curves for Victoria columns, Set 2 design, Case II, X1: (a) tied column, (b) spiral column.

The Victoria Set 2 tied column is comparable to the other columns for Victoria, and the reinforcement reaches stresses of 450 MPa right near the point of maximum displacement. The displacement curve for the Victoria Set 2 spiral column, seen in Fig. 5.23b, shows that it

performed similarly to the spiral column for Set 1. A minor difference is that the reinforcement surpassed stresses of 450 MPa approximately 8 ms later than the Set 1 column. For Case I, the two spiral columns experienced failure mechanisms faster in time than the two tied columns. For Case II, the difference in the timing of failure mechanisms between the two tied and spiral columns is not as noticeable, and the performance of the spiral columns is slightly better than the tied columns.

5.2.2.4 Comparison of results for all columns of Case II

Qualitative comparison

Table 5.3 summarizes the qualitative results for the failure mechanisms of the eight columns examined. When comparing the results to Case I (Table 5.1), both Toronto columns and the Vancouver tied column performed significantly worst in Case II. The Vancouver spiral column and all Victoria columns performed similarly to Case I, indicating that for charge height X1, these columns are adequately reinforced to resist the blast load. The Toronto spiral column and the Vancouver spiral column have the same spacing of transverse reinforcement, and the difference between the two columns is the Vancouver column has bigger transverse reinforcement bars (Toronto: 20M; Vancouver: 25M, Table 3.2). The performance between these two columns is more noticeable in Case II than it was in Case I. It can be concluded that as the blast becomes more severe, bigger transverse reinforcement bar size is more effective in reducing damage to the column, but for lower levels of blast, it might not be efficient to use a bigger bar size as the difference will not be very noticeable. Lastly, the results of Table 5.3 indicate that for all four Victoria columns, the best performance is for the Set 1 spiral column.

Table 5.3 Summary of failure mechanisms for all columns, Case II, X1.

Failure mechanism		Toronto		Vancouver		Victoria			
		Tied	Spiral	Tied	Spiral	Set 1,Tied	Set 2, Tied	Set 1, Spiral	Set 2, Spiral
Erosion at boundaries	outside core	Yes	Yes	Yes	Yes	Yes	Yes	Yes	Yes
	inside core	High	Low	High	Medium	Medium	Medium	Low	Medium
Crushing	outside core	Yes	Yes	Yes	Yes	Yes	Yes	Yes	Yes
	inside core	High	High	High	Low	No	No	No	No
Spalling	outside core	Yes	Yes	Yes	Yes	Yes	Yes	Yes	Yes
	inside core	High	High	High	Medium	Low	Low	Low	Low
Severe rebar deformation		Yes	Yes	Yes	No	No	No	No	No
Breakage of column		Yes	Yes	Yes	No	No	No	No	No
Steel Stress	400 Mpa	After	Before	Before	Before	Before	Before	Before	Before
	450 Mpa	After	After	After	After	After	After	After	After
	500 Mpa	No	No	After	No	After	No	No	No

Comparison of maximum displacements

The maximum displacement of the columns examined in Case II is about 10%-19% larger than in Case I (Table 5.2). Similar to Case I, the Toronto tied column did not reach its maximum displacement within the 80 ms simulation time. It is necessary to mention that the

Table 5.4 Maximum displacement for all columns, Case II, X1.

Location	Column	Maximum displacement (mm)	Percent difference from Case I
Toronto	tied	47.9	18.0%
	spiral	43.8	18.9%
Vancouver	tied	39.6	10.7%
	spiral	35.1	11.3%
Victoria	Set 1, tied	32.7	10.3%
	Set 2, tied	32.0	10.4%
	Set 1, spiral	32.5	10.7%
	Set 2, spiral	32.7	10.8%

performance of the Vancouver tied column in Case II is very different than in Case I even though the difference in maximum displacement between the two cases is not significant (i.e., only 11%). This is because the column experienced breakage in Case II and breakage did not occur in Case I. For the Victoria columns, it can be concluded that the Set 1 columns performed

better than the Set 2 columns by taking into account the concrete failure mechanisms, stress in steel reinforcement, and maximum displacement.

Comparison of displacement curves

Figure 5.24 shows the displacement curves for all eight columns. The first observation is that the curves for the Vancouver tied and spiral columns intersect each other. Note that in Case I, the curve for the Vancouver spiral column intersected the curves for the Victoria columns, while the curve for the Vancouver tied column was further away (Fig. 5.12). Therefore, the results in Fig. 5.24 indicate that, although the Vancouver spiral column performed relatively well in Case II, it definitely did not perform as well as it did in Case I.

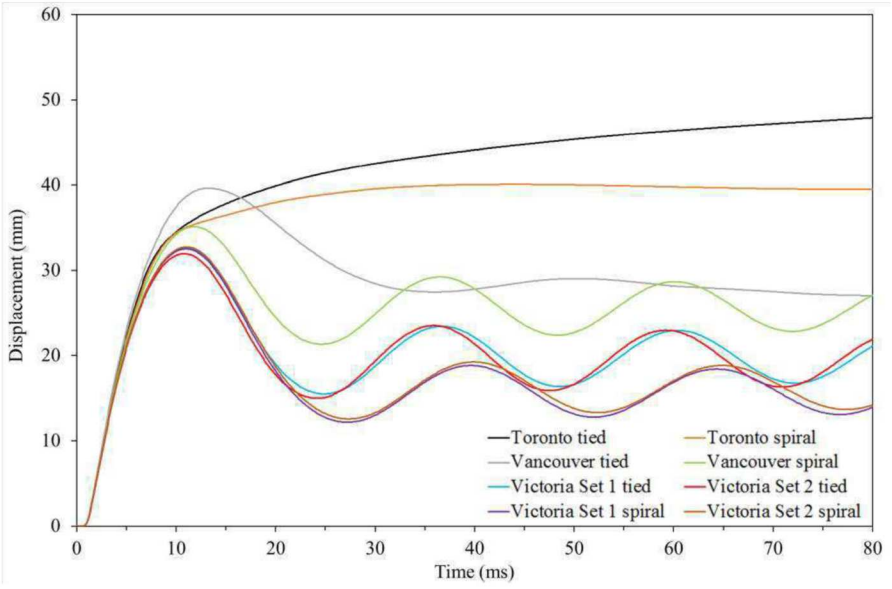

Figure 5.24 Displacement curves for all columns, Case II, X1.

The curves for the Victoria tied columns follow each other more closely than they did in Case I, and the same applies for the spiral columns. In addition, the spiral columns also experience a bigger rebounding displacement, which contributes to some limited residual

damage that occurred after maximum displacement. As a result of their strong performance during the positive pressure phase, rebounding has less of an effect on Victoria.

5.2.3 Case III (Charge distance is 12% closer than Case I)

5.2.3.1 Toronto columns

Concrete failure mechanisms

Figure 5.25 shows the effective plastic strain in concrete at 5 ms, 15 ms, and 30 ms for the Toronto tied and spiral columns. The tied column experiences significant breakage in Case III, and as a result, the tied column is not able to resist blast. It can also be seen in the figure that the shear surface failure follows a 45 degree line for both the top and bottom plastic hinge regions. Note that the pattern discussed above was also observed in Case I and Case II.

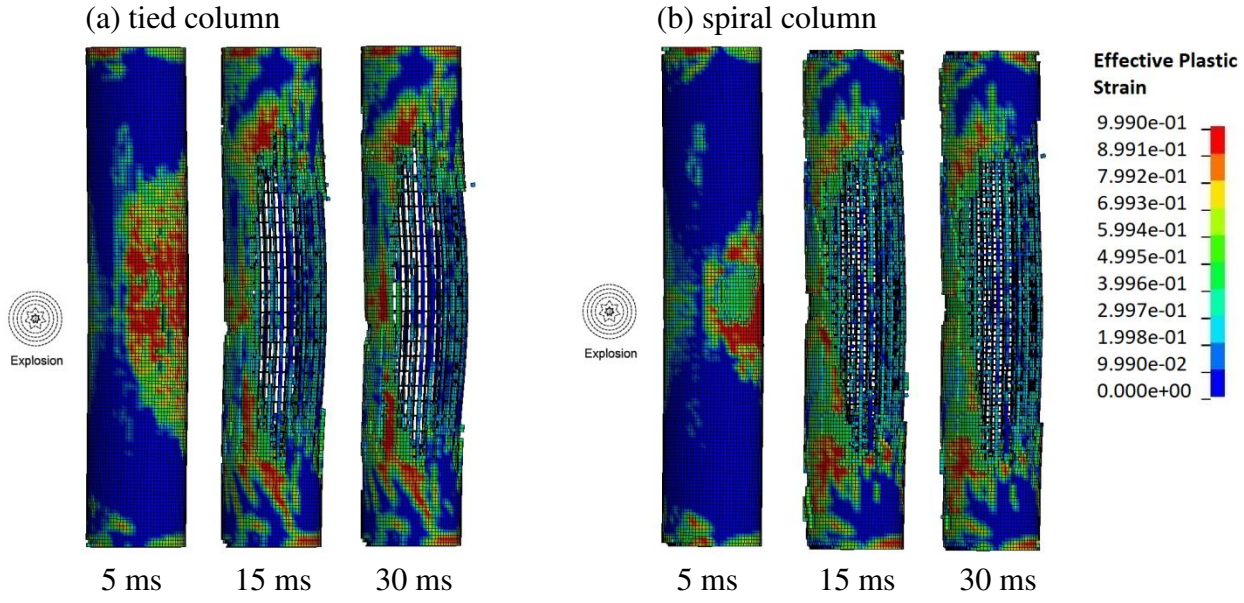

Figure 5.25 Contour of the effective plastic strain in Toronto columns, Case III, X1.

Similar to the tied column, the Toronto spiral column also experiences breakage. Fig. 5.24 shows noticeable crushing of concrete on the front face of the plastic hinge zone at the base due to resistance from the transverse reinforcement. Although the column breaks, its ability to

resist blast is better in this case than in Case I and Case II, which indicates standoff distance has less effect on column performance than charge weight.

Reinforcement stress and behaviour

Unlike Case I and Case II, the Toronto tied column in Case III does not experience pullout of ties, and the reinforcement reaches yield stress right before breakage of the column has occurred. Generally speaking, in the first two cases, columns that experienced breakage had a mechanism where stress in the longitudinal bars shifted up at the back of the column while the stress in the top of the column shifted down on the front side, which is shown in Fig. 5.3. Columns that were able to successfully resist the blast and have rebounding had a mechanism where stress shifted back and forth at mid-height, as illustrated in Fig. 5.6. However, the stress distribution observed in the tied column of Case III is a combination of those in Case I and Case II. More specifically, stress in the longitudinal reinforcement starts to shift upwards, similar to Fig. 5.3, but does not get to the top of the column; instead, it accumulates at mid-height and shifts back and forth, similar to Fig. 5.6. The tied column breaks but it showed more resistance in Case III than in Cases I and II.

The reinforcement for the Toronto spiral column also shows more resistance in Case III than in Cases I and II. Similar to the other two cases, the spirals reached yield stress earlier than the ties. In addition, the reinforcement stayed in stress ranges above 400 MPa much longer in Case III than in Cases I and II, which indicates that a longer period of yielding allowed for greater energy dissipation. The spiral column experiences breakage, but a very minor form of rebounding is observed.

Displacement curves

The Toronto tied column experiences a minor form of rebounding and does obtain maximum displacement within the 80 ms simulation time, which was not seen in Cases I and II. It can be seen in Fig. 5.26 that the reinforcement initially reaches yield stress right before column

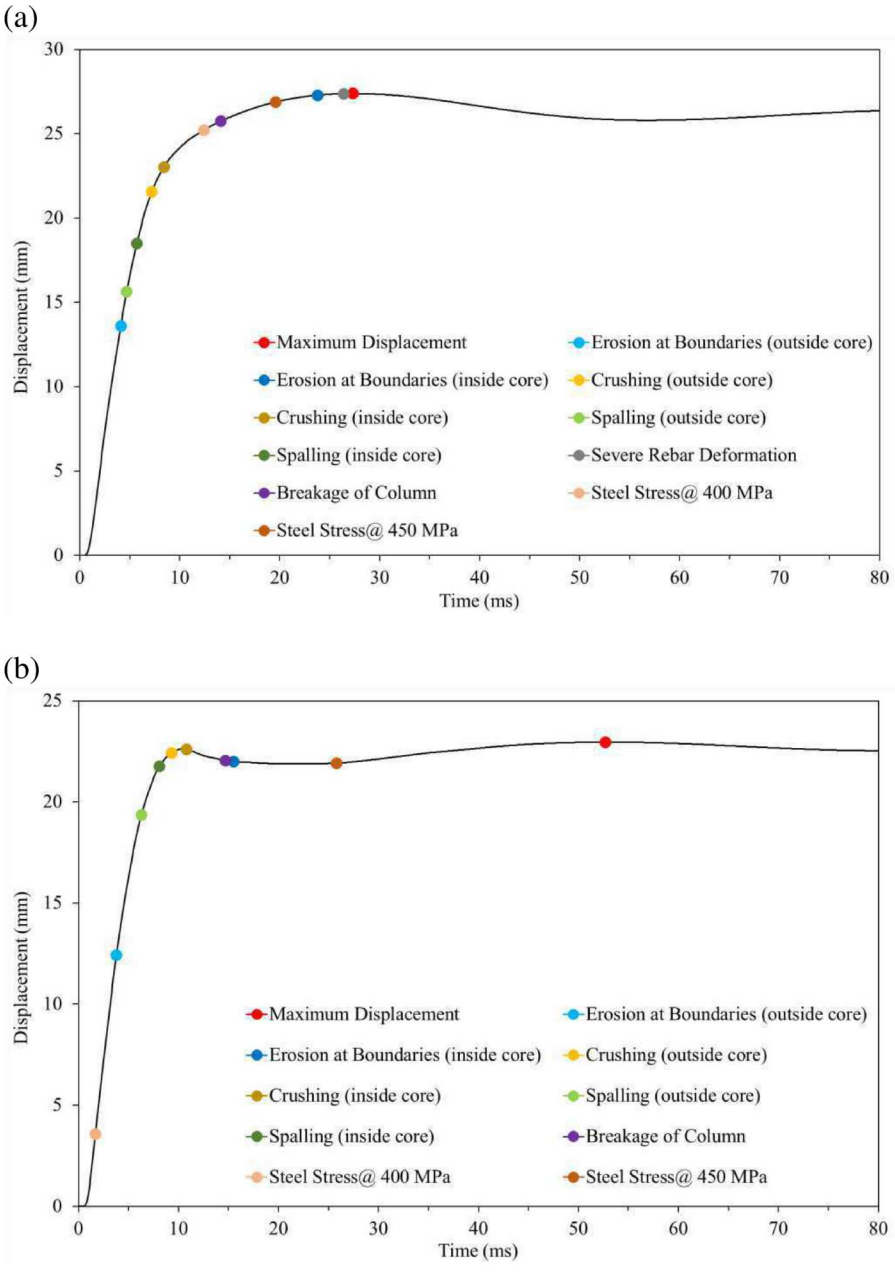

Figure 5.26 Displacement curves for Toronto columns, Case III, X1: (a) tied column, (b) spiral column.

breakage and progressively reaches higher levels of stress as the column reaches maximum displacement. The Toronto spiral column experiences boundary erosion inside the core at approximately the same time as the column breaks (Fig. 5.26b), and this occurs for all three cases. However, erosion inside the boundary core is less than in Cases I and II. Moreover, the total maximum displacement of this model is reduced by about 45% when compared to Case I.

5.2.3.2 Vancouver columns

Concrete failure mechanisms

The Vancouver columns perform better in Case III when compared to Case I and Case II. For Cases I and II, only the spiral column demonstrated an ability to successfully resist blast. In this case, both the tied and spiral column demonstrates the ability to resist the blast. Figure 5.27 shows the effective plastic strain in concrete at 5 ms, 15 ms, and 30 ms for the Vancouver tied and spiral columns. It was found that the concrete in the tied column sustained less core penetration than the first two cases. There is noticeably more crushing on the front base of the

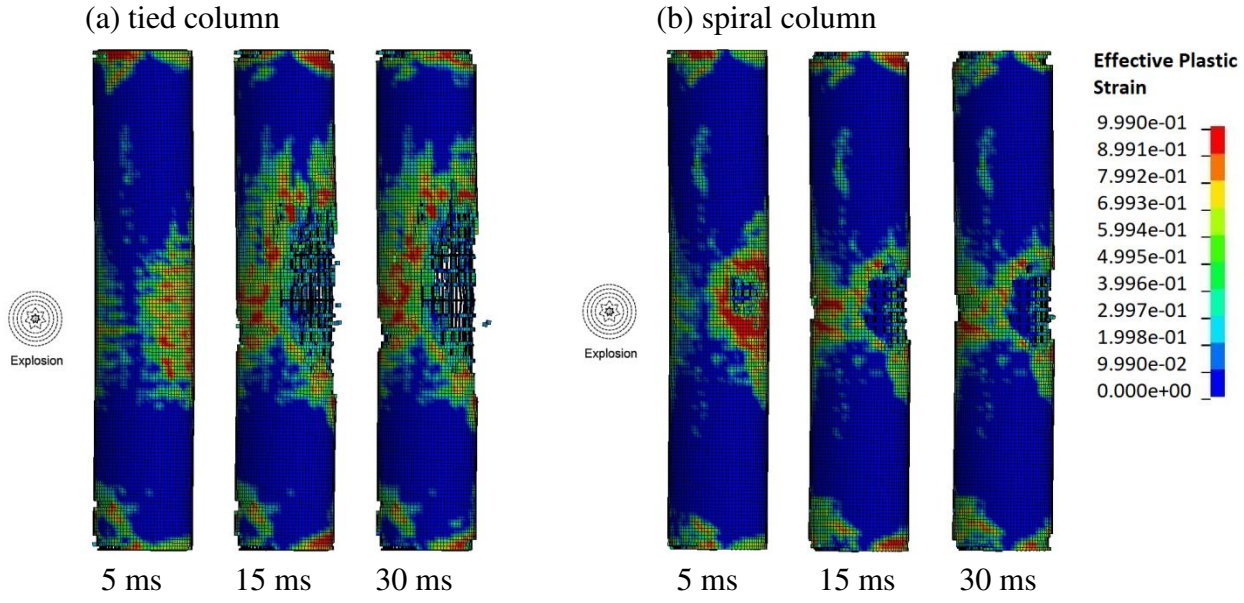

Figure 5.27 Contour of the effective plastic strain in Vancouver columns, Case III, X1.

column as compared to Case I and Case II, which shows the contribution of reinforcement to blast load resistance. The reduction is spalling on the tension side is not as noticeable, and shows that greater reinforcement would be required to optimize the columns performance.

Figure 5.28 shows the front view of the Vancouver spiral column at the end of simulation for Case I, Case II, and Case III, and it is clear that no penetration of core concrete occurred for Case III. It can also be seen in Fig. 5.28 that the column sustains more erosion at the base in Case III than in Case I and Case II. As a column shows more resistance to blast, erosion at the front of the column prevents spalling at the back. Since the Vancouver spiral column showed more resistance to the blast in Case III than in previous cases, it experienced slightly more erosion at the front of the column. The spiral column does not experience crushing that penetrates the core, which has not been seen in the previous two cases.

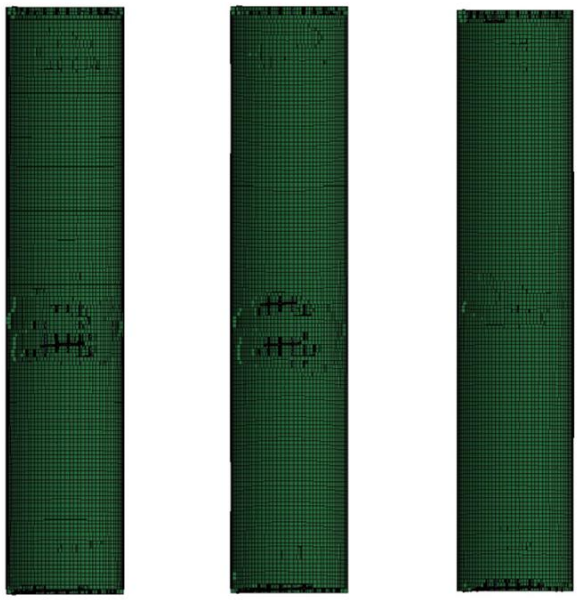

Case I Case II Case III

Figure 5.28 Front view of the Vancouver spiral columns at the end of simulations, X1.

Reinforcement stress and behaviour

The effects of scaled standoff on column response can clearly be seen in the Vancouver columns for Case III. The tied column experiences lower stresses in Case III than in the previous cases. Severe deformation of longitudinal reinforcement occurs at the peak of the first rebounding cycle in Case III, while it occurred during the positive pressure phase in Case I and Case II, which is not desirable. Furthermore, the stress of the reinforcement did not exceed 500 MPa in Case III; however, it did in the previous two cases. In terms of the spiral column, the spirals yielded, but the longitudinal reinforcement did no yield; however, in Case I and Case II, the stress in the longitudinal reinforcement did yield. The reinforcement of both the tied and spiral columns only experience stresses above 450 MPa during rebounding and not during the positive pressure phase.

Displacement curves

Figure 5.28 illustrates that the failure mechanisms for the tied column in Case III occur much later than in Case I (Fig. 5.7a) and Case II (5.19a), and they occur slightly earlier before the column reaches its maximum displacement. For both Case I and Case III, severe deformation of longitudinal reinforcement occurs at the peak of the first rebounding cycle. The tied column only experiences crushing inside the core after the positive pressure phase. For the Vancouver spiral column, erosion at the boundaries that penetrates the core occurs as a result of rebounding and not as a result of the positive pressure phase. Moreover, the spiral column experiences limited spalling that penetrates the core during the positive pressure phase. When considering failures for erosion at boundaries, crushing, and spalling, the Vancouver spiral column experienced extremely limited concrete failure during the positive pressure phase, and some of

the failures are attributed to rebounding. In summary, the spiral column performs better than the tied column.

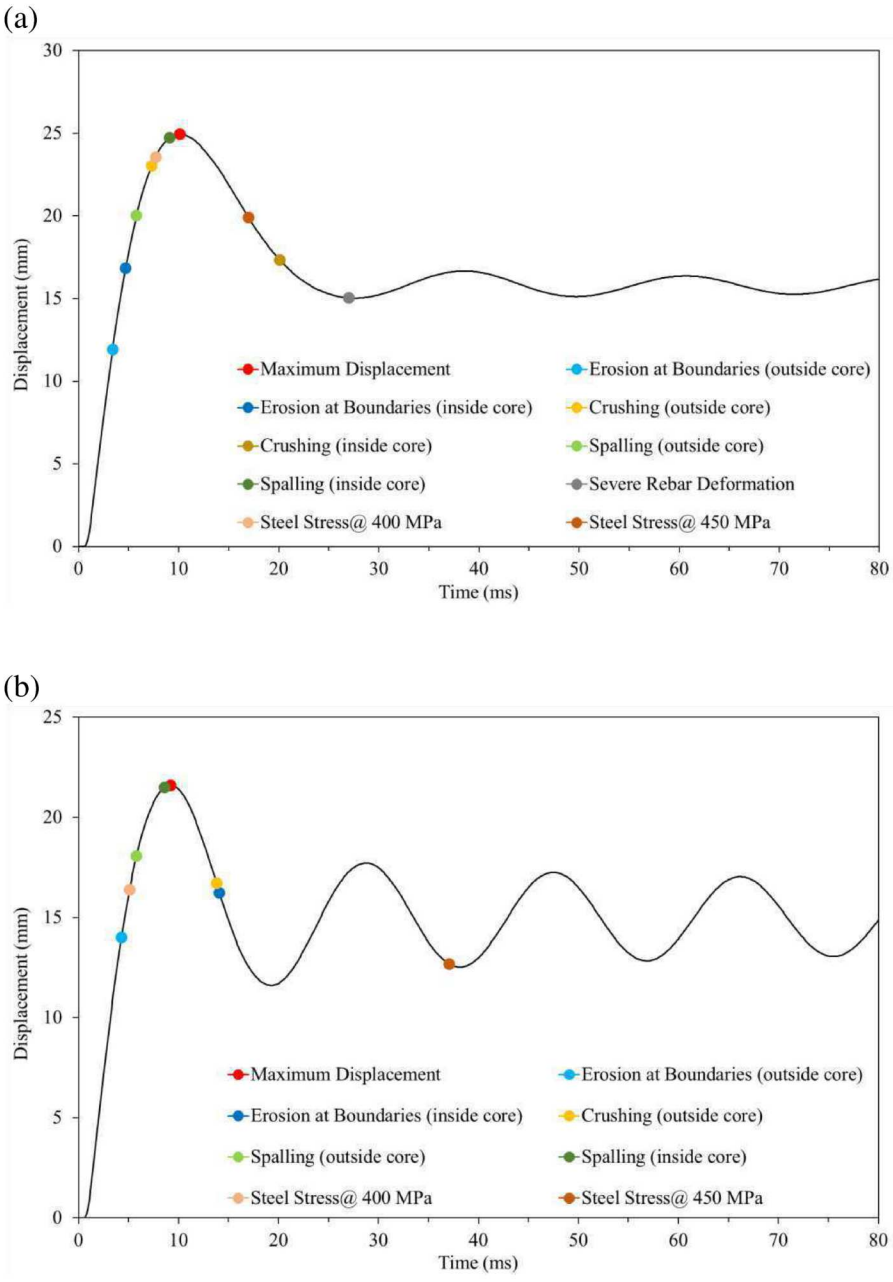

Figure 5.28 Displacement curves for Vancouver columns, Case III, X1: (a) tied column, (b) spiral column.

5.2.3.3 Victoria columns

Concrete failure mechanisms

In general, all four Victoria columns performed well against the scaled standoff blast defined in Case III. Although the failure mechanisms from Case I and Case II are still observed in this case, they are mainly due to rebounding and not from the positive phase pressure. Figures 5.29 and 5.30 show the effective plastic strain in concrete at 5 ms, 15 ms, and 30 ms for the Victoria Set 1 and Set 2 columns, respectively. It has been noticed that concrete erosion is extremely similar for all four columns. There was more of a difference in concrete erosion between the four Victoria columns in the last two cases where the blast loads were quite high. Even with the relatively lighter blast load of Case III, the Victoria columns still experience minor spalling at the back of the columns. Therefore, the Victoria columns, which have the most adequate reinforcement of all columns, experience spalling for all three cases of blast at mid-height.

As explained in the previous sections for the results from Case I and Case II, all Victoria columns experienced crushing outside the core before reaching maximum displacement. In Case III, crushing outside the core occurred after the columns reached maximum displacement and this failure mechanism was not observed during the positive pressure phase. Furthermore, the overall core penetration of concrete is less for Set 1 columns than for Set 2 columns. The difference in overall core penetration between Set 1 and Set 2 is more obvious for the spiral columns than the tie columns, and this was also the scenario for Case I and Case II. Therefore, with regards to concrete erosion and core penetration, the Set 1 spiral column performs better than the Set 2 spiral column for all three cases of blast at mid-height.

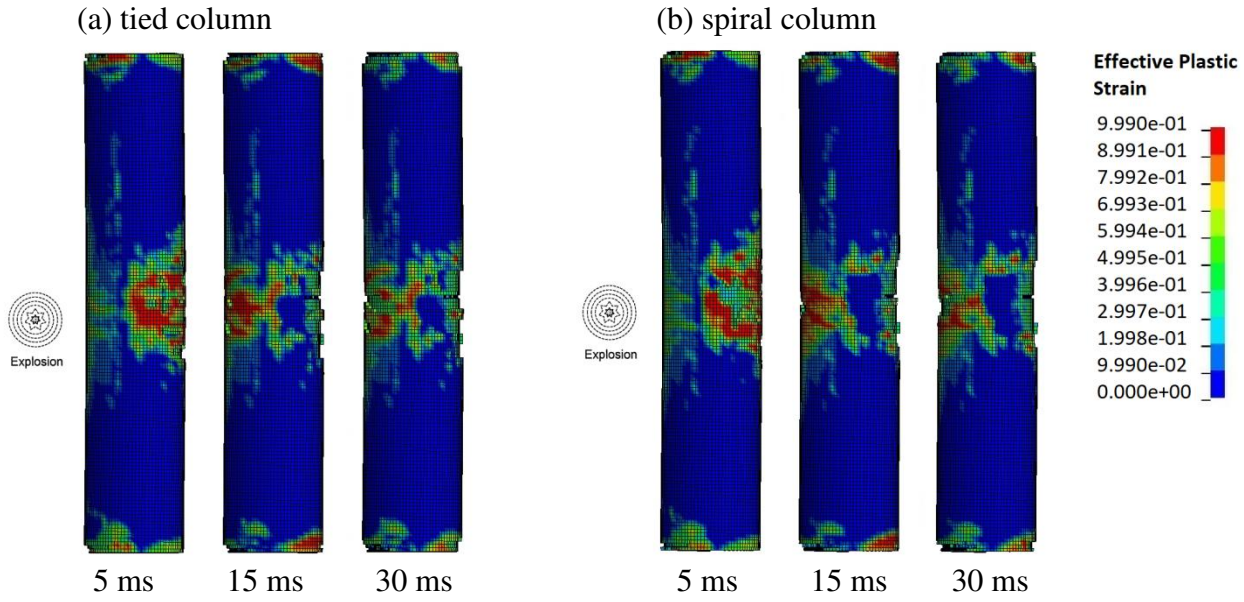

Figure 5.29 Contour of the effective plastic strain in Victoria columns, Set 1 design, Case III, X1.

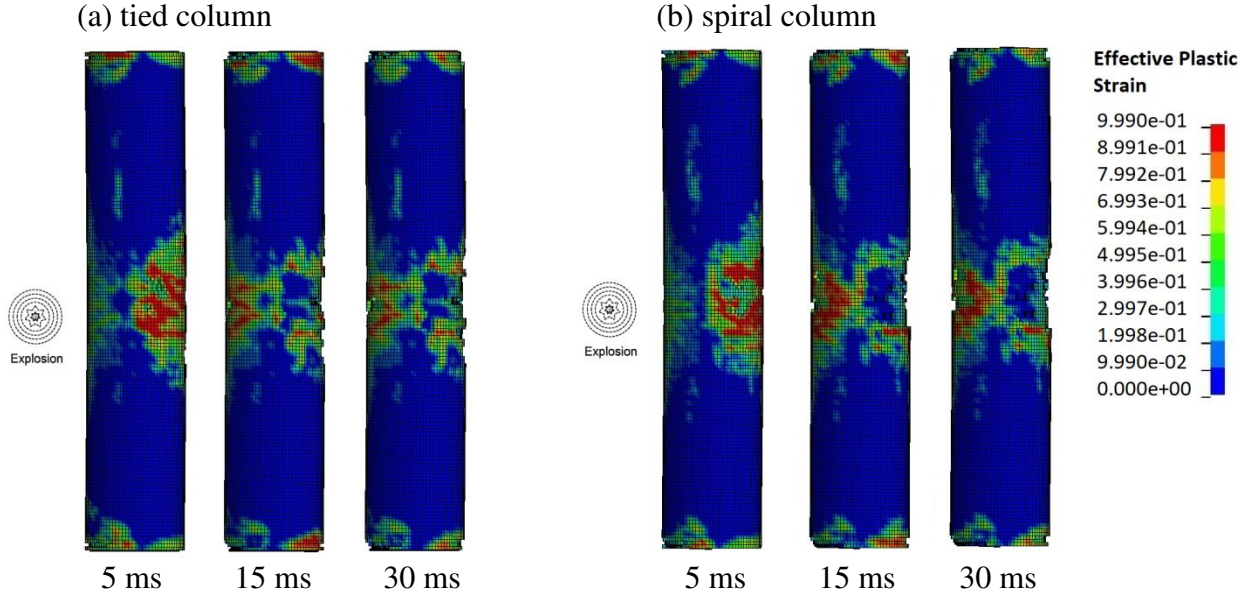

Figure 5.30 Contour of the effective plastic strain in Victoria columns, Set 2 design, Case III, X1.

Reinforcement stress and behaviour

As the stress distribution of the Victoria models is similar to the other cases, the discussion is focussed on the time when the reinforcement exceeds stresses of 450 MPa, as stress in the reinforcement never exceeds 500 MPa. For both the tied and spiral columns for Set 1, the

reinforcement exceeds 450 MPa right at the peak of the first rebounding cycle. For the tied column of Set 2, it occurred before the peak of the first rebounding cycle, while for the spiral column of Set 2, it occurred much later.

Displacement curves

The displacement curve for the Victoria Set 1 tied column (Fig. 5.31a) illustrates that except spalling, any erosion into the core occurs as a result of rebounding. For Case I and Case II, there was penetration into the core with mechanisms other than spalling. The Set 1 spiral column experiences concrete failure mechanisms at a faster rate than the tied column, which has been in previous cases. It is also concluded that the spiral columns reach higher stress levels later in time compared to the tied columns.

The Set 2 tied column is extremely similar to the Set 1 tied column in terms of timing for failure mechanisms. The reinforcement of the Set 1 tied column experiences stresses above 450 MPa right at the first rebounding peak. The displacement curve for the Victoria Set 2 spiral column (Fig. 5.32b) shows that the reinforcement reaches 450 MPa well past 30 milliseconds into the simulation.

The discussion is further focussed on the time when the reinforcement exceeds stress of 450 MPa, which is the maximum stress level developed. For both the tied and spiral columns of Set 1, it occured right at the peak of the first rebounding cycle. For the tied column of Set 2, it occurred before the peak of the first rebounding cycle, and the Set 2 spiral column is the last of all Victoria columns to surpass stresses of 450 MPa. In summary, the results of concrete erosion and reinforcement analysis indicate that the Set 1 columns (both tied and spiral) performed better than the Set 2 columns.

(a)

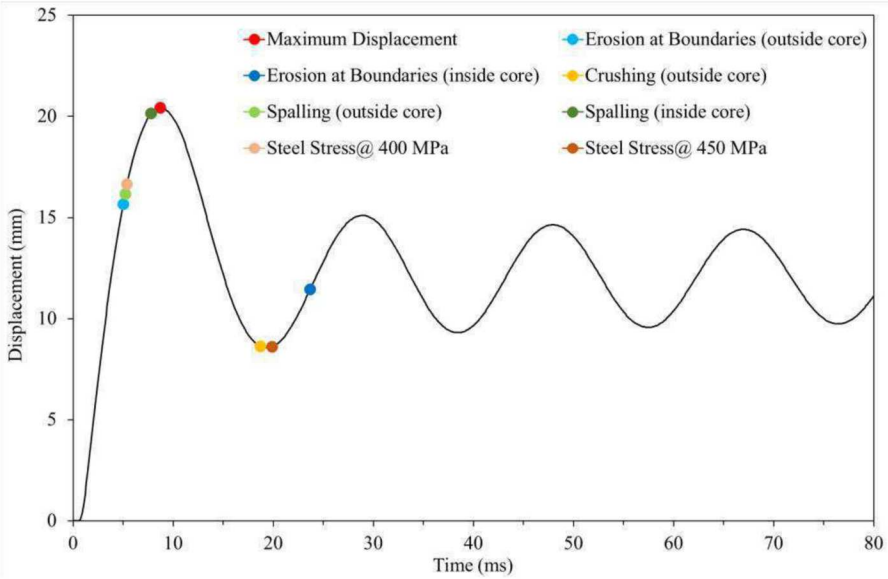

(b)

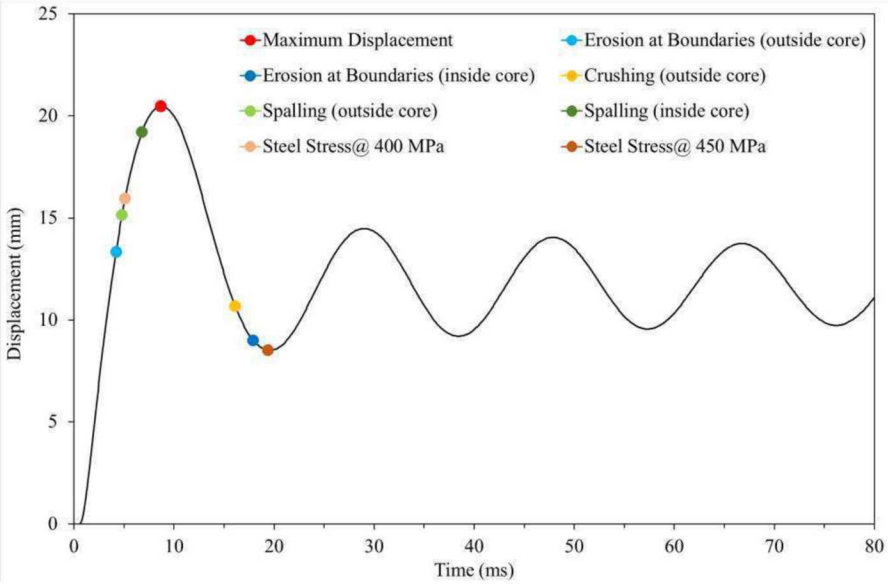

Figure 5.31 Displacement curves for Victoria columns, Set 1 design, Case III, X1: (a) tied column, (b) spiral column.

(a)

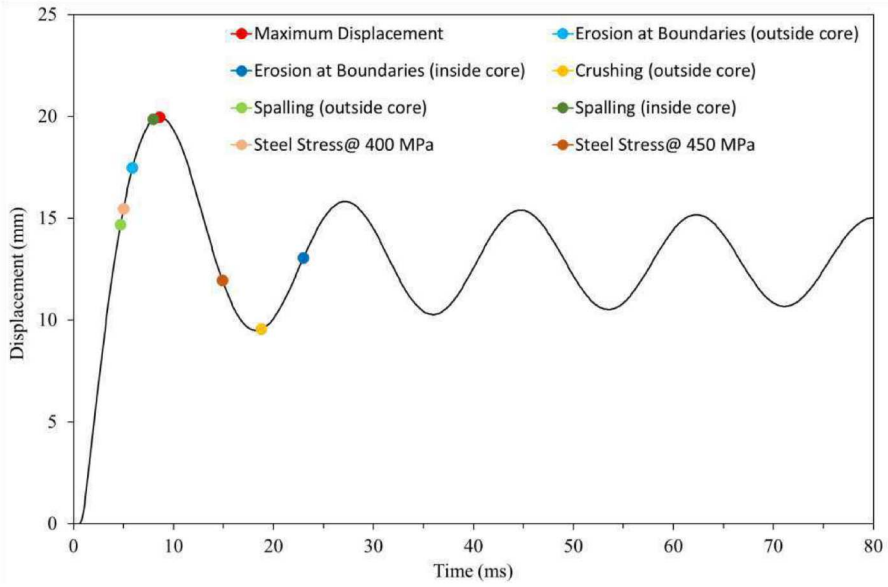

(b)

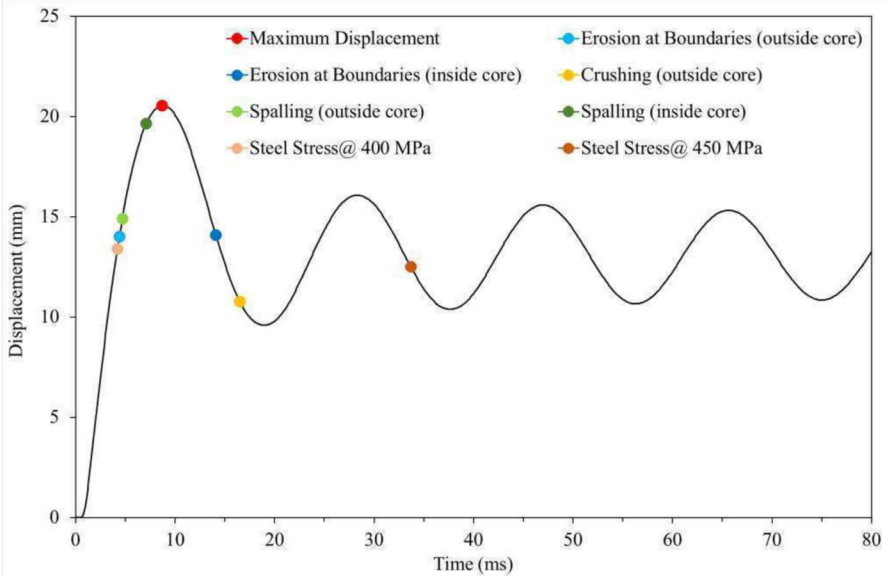

Figure 5.32 Displacement curves for Victoria columns, Set 2 design, Case III, X1: (a) tied column, (b) spiral column.

5.2.3.4 Comparison of results for all Columns of Case III

Qualitative comparison

The major observation for concrete failure mechanisms from the Case III simulations is that erosion would occur outside the core even for low blast pressures. Damage to the interior

core should be avoided in order for the column to carry the required axial loads and to prevent progressive collapse of the bridge. For Case III, even though the core concrete is penetrated in some columns, the penetration occurs much later in time as compared to Case I and Case II, and it occurs mostly as a result of rebounding and not from the positive pressure phase. With regards to reinforcement, Case III is the only case where all columns experienced yield stress before maximum displacement and/or breakage of the column. In the first two cases, the Toronto tied column was the only column to not experience yield stress before maximum displacement and/or breakage.

The final results from Table 5.5 indicate that both Vancouver columns and all Victoria columns successfully resisted the blast. The Vancouver tied column is the first example in Case III showing a satisfactory performance of a tied column against blast load. It is necessary to mention that this column did not break in Case I but was not considered successful due to excessive concrete erosion, and the column experienced complete breakage in Case II.

Table 5.5 Summary of failure mechanisms for all columns, Case III, X1.

Failure mechanism		Toronto		Vancouver		Victoria			
		Tied	Spiral	Tied	Spiral	Set 1,Tied	Set 2, Tied	Set 1, Spiral	Set 2, Spiral
Erosion at boundaries	outside core	Yes	Yes	Yes	Yes	Yes	Yes	Yes	Yes
	inside core	Low	Low	Medium	Medium	Low	Medium	Medium	Medium
Crushing	outside core	Yes	Yes	Yes	Yes	Yes	Yes	Yes	Yes
	inside core	High	High	Low	No	No	No	No	No
Spalling	outside core	Yes	Yes	Yes	Yes	Yes	Yes	Yes	Yes
	inside core	High	High	High	Medium	Low	Low	Low	Low
Severe rebar deformation		Yes	No	Yes	No	No	No	No	No
Breakage of column		Yes	Yes	No	No	No	No	No	No
Steel Stress	400 Mpa	Before	Before	Before	After	Before	Before	Before	Before
	450 Mpa	After	After	After	After	After	After	After	After
	500 Mpa	No	No	No	No	No	No	No	No

Comparison of maximum displacements

Table 5.6 shows that the greatest reduction in maximum displacement for Case III as compared to Case I is about 45% for the Toronto spiral column. For the Vancouver and Victoria columns, the average reduction is about 35% and 37%, respectively. Furthermore, Case III is the only case for charge height X1 where all columns reached peak maximum displacement within the 80 millisecond simulation time.

Table 5.6 Maximum displacement for all columns, Case III, X1.

Location	Column	Maximum displacement (mm)	Percent difference from Case I
Toronto	tied	27.4	-37.4%
	spiral	23.0	-44.9%
Vancouver	tied	25.0	-35.2%
	spiral	21.6	-36.9%
Victoria	Set 1, tied	20.4	-36.3%
	Set 2, tied	20.0	-36.2%
	Set 1, spiral	20.5	-35.2%
	Set 2, spiral	20.5	-35.5%

Comparison of displacement curves

It is found in this study that all columns in Case III have experienced some degree of rebounding, which was not observed in the two previous cases including both Toronto columns Furthermore, it is observed that the spiral column experiences greater rebounding than the tied column. It is interesting to note that the Victoria Set 1 columns experienced a bigger rebounding deflection than the Set 2 columns, which indicates that they better resisted blast during the positive pressure phase. The Set 1 and Set 2 columns have similar concrete failures and reinforcement stress patterns at the end of the simulations, and accounting for the displacement curves, it is concluded that the Set 1 columns performed better than the Set 2 columns during the positive pressure phase.

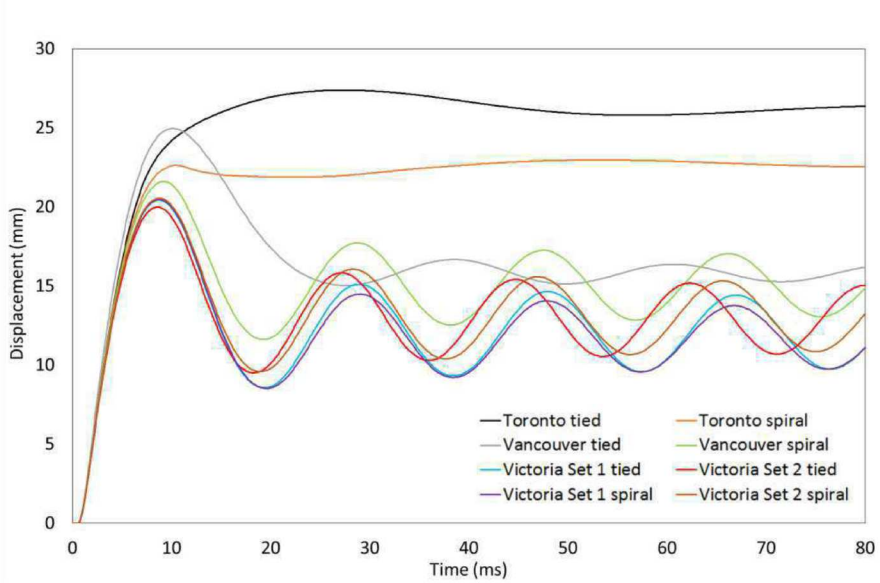

Figure 5.33 Displacement curves for all columns, Case III, X1.

Chapter 6: Analysis and Results – Charge Height X2

6.1 Introduction

Charge height X2 is compatible with the range of location for hand placed or vehicle delivered bombs recommended by the Department of Defense (Winget et. al, 2005a). The value of scaled standoff for Case I, Case II, and Case III remains the same as the simulations for charge height X1. Since charge height X2 is closer to the base of the column, attention was given to the fixed boundary condition at the base in order to determine its impact on the column's ability to resist blast. Following the same evaluation procedures presented in Chapter 5, both qualitative and quantitative results will be recorded from LS-DYNA for charge height X2. In the end, the analysis results from charge height X2 are compared with charge height X1 in order to identify which case is critical for blast load analysis.

6.2 Analysis of Results for Charge Height X2 (close to the ground)

6.2.1 Case I (reference case)

6.2.1.1 Toronto columns

Concrete failure mechanisms

Figure 6.1 shows the effective plastic strain in concrete at 5 ms, 15 ms, and 30 ms for the Toronto tied and spiral columns. The results show that failure of the tied column is very severe in this case and occurs within the first few milliseconds of simulation. During the simulation, it has been found that when the shock front makes contact with the columns front surface at approximately 3 ms, strain occurs on the tension side around the height of the blast. At the front

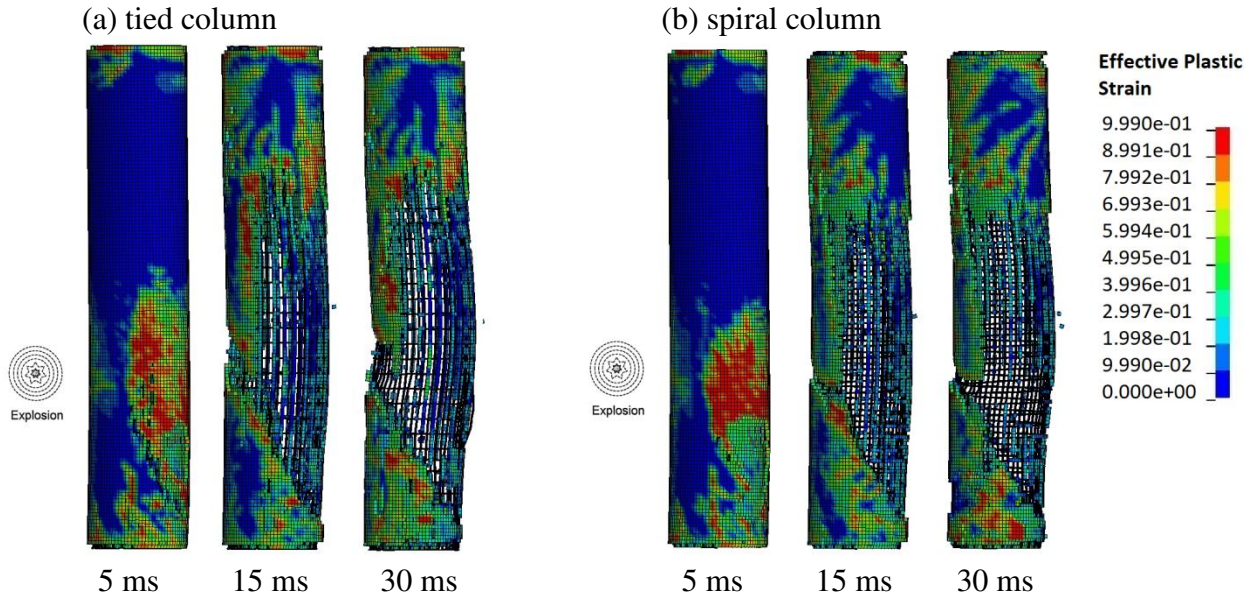

Figure 6.1 Contour of the effective plastic strain in Toronto columns, Case I, X2.

of the column, a 45 degree shear crack starts to occur in the plastic hinge region of the base. At 11 ms, core concrete has been eroded and the column has lost any ability to carry axial load. The results indicate that the Mach front has had a severely negative impact on the column. As explained in Chapter 2, a Mach front is a super positioning of waves due to reflection that causes greater damage to the structure. The Mach front was not noticeably concerning for charge height X1, but it is having a severely negative impact for charge height X2. Moreover, the ability of the tied column to resist blast is affected by its seismic design. The column is not adequately reinforced in the plastic hinge regions and it shows no ability in resisting the blast in at the base. As illustrated in Fig. 6.2, the tied column experiences breakage along a 45 degree shear line and at 38 ms the column experiences complete erosion of the base.

Figure 6.2 Erosion at the base of the Toronto tied column at 38 ms, Case I, X2.

The spiral column also experiences a distribution of strain that covers a large area on the tension side of the column (Fig. 6.1b). The column experiences breakage at approximately 10ms due to 45 degree shearing in the plastic hinge region at the base, and by the end of the simulation there is complete erosion at the base. The spiral column experiences greater crushing in the front of the plastic hinge region at the base as compared to the tied column. As mentioned in the analysis of results for charge height X1, crushing from compression at the front is more desirable than spalling from tension at the back. Similar to the results for X1, this crushing pattern demonstrates that spiral columns show greater resistance to blast than tied columns in the plastic hinge region at the base.

Reinforcement stress and behaviour

The tied column experiences stress on the front and back of the ties in the bottom plastic hinge region as the shock front arrives. Stress also occupies the back of ties in the non-plastic hinge region around charge height. Figure 6.3 illustrates that axial force in ties at the base, which is directly proportional to stress, occurs in a 45 degree pattern, indicating high shear stress. This pattern starts at charge height and moves down into the back of the bottom plastic hinge region. As pressure continues to increase, all of the ties below mid-height of the column experience yield stress. At 11 ms, which is critical as core concrete has been eroded and the column has lost any ability to carry axial load, some ties experience severe deformation while others experience pullout, and the majority of ties below mid-height experience stress above 400 MPa. After 11ms, the ties at the top plastic hinge region are also yielding. For charge height X1, stress in reinforcement dissipated by the end of the simulation for the tied column, while for this charge height X2, the ties are actively yielding until the end of the simulation.

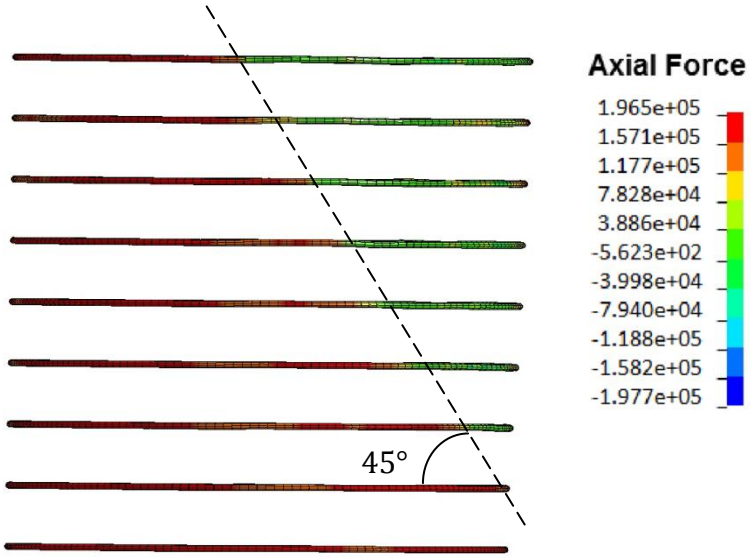

Figure 6.3 Axial force on ties of the Toronto tied column, Case I, X2.

The behavior of longitudinal reinforcement for this column is similar for both charge height X1 and X2. It first experiences stress at blast height and the stress then shifts to the top of the column. The longitudinal reinforcement does not yield during this process, i.e., the first time yielding occurs is after breakage of the column. As illustrated in Fig. 6.4, the reinforcement experiences severe deformation in a 45 degree shear pattern starting at the front of the column and continuing into the bottom plastic hinge region. As presented in Chapter 5 for Case I, deformation of longitudinal reinforcement occurred in a horizontal pattern, which indicates flexural failure.

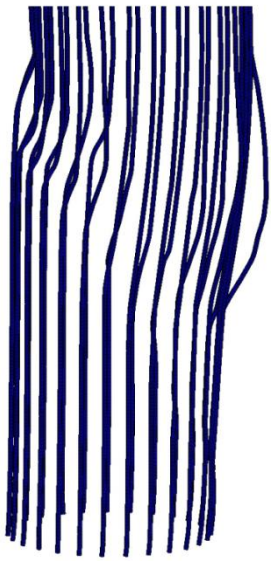

Figure 6.4 Deformation of longitudinal bars for the Toronto tied column, Case I, X2.

With respect to the spiral column, the transverse reinforcement of the spiral column yields almost instantaneously and stress in the spirals exceeds 450 MPa before 10 ms. The stress distribution pattern is the same as the tied column, i.e., it first starts at charge height and the bottom plastic hinge region. The stress then spreads in a 45 degree shear pattern. Similar to the tied column, yield stress only reaches the spirals in the top plastic hinge region after it has

engulfed the rest of the column. The blast is so severe that spirals experience severe deformation at approximately 26 ms. Stress in the longitudinal reinforcement starts at blast height and shifts towards the top plastic hinge region without yielding. The longitudinal reinforcement only yields in the bottom plastic hinge region after breakage of the column.

Displacement curves

The displacement curves for the tied and spiral columns are presented in Fig. 6.5a and 6.5b, respectively. The tied column experiences reinforcement yielding only after the column has experienced breakage, which indicates that the majority of energy was dissipated through concrete erosion. For charge height X1, this column experienced crushing at the front of the column after breakage for this case. But this mechanism occurs before column breakage. Since charge height X2 is closer to base, the majority of crushing at the front occurs in the bottom plastic hinge region. The tied and spiral columns both experience erosion at the boundaries inside the core after column breakage, which also occurred for these columns for charge height X1. For the reinforcement, when compared to charge height X1, the spiral column yielded later in time and experienced high levels of stress for longer periods of time. The reinforcement of this column exceeds stress of 500 MPa, but the column for X1 did not.

(a)

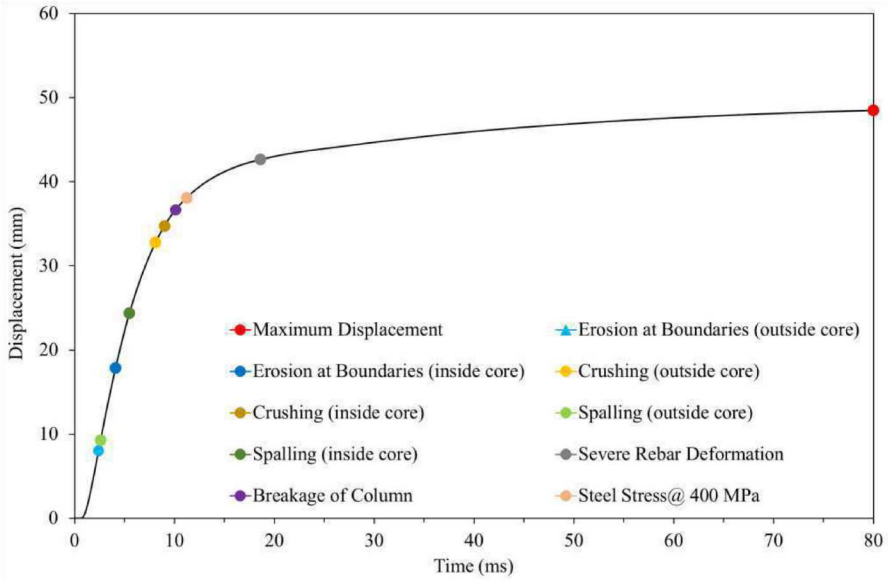

(b)

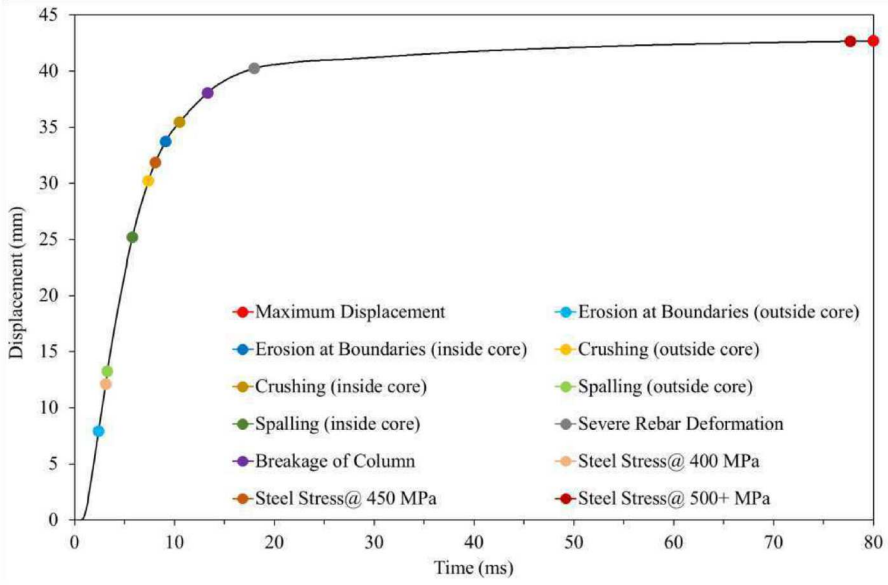

Figure 6.5 Displacement curves for Toronto columns, Case I, X2: (a) tied column, (b) spiral column.

6.2.1.2 Vancouver columns

Concrete failure mechanisms

For the simulations of this case at charge height X1, the Vancouver tied column failed to resist the blast and the spiral column did resist the blast. However, both columns performed poorly for charge height X2 compared to charge height X1. Figure 6.6 shows the effective plastic strain in concrete at 5 ms, 15 ms, and 30 ms for the Vancouver tied and spiral columns. The results indicate that the tied column performed better than the spiral column, which is surprising. More specifically, concrete in the plastic hinge region of the base remains fairly intact for the tied column but the spiral column experiences significant erosion (Fig. 6.6). Furthermore,

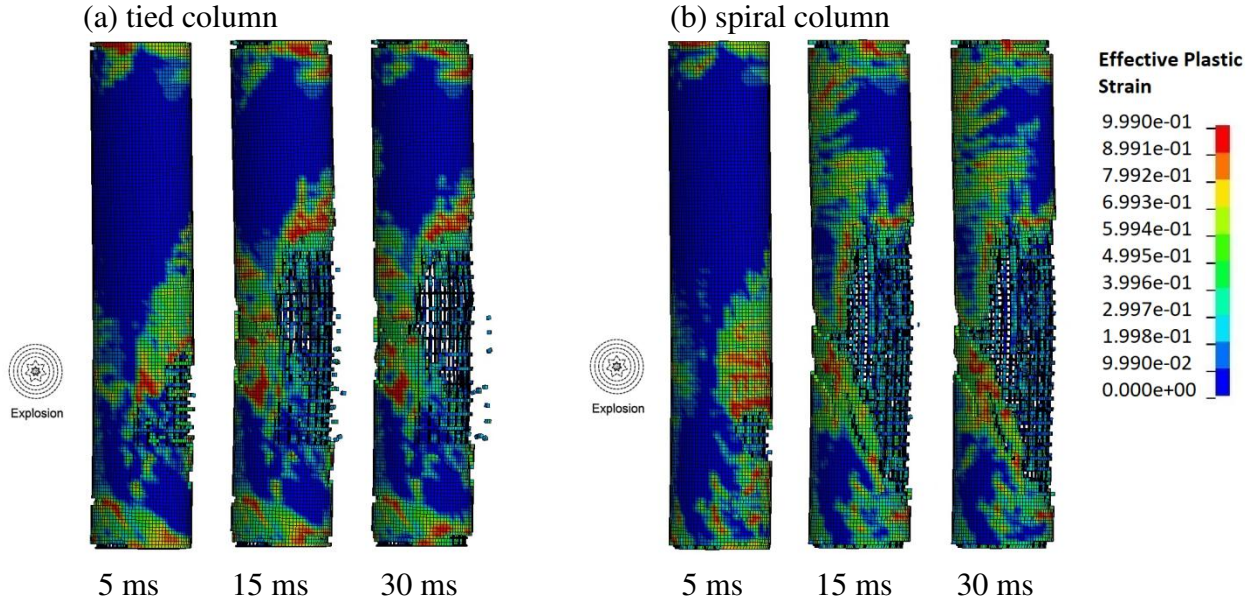

Figure 6.6 Contour of the effective plastic strain in Vancouver columns, Case I, X2.

results in Fig. 6.6 show that both columns experience shearing in a 45 degree pattern; however, the shear does not penetrate the core of the bottom plastic hinge region for the tied column. The tied column experiences breakage at mid-height, which is similar to the results for charge height X1. The spiral column experiences breakage along the 45 degree shear line that penetrates the

base. In addition, Fig 6.7 shows that the tied column experiences crushing not spalling into the core on the front base of the column due to insufficient transverse reinforcement This mechanism is not observed for the spiral column.

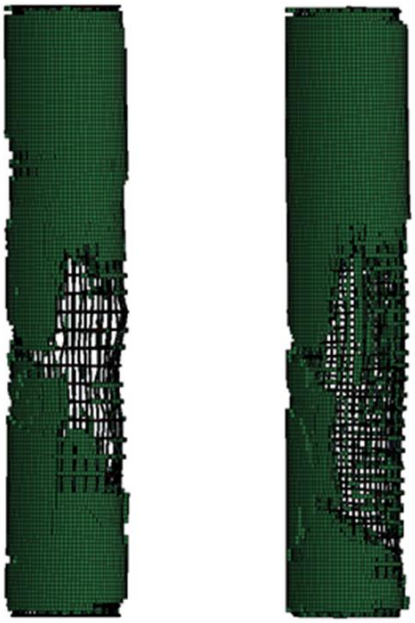

Tied Spiral

Figure 6.7 Side view of the Vancouver spiral columns at the end of simulations, Case I, X2.

One of the conclusions described in Chapter 5, for charge height X1 simulation where the blast was located at mid-height, was the spiral column performed better. This is mainly because the spacing of transverse reinforcement in the spiral column outside the plastic hinge region is smaller than the tied column. However, for charge height X2 where the blast is closer to the base, the spiral column performs poorly because spacing inside the plastic hinge region is larger than the tied column. In addition, it is interesting to compare the behavior of the Vancouver spiral column with the Toronto spiral column since both have the same transverse reinforcement spacing (150 mm) but the Vancouver column uses a bigger bar size of 25M *(*20M for Toronto). The results from charge height X1 (Chapter 5) revealed that the bar size had a major impact on

the resistance as the Toronto spiral columns failed and the Vancouver spiral columns succeeded in resisting blast. But this observation was not achieved in this case, i.e., the bigger bar size did not have a noticeable impact on the Vancouver spiral columns ability to resist blast.

Reinforcement stress and behaviour

The tied column experiences breakage, but the ties yielded before maximum displacement and prevented further deflection. Before reaching maximum displacement, stress in ties is concentrated in the bottom plastic hinge region and at blast height. Note that blast height is slightly above the bottom plastic hinge region. Ties in the top plastic hinge region only experience noticeable stress afterwards. There is pullout of ties near blast height during the positive pressure phase. Stress in the longitudinal bars begins at the back of the column around blast height and starts to shift up before accumulating at mid-height. When longitudinal reinforcement is able to limit displacement, the stress accumulates at mid-height and does not shift up to the top of the column. The longitudinal reinforcement of the tied column experiences severe deformation in a horizontal pattern around mid-height and not in a 45 degree shear pattern near the base. The reinforcement of the spiral column experiences similar stress patterns as the Toronto spiral column. Stress starts at charge height and penetrates into the bottom plastic hinge region. The spirals reached yield stress within a few milliseconds of pressure impacting the column, but there is not enough reinforcement to prevent failure through concrete erosion.

Displacement curves

It can be seen in Fig. 6.8a that the tied column only experiences crushing inside the core during rebounding, but the spiral column experienced this mechanism during the positive pressure phase. Both columns experience breakage after maximum displacement, which indicates that there was severe damage during the positive pressure phase that rebounding caused

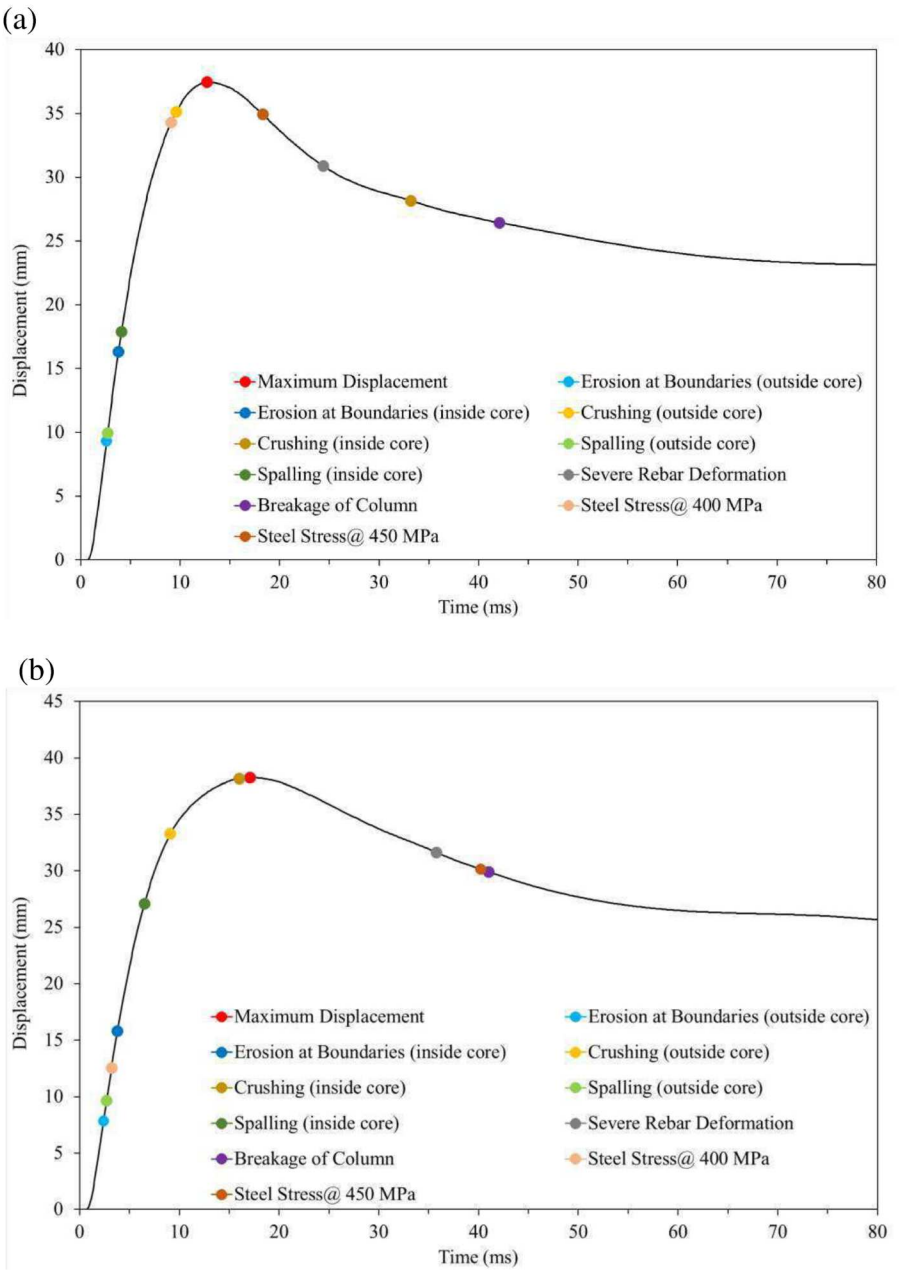

Figure 6.8 Displacement curves for Vancouver columns, Case I, X2:
(a) tied column, (b) spiral column.

the column to break. Moreover, the reinforcement of the tied column exceeds the stress of 450 MPa before severe deformation of reinforcement, but the spiral column exceeds the stress of 450 MPa after severe deformation. This demonstrates that the reinforcement of the tied column had more of a positive impact on the columns ability to resist blast.

It is necessary to mention that both the tied and spiral columns experienced multiple rebounding cycles for charge height X1 (Figs. 5.7a and 5.7b), but neither column completes a full rebounding cycle for this case.

6.2.1.3 Victoria columns

Concrete failure mechanisms

The severity of the blast at charge height X2 does not have a significant impact on the Victoria columns. Figures 6.9 and 6.10 show the effective plastic strain in concrete at 5 ms, 15 ms, and 30 ms for the Victoria Set 1 (Transverse reinf. 25M@80 mm) and Set 2 columns (30M@100 mm for tied, 125 mm for spiral), respectively. When the strain on the back of the Victoria columns shifts up from charge height it does not go to the top of the column and instead accumulates around mid-height. The area of this strain is small when compared to the Toronto and Vancouver columns, which results in limited concrete erosion on the Victoria columns. Moreover, as concrete erosion occurs mostly at mid-height and not at the base, a portion of concrete erosion is attributed to the shifting of tension from the back of the column to the front as a result of rebounding.

For the two tied columns, Figures 6.9a and 6.10a show that they perform similarly for erosion at the boundaries and crushing, except the Set 1 column has more spalling at the back. Therefore, it can be concluded that the tied column of Set 2 performed better than the Set 1 column. For the spiral columns illustrated in Figs. 6.9b and 6.10b, the noticeable difference is also for spalling at the back of the column. The Set 1 spiral column has more spalling compared to Set 2. With closer examination, it is noticed that although the Set 1 spiral column experiences more spalling overall, it experienced less spalling during the positive pressure phase compared to the Set 2 column. It is desirable that spalling is reduced during the positive pressure phase rather

than it occurring as a result of rebounding. Accordingly, the Set 1 spiral column performs better than the Set 2 column.

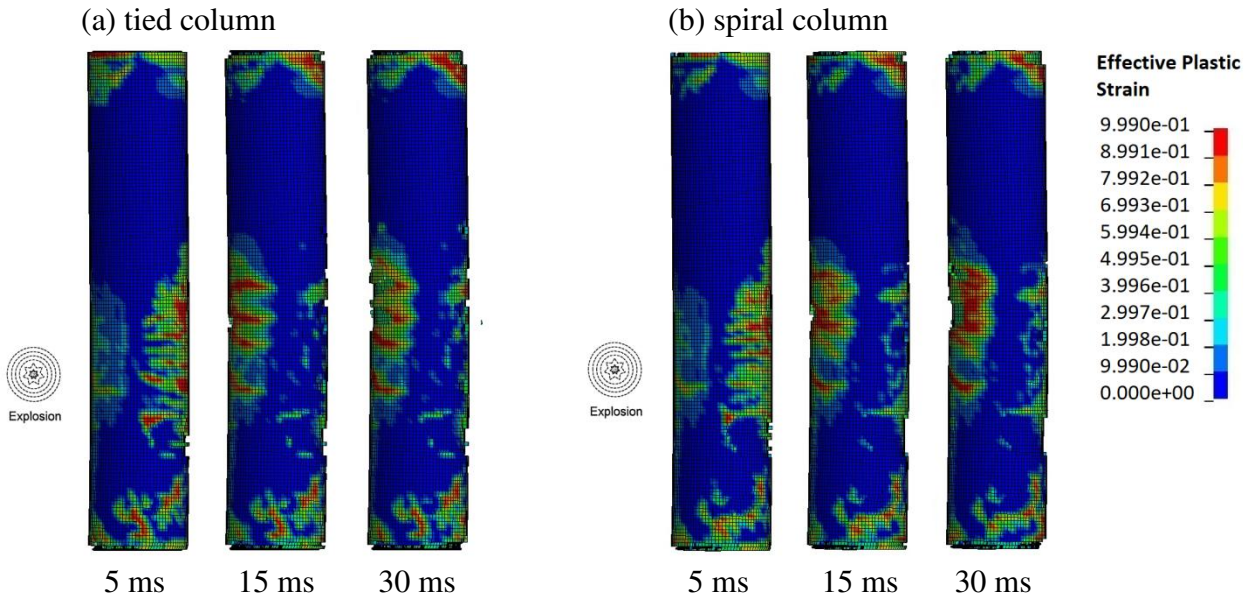

Figure 6.9 Contour of the effective plastic strain in Victoria columns, Set 1 design, Case I, X2.

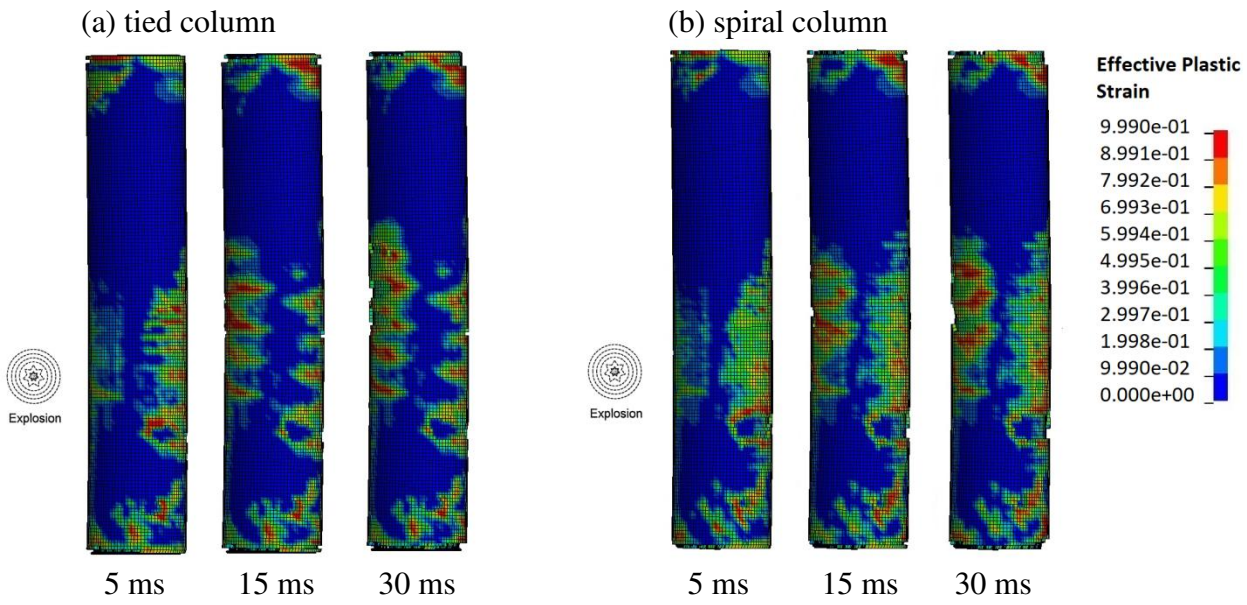

Figure 6.10 Contour of the effective plastic strain in Victoria columns, Set 2 design, Case I, X2.

In all of the simulations for charge height X1, the Victoria columns experienced spalling at the back that penetrated the core. In this case (charge height X2), spalling only occurs outside the core, and not inside the core. This is a rare example where the fixed boundary condition prevented severe spalling at the back of the column. The fixed boundary does not allow rotation and increases shear failure, but this decreases flexural failures like spalling. Since the Victoria columns are adequately reinforced and and there is no shear or spalling inside the core.

Reinforcement stress and behaviour

As discussed above, at the end of the 80 ms simulation, the reinforcement of the Toronto and Vancouver columns were still experiencing augmented levels of stress. However, the level of stress in the reinforcement of the Victoria columns is significantly lower by the end of the simulation. For example, the reinforcement of the two tied columns surpasses stresses of 400 MPa before the occurrence of maximum displacement. The two spiral columns also experience similar stress patterns, which is consistent with the finding from the results for charge height X1, i.e., high stress levels stayed longer in spirals than in ties. It should be noted that the Victoria columns are the only columns in Case I (neither Toronto nor Vancouver columns) to experience the rebounding effect. As a result, their longitudinal reinforcement experienced the shift in tension from the back to the front of the column as rebounding occurred.

Displacement curves

Figures 6.11 and 6.12 illustrate the displacement curves for the Victoria Set 1 and Set 2 columns, respectively. The Set 1 tied column first experiences crushing slightly before maximum displacement. The Set 1 spiral column experiences no form of crushing before maximum displacement, and crushing outside the core only occurs after maximum displacement and as a result of rebounding. The Set 2 tied column experiences crushing before maximum displacement

(a)

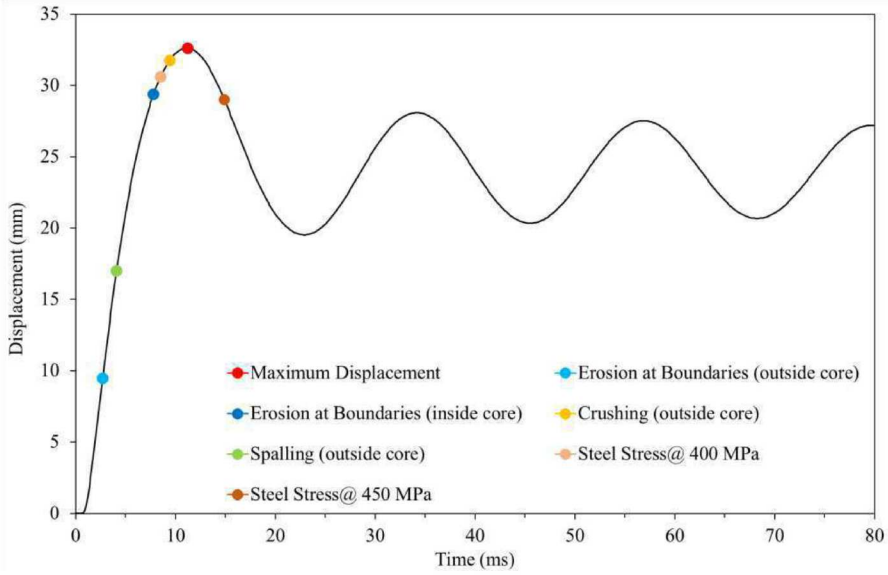

(b)

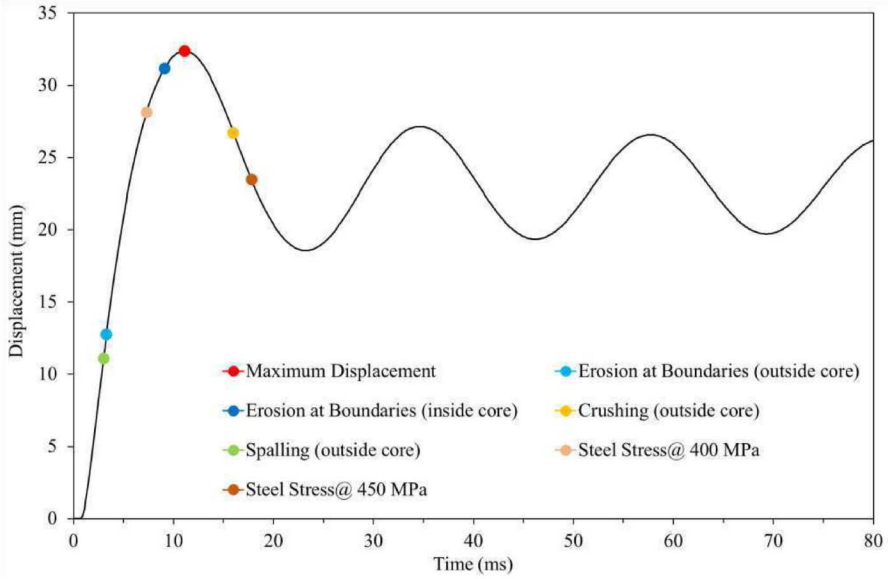

Figure 6.11 Displacement curves for Victoria columns, Set 1 design, Case I, X2: (a) tied column, (b) spiral column.

(a)

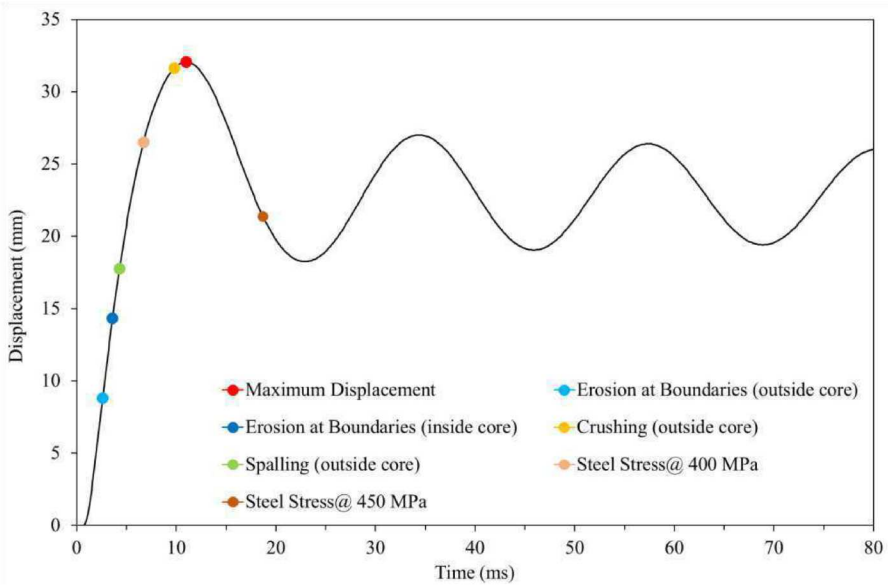

(b)

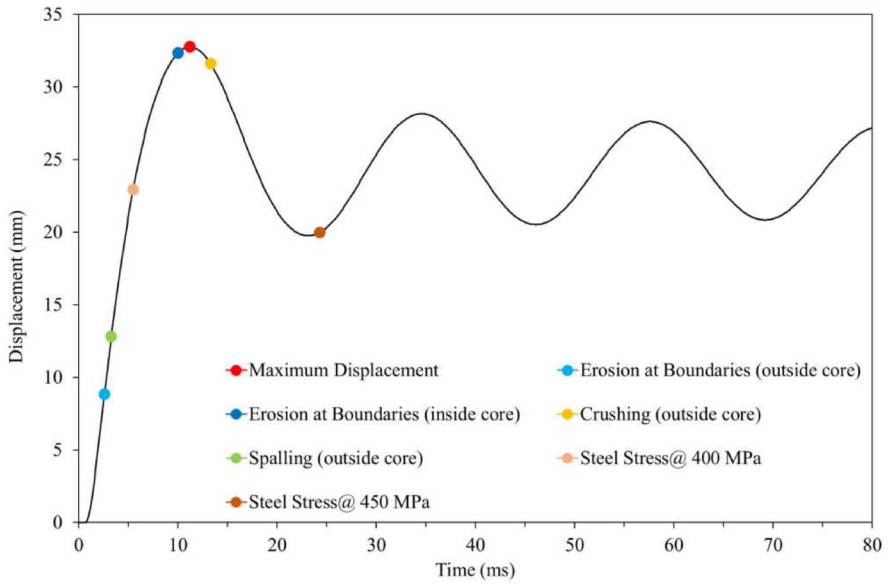

Figure 6.12 Displacement curves for Victoria columns, Set 2 design, Case I, X2: (a) tied column, (b) spiral column.

and the Set 2 spiral column also experiences crushing after maximum displacement. The two spiral columns experienced less concrete erosion during the positive pressure phase as compared to the two tied columns and their performance is superior.

The reinforcement of the two spiral columns reaches yield stress at approximately the same time as the two tied columns. This is different to the findings for charge height X1, where the reinforcement of the two spiral columns reached yield stress much faster than the tied columns. From all four Victoria columns, the reinforcement of the Set 2 spiral column is the last to reach stresses of 450 MPa. Therefore, for spiral columns, the reinforcement of the Set 1 column had more of a positive impact in resisting the blast. In summary, it is concluded that the Set 2 design demonstrates better blast resistance for tied columns and the Set 1 design demonstrates better blast resistance for spiral columns.

6.2.1.4 Comparison of results for all Columns of Case I

Qualitative comparison

The qualitative results for charge height X2 are presented in Table 6.1. It can be seen that the blast load has caused severe damage to all of the Toronto and Vancouver columns. Specifically, the Vancouver spiral column is the most underperforming column, especially in terms of concrete erosion. The four Victoria columns have successfully resisted the blast.

Table 6.1 Summary of failure mechanisms for all columns, Case I, X2.

Failure mechanism		Toronto		Vancouver		Victoria			
		Tied	Spiral	Tied	Spiral	Set 1,Tied	Set 2, Tied	Set 1, Spiral	Set 2, Spiral
Erosion at boundaries	outside core	Yes	Yes	Yes	Yes	Yes	Yes	Yes	Yes
	inside core	High	High	Medium	Medium	Medium	Medium	Medium	Medium
Crushing	outside core	Yes	Yes	Yes	Yes	Yes	Yes	Yes	Yes
	inside core	High	High	High	High	No	No	No	No
Spalling	outside core	Yes	Yes	Yes	Yes	Yes	Yes	Yes	Yes
	inside core	High	High	High	High	No	No	No	No
Severe rebar deformation		Yes	Yes	Yes	Yes	No	No	No	No
Breakage of column		Yes	Yes	Yes	Yes	No	No	No	No
Steel Stress	400 Mpa	After	Before	Before	Before	Before	Before	Before	Before
	450 Mpa	No	Before	After	After	After	After	After	After
	500 Mpa	No	After	No	No	No	No	No	No

Comparison of maximum displacements

The average maximum displacement values (charge height X2) in Table 6.2 are 13% greater than those from the same case of charge height X1 (Table 5.2). This demonstrates that charge height X2 is more critical for maximum displacement than charge height X1 (mid-height). This is the first time that both Toronto columns (tied and spiral) do not reach their peak maximum displacement within the 80 ms simulation, which did not occur for the simulations of charge height X1. The average maximum displacement for the Victoria columns increased by about 10% when compared to charge height X1.

Table 6.2 Maximum displacement for all columns, Case I, X2.

Location	Column	Maximum displacement (mm)
Toronto	tied	48.5
	spiral	42.7
Vancouver	tied	37.4
	spiral	38.2
Victoria	Set 1, tied	32.6
	Set 2, tied	32.1
	Set 1, spiral	32.4
	Set 2, spiral	32.8

Comparison of displacement curves

Figure 6.13 illustrates the displacement curves for all of the columns. For the Toronto columns, the spiral column performed best and shows limited displacement compared to the tied column. The Vancouver columns start the rebounding process but never complete a full cycle. The Vancouver tied column experiences better deflection recovery from the blast as compared to the spiral column. However, the results from charge height X1 suggest the opposite, i.e, the Victoria columns are the only columns to experience at least one full rebounding cycle, which indicates that the Vancouver tied column has a more desirable curve than the spiral column.

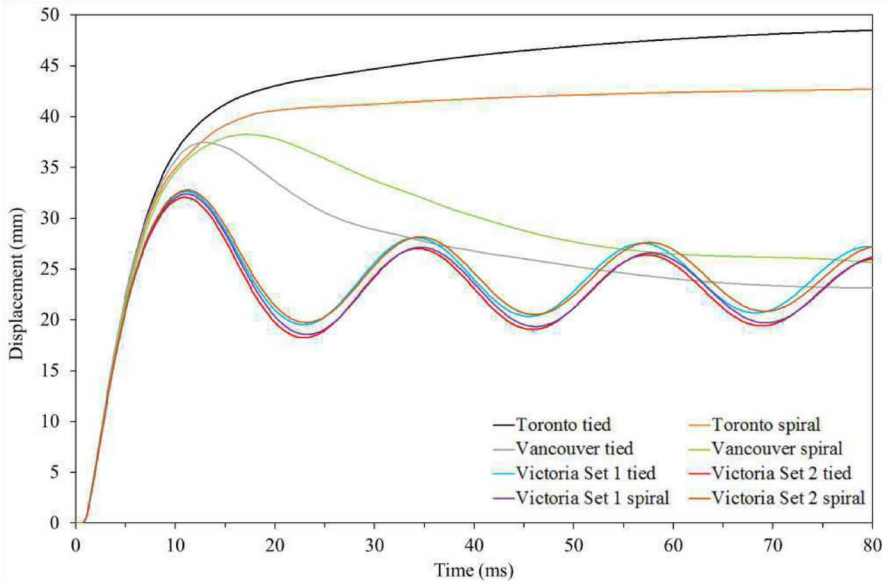

Figure 6.13 Displacement curves for all columns, Case I, X2.

6.2.2 Case II (Charge weight is 12% heavier than Case I)

6.2.2.1 Toronto columns

Concrete failure mechanisms

Figure 6.14 illustrates the effective plastic strain in concrete at 5 ms, 15 ms, and 30 ms for the Toronto tied and spiral columns. The pattern of concrete failure for the tied column is similar to Case I (Fig. 6.1). However, the critical 45 degree shear line that penetrates into the bottom plastic hinge region occurs sooner (5 ms *vs* 8 ms), indicating the blast was more severe. Similar to the results of Case I, this column again experiences complete concrete erosion at the base, while the spiral column performs poorly and concrete failure occurs at a much faster pace than it did in Case I. Furthermore, the column experiences less crushing at the front as compared to Case I. This indicates that more energy was dissipated through spalling rather than crushing, which is not desirable. Moreover, the column experiences complete erosion at the base like the tied column.

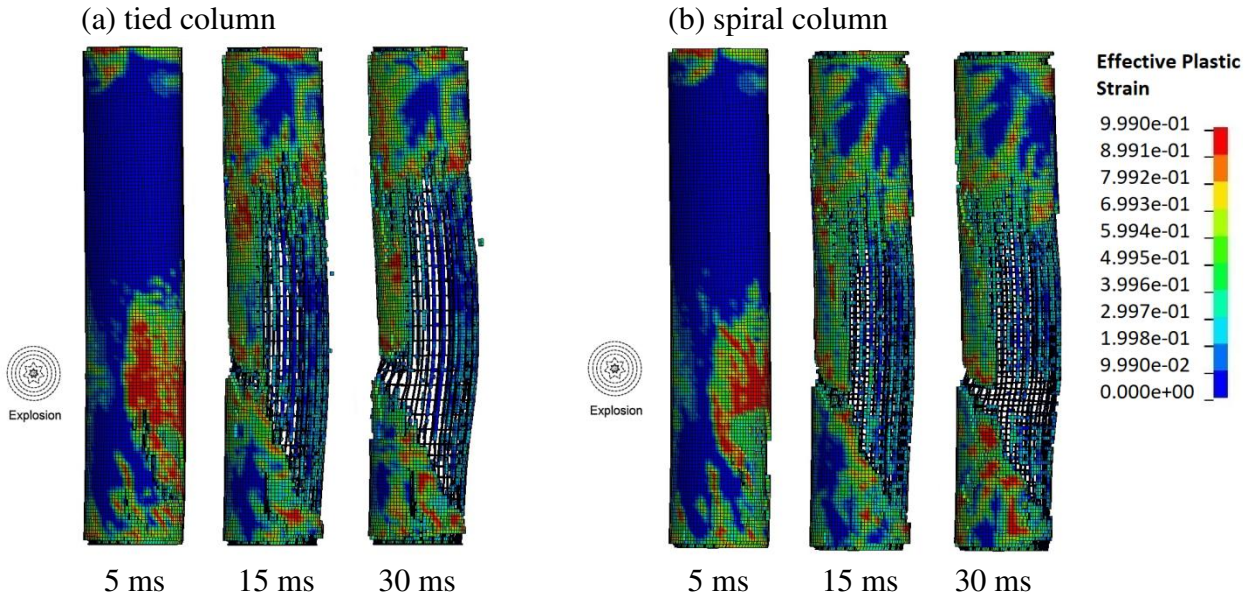

Figure 6.14 Contour of the effective plastic strain in Toronto columns, Case II, X2.

Reinforcement stress and behaviour

The tied column experiences pullout of ties at 7ms, which is the fastest time recorded for this mechanism in all of the simulations of this study. Furthermore, the reinforcement reaches yield stress at a faster pace compared to Case I, and the reinforcement retains these high stress levels for longer periods of time. The longitudinal reinforcement experiences deformation in a 45 degree pattern which starts at the front of the column near charge height and penetrates into the plastic hinge region at the base. Severe deformation of longitudinal bars, as shown in Fig 6.4, occurs at 15 ms, which is the fastest time recorded in this study. The spiral column experiences the same stress distribution and severe deformation of reinforcement as it did in Case I; however, all indicators of stress and failure occur much faster in time. Both the spirals and longitudinal reinforcement of this column experience severe deformation, which was unexpected.

Displacement curves

Figure 6.15 illustrates the displacement curves for the Toronto tied and spiral columns. It is interesting to report herein that the tied and spiral columns do not reach peak maximum displacement in the simulation. The reinforcement of the tied column yields at the exact time of

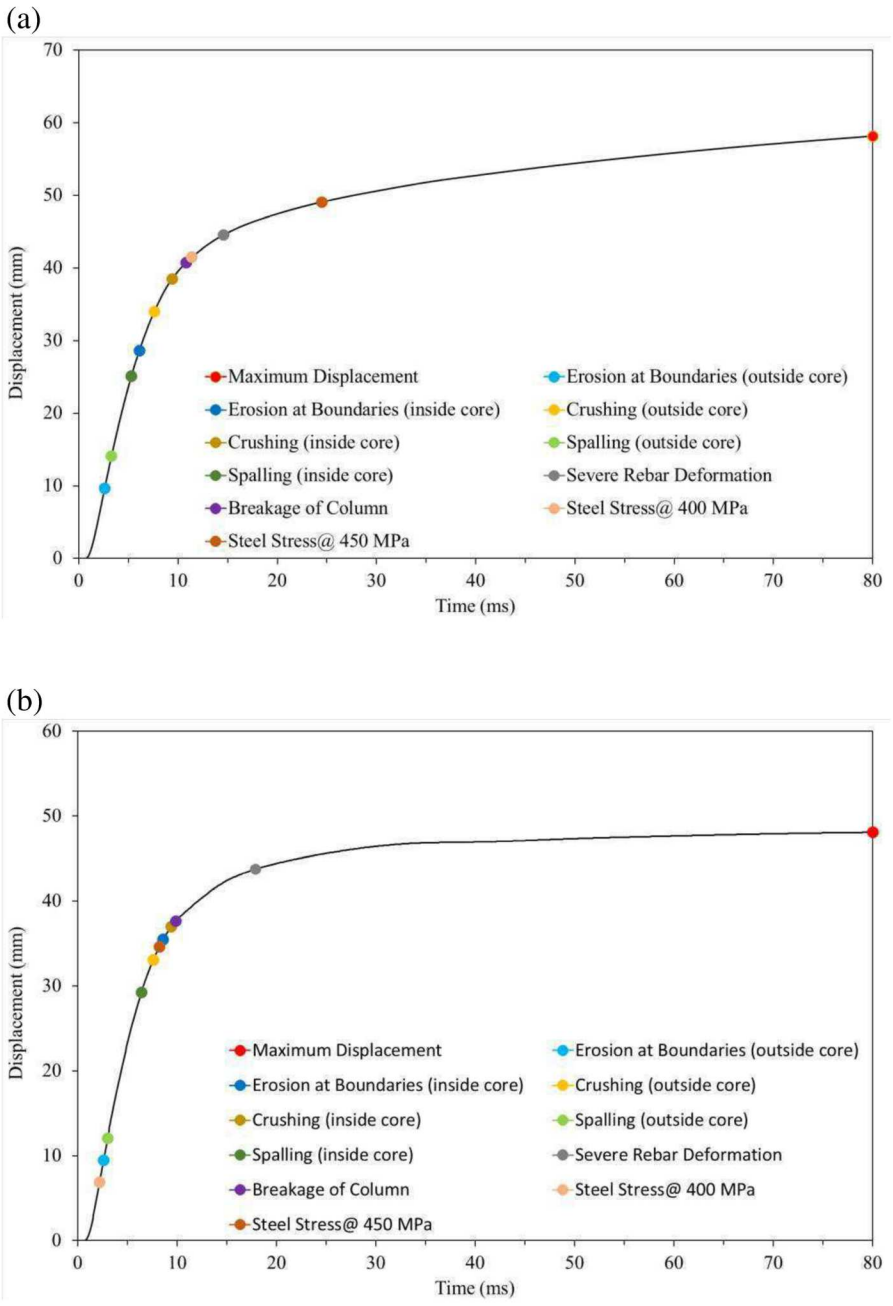

Figure 6.15 Displacement curves for Toronto columns, Case II, X2: (a) tied column, (b) spiral column.

column breakage, and reinforcement surpassed stresses of 450 MPa, which did not occur for Case I. Comparing the slope of the displacement curve for the tied and spiral columns, it is found that the increase in displacement is not as steep for the spiral column. Therefore, the spiral column shows more resistance than the tied column for the most severe blast case.

6.2.2.2 Vancouver columns

Concrete failure mechanisms

Figure 6.16 shows the effective plastic strain in concrete at 5 ms, 15 ms, and 30 ms for the Vancouver tied and spiral columns. Throughout the height of the column, the tied and spiral column experience similar levels of concrete erosion, except at the bottom plastic hinge region. The tied column does not experience a lot of erosion near the base due to smaller spacing of transverse reinforcement in that region.

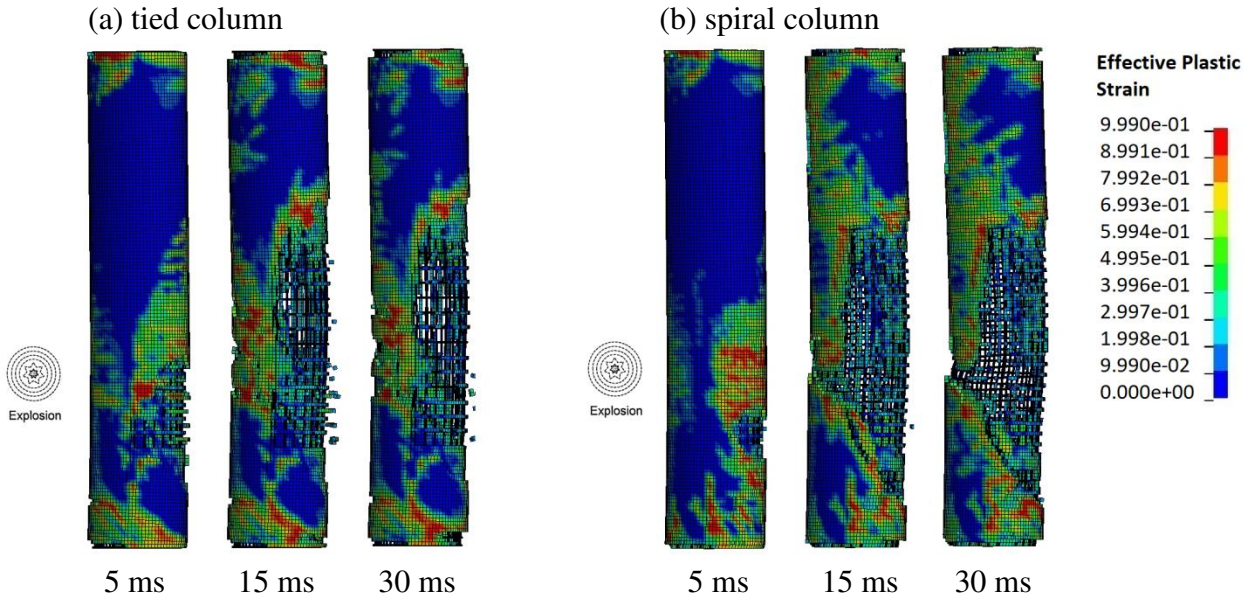

Figure 6.16 Contour of the effective plastic strain in Vancouver columns, Case II, X2.

Figure 6.17 shows both columns at the end of simulation. It can be seen in the figure that the tied column does not experiences breakage along a 45 degree shear line, while the spiral column does and it penetrates the bottom plastic hinge region.

Tied Spiral

Figure 6.17 Side view of the Vancouver columns at the end of simulations, Case II, X2.

Reinforcement stress and behaviour

The transverse reinforcement of the tied column experiences the same stress distribution pattern as it did in Case I, but there is a difference for the longitudinal reinforcement. For Case I, when pressure from the blast impacted the column, stress on longitudinal bars shifted upwards without yielding. In this case, stress on longitudinal bars shifts up and yielding does occur. Severe deformation of longitudinal bars occurs at the back of the column around mid-height, which is similar to Case I.

For the spiral column, the spirals experience severe deformation before the occurrence of maximum displacement. The longitudinal bars at the front of the bottom plastic hinge region experienced high yield stress, which did not happen in Case I. In addition, severe deformation of bars occurs along a 45 degree pattern into the bottom plastic hinge region, similar to Case I (Fig. 6.4). This is the most severe pattern for deformation of longitudinal reinforcement.

Displacement curves

The displacement curves for the Vancouver columns are shown in Figure 6.18. The reinforcement of the tied column experiences stress of 450 MPa and severe deformation after maximum displacement. However, in Case I, these mechanisms occurred before column breakage. In this case, the reinforcement of the tied column dissipated less energy than it did in Case I, and as a result, the column experienced greater concrete erosion. For this case, these mechanisms occurred after column breakage as concrete eroded at a much faster pace and the reinforcement did not have the same positive impact on the columns ability to resist blast. The displacement curve of the spiral column indicates that it experienced no form of rebounding. In this study, this is the only simulation where the Vancouver spiral column experienced no rebounding. In Case I, this column experienced maximum displacement before column breakage. However, in this case, the column experiences maximum displacement after breakage.

(a)

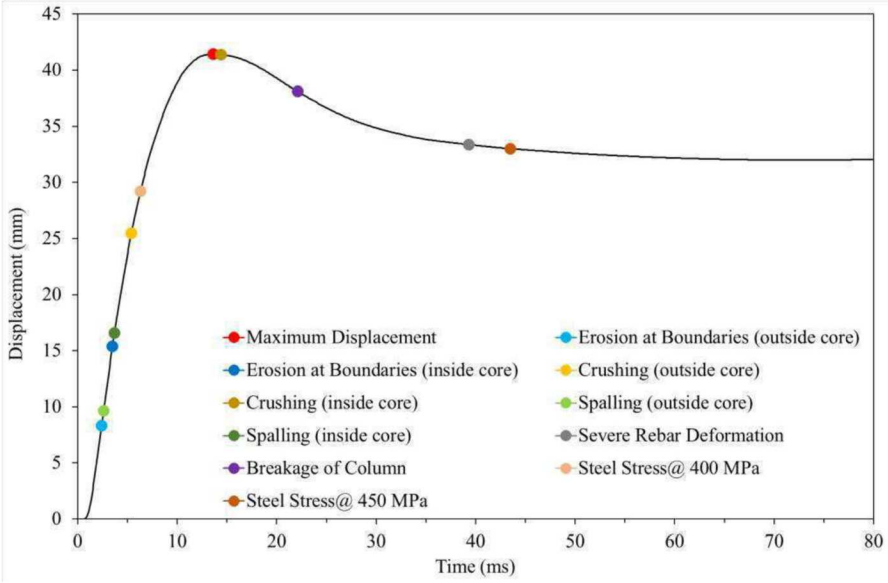

(b)

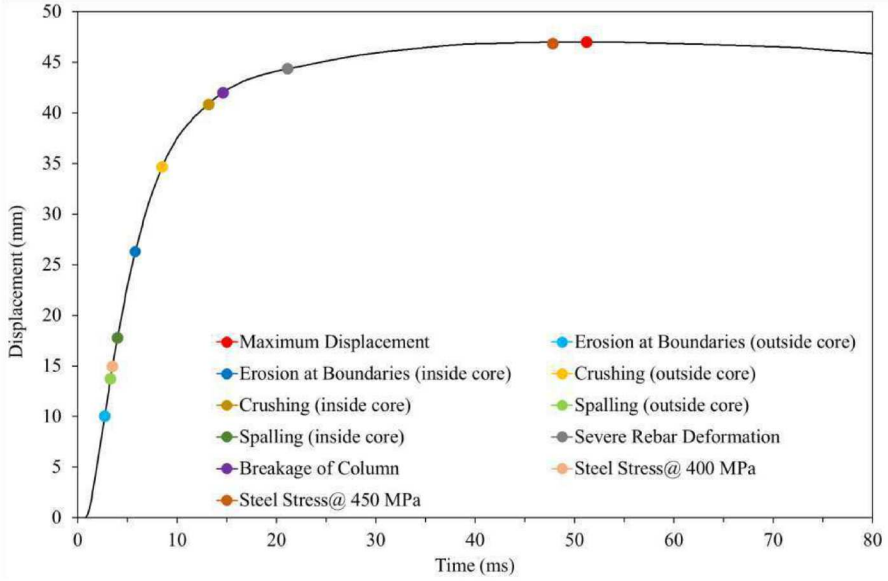

Figure 6.18 Displacement curves for Vancouver columns, Case II, X2: (a) tied column, (b) spiral column.

6.2.2.3 Victoria columns

Concrete failure mechanisms

All Victoria columns successfully resist the blast, which demonstrates that they are adequately reinforced to resist the worst possible scenario considered in this study. Figures 6.19 and 6.20 show the effective plastic strain in concrete at 5 ms, 15 ms, and 30 ms for the Victoria Set 1 and Set 2 columns, respectively. The two sets of tied columns perform similarly, except that the Set 2 column experiences less erosion of concrete. Therefore, it design is considered to be more favorable than Set 1. For spiral columns, the distinguishing failure mechanism is spalling. The spiral column for Set 2 experiences spalling at the back of the bottom plastic hinge region which penetrates the core, which was not observed for Set 1. Therefore, the spiral column for Set 1 has superior design for this blast case.

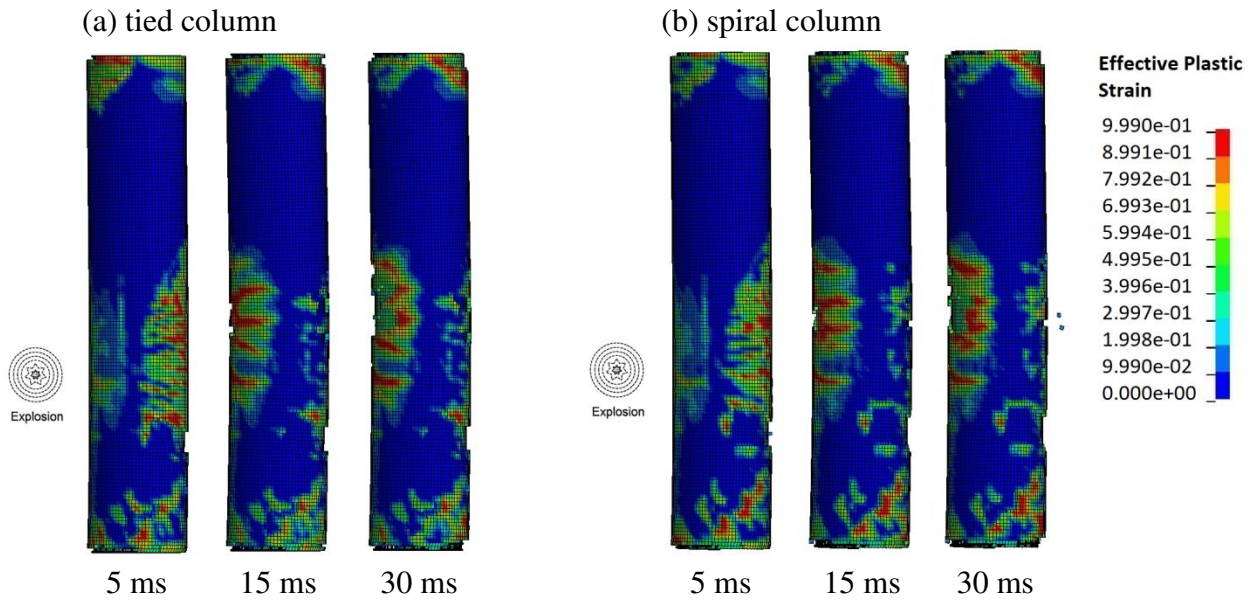

Figure 6.19 Contour of the effective plastic strain in Victoria columns, Set 1 design, Case II, X2.

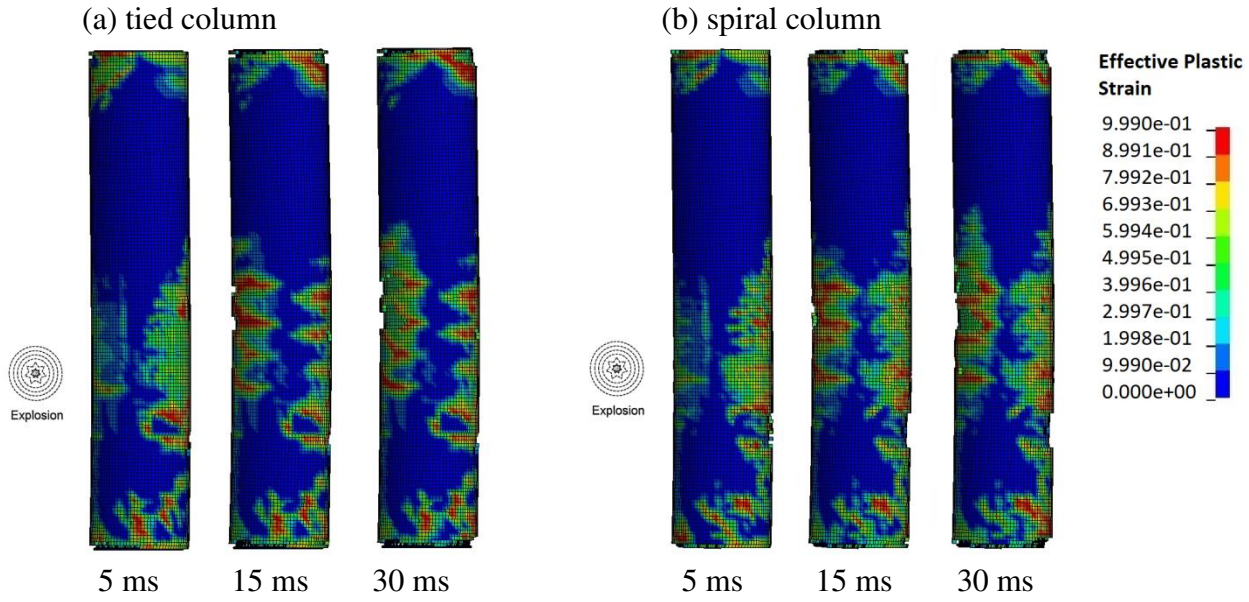

Figure 6.20 Contour of the effective plastic strain in Victoria columns, Set 2 design, Case II, X2.

Reinforcement stress and behaviour

The reinforcement for all Victoria columns performs similarly to Case I. The level of stress in the reinforcement of the columns is reduced to relatively minimum levels by the end of the simulations. Moreover, the time at which the columns reach stresses of 400 MPa and 450 MPa is similar to Case I. For the four Victoria columns, the reinforcement of the Set 2 spiral column is the last to reach stresses of 450 MPa. The sooner reinforcement yields, the more energy it can dissipate and prevent concrete erosion.

Displacement curves

The displacement curves for the Victoria Set 1 and Set 2 columns are shown in Figs 6.21 and 6.22, respectively. For the tied columns, it is worth mentioning that the reinforcement for the Set 2 design experiences yielding stress sooner than the Set 1 design, which is beneficial for the columns to dissipate energy from the blast and reducing concrete erosion. The reinforcement of the two spiral columns yielded faster than the tied columns, which has also been noted in

previous cases. The displacement curve for the Set 2 spiral column demonstrates that spalling, which penetrated the core, occurred during the positive pressure phase. This shows that the Set 1 spiral column performed better than the Set 2 column during the positive pressure phase and the rebounding phase.

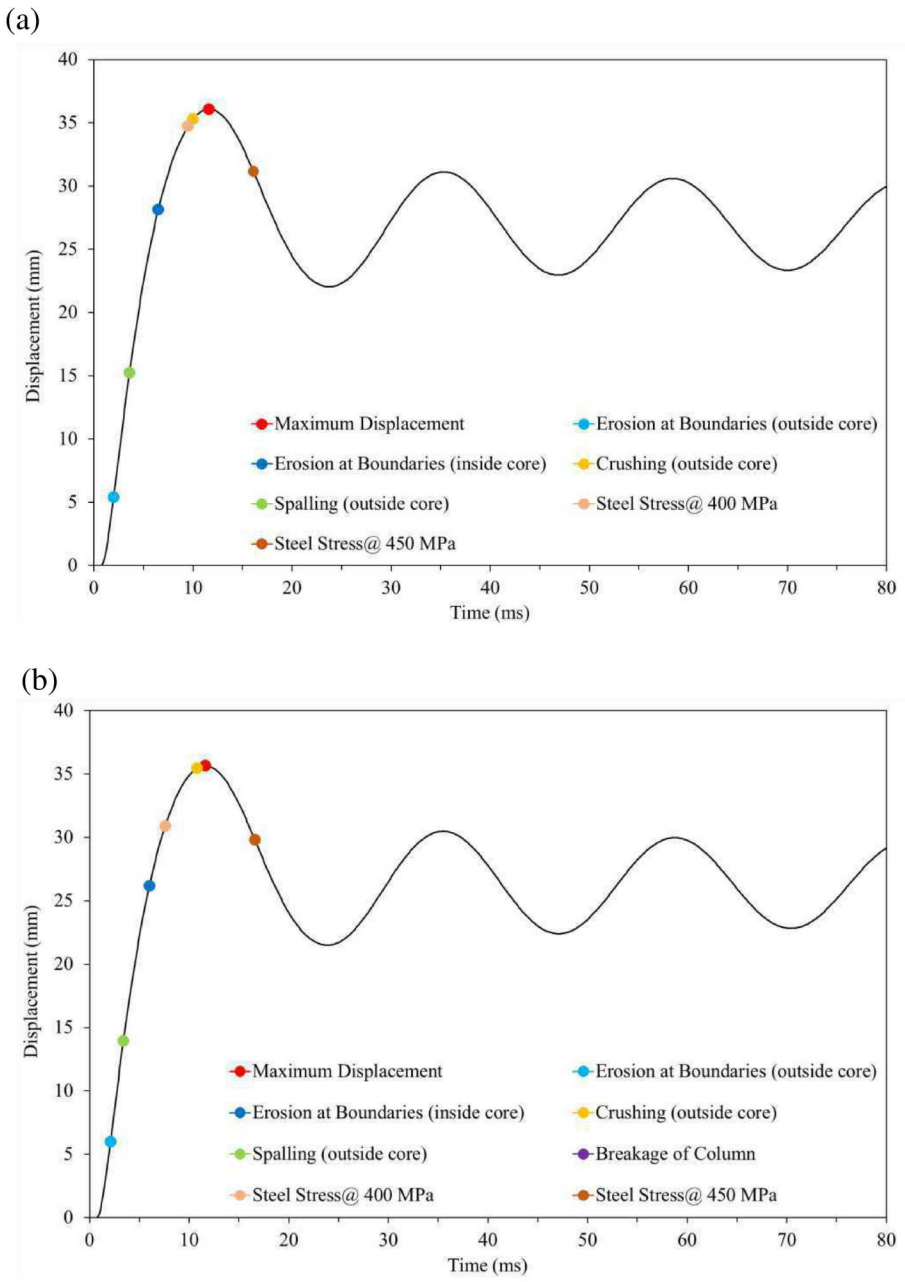

Figure 6.21 Displacement curves for Victoria columns, Set 1 design, Case II, X2: (a) tied column, (b) spiral column.

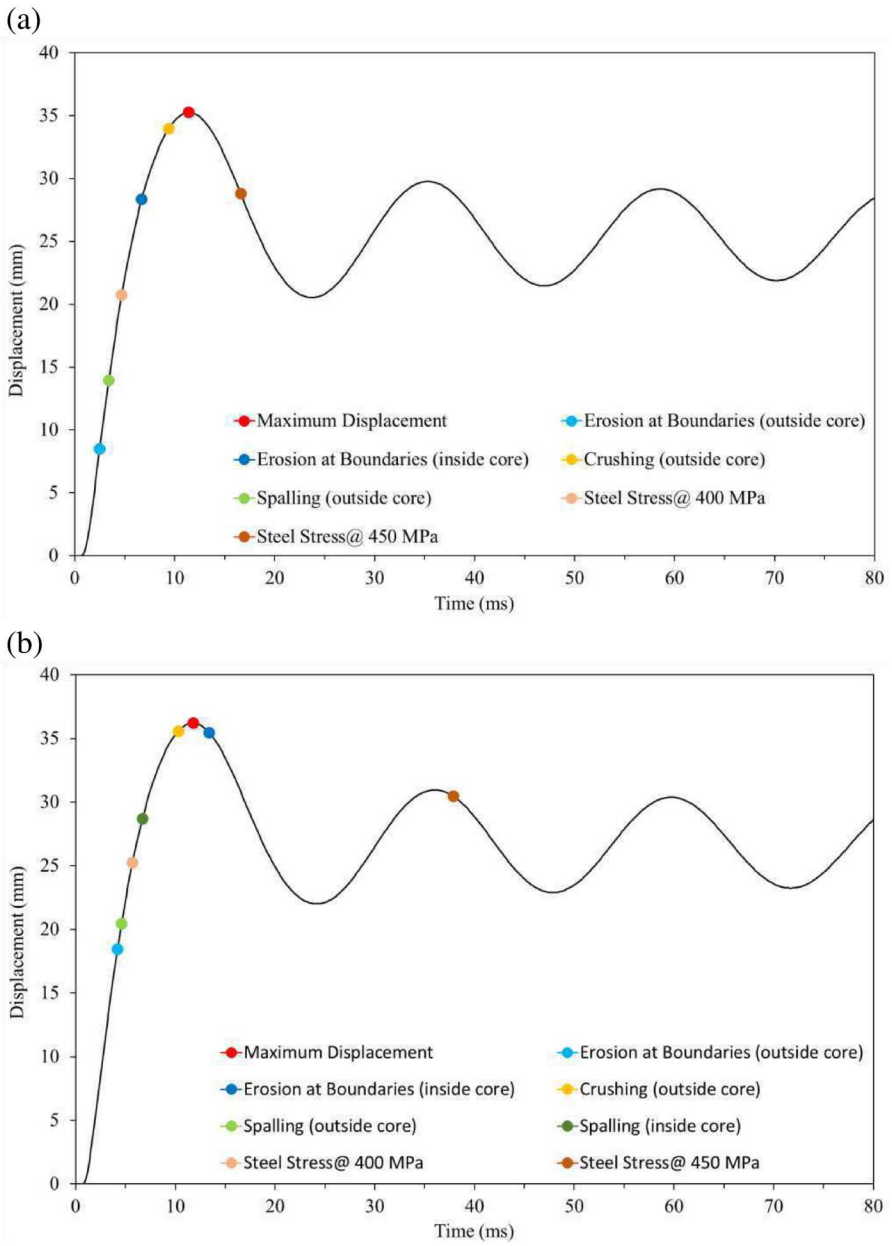

Figure 6.22 Displacement curves for Victoria columns, Set 2 design, Case II, X2: (a) tied column, (b) spiral column.

6.2.2.4 Comparison of results for all Columns of Case II

Qualitative comparison

The qualitative results in Table 6.3 show that for Case II, which is considered to be the worst case scenario of all simulations, the Toronto and Vancouver columns had worst

performances than Case I, and only the Victoria columns successfully resisted the blast. The column that underperformed most as compared to Case I is the Vancouver spiral column.

Table 6.3 Summary of failure mechanisms for all columns, Case II, X2.

Failure mechanism		Toronto		Vancouver		Victoria			
		Tied	Spiral	Tied	Spiral	Set 1,Tied	Set 2, Tied	Set 1, Spiral	Set 2, Spiral
Erosion at boundaries	outside core	Yes	Yes	Yes	Yes	Yes	Yes	Yes	Yes
	inside core	High	High	Medium	High	Medium	Medium	Medium	Medium
Crushing	outside core	Yes	Yes	Yes	Yes	Yes	Yes	Yes	Yes
	inside core	High	High	High	High	No	No	No	No
Spalling	outside core	Yes	Yes	Yes	Yes	Yes	Yes	Yes	Yes
	inside core	High	High	High	High	No	No	No	Low
Severe rebar deformation		Yes	Yes	Yes	Yes	No	No	No	No
Breakage of column		Yes	Yes	Yes	Yes	No	No	No	No
Steel Stress	400 Mpa	After	Before	Before	Before	Before	Before	Before	Before
	450 Mpa	After	Before	After	After	After	After	After	After
	500 Mpa	No	No	No	No	No	No	No	No

Comparison of maximum displacements

The Vancouver spiral column performs extremely worst in terms of the maximum displacement. Table 6.4 shows that the Vancouver spiral column experiences the greatest percentage increase in displacement when compared to the Case I simulations. The Vancouver

Table 6.4 Maximum displacement for all columns, Case II, X2.

Location	Column	Maximum displacement (mm)	Percent difference from Case I
Toronto	tied	58.2	18.1%
	spiral	48.1	11.9%
Vancouver	tied	41.4	10.1%
	spiral	47.0	20.6%
Victoria	Set 1, tied	36.1	10.1%
	Set 2, tied	35.3	9.5%
	Set 1, spiral	35.7	9.6%
	Set 2, spiral	36.2	10.0%

tied column has a maximum displacement similar to the Victoria columns due to adequate reinforcement. In summary, the columns for Case II experienced an average increase in maximum displacement of 13% as compared to Case I.

Comparison of displacement curves

The resulting displacement curves for all columns (Fig. 6.23) illustrates the poor performance of the Vancouver spiral column because the displacement curve of this column is almost identical to the Toronto spiral column. This has not previously occurred as the Vancouver spiral column tends to perform better than the Toronto columns. The displacement curves of the Victoria columns show that for tied columns, the Set 2 design had a better recovery towards the columns original position, and for spiral columns the same applies for the Set 1 design. Therefore, in conclusion, when including results for concrete erosion, stress and behaviour of reinforcement, and displacement curve, it is noted that for tied columns the Set 2 design is superior while for spiral columns the Set 1 design is superior.

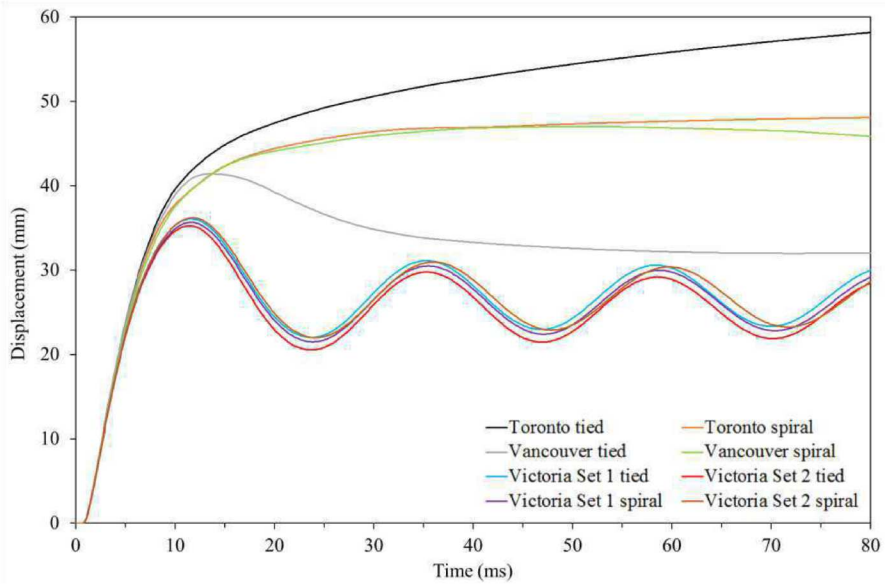

Figure 6.23 Displacement curves for all columns, Case II, X2.

6.2.3 Case III (Charge distance is 12% closer than Case I)

6.2.3.1 Toronto columns

Concrete failure mechanisms

Figure 6.24 shows the effective plastic strain in concrete at 5 ms, 15 ms, and 30 ms for the Toronto tied and spiral columns. The tied column shows minor improvement compared to Case I (Fig. 6.1a) and Case II (6.14a) as concrete failure mechanisms occurred later in time. The column still experiences breakage, and more importantly, the column breaks along the 45 degree shear line that penetrates the bottom plastic hinge region. The column experiences complete erosion at the base.

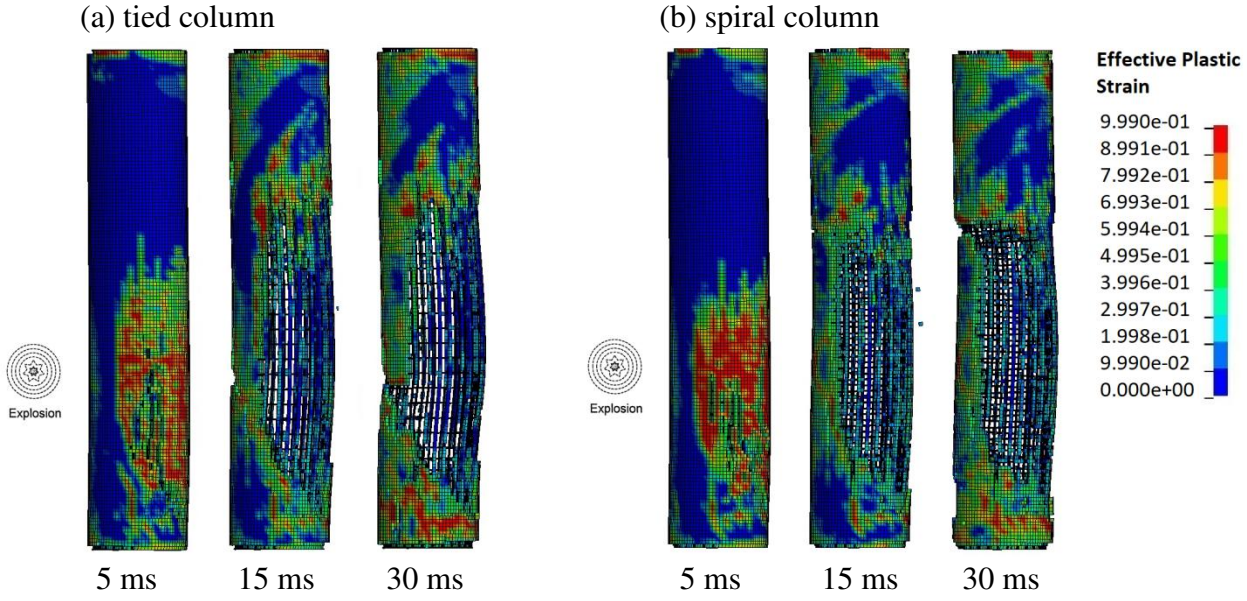

Figure 6.24 Contour of the effective plastic strain in Toronto columns, Case III, X2.

The spiral column experiences breakage from a different pattern than for Case I (Fig. 6.1b) and Case II (Fig. 6.14b). More specifically, in Cases I and II, the column broke along a 45 degree shear line that penetrated the bottom plastic hinge region. However, in Case III (Fig. 6.24b), the breakage line for this case is horizontal and occurs slightly above mid-height. As seen

in the results of charge height X1, horizontal failure around mid-height is indicative of flexural failure. Therefore, failure of this column was not due solely to shear, and flexural failure occurred as well. The results in Fig. 6.25 show that the column did not experience complete erosion at the base, which is only observed in Case III, and not in Cases I and II.

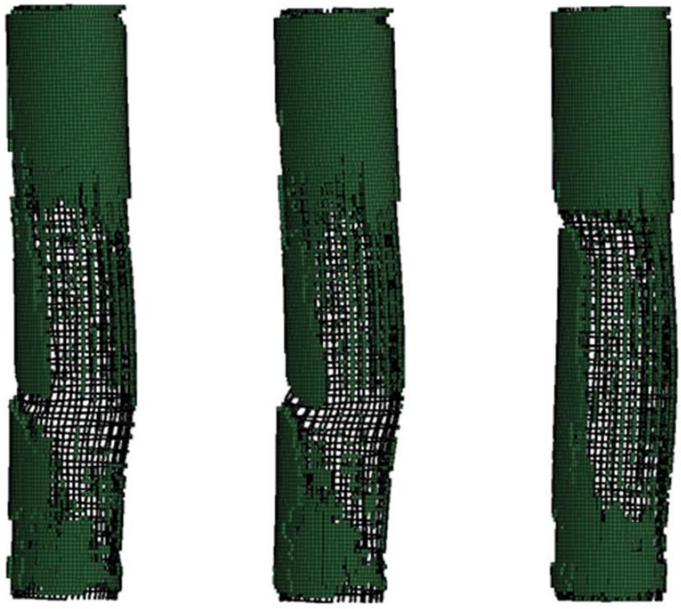

Case I Case II Case III

Figure 6.25 Side view of the Toronto spiral columns at the end of simulations, X2.

Reinforcement stress and behaviour

Although the pressure of the Case III blast is the lowest among the three cases considered, the tied column still experiences pullout of ties and severe deformation of longitudinal reinforcement. It is also noted that yielding and severe deformation of reinforcement occurs before column breakage, which is opposite to the finding in Cases I and II. Furthermore, stress in the reinforcement of the spiral column is much less than in the first two cases, and stress decreases towards the end of the simulation. Moreover, severe deformation of longitudinal bars in the spiral column occurs before breakage of the column. However, this occurred after column

breakage in Cases and I and II. This demonstrates that that the longitudinal reinforcement had more positive impact on blast resistance as energy dissipation is much faster than in the first two cases. This allowed for a reduction in concrete erosion and avoided shear failure of the column.

Displacement curves

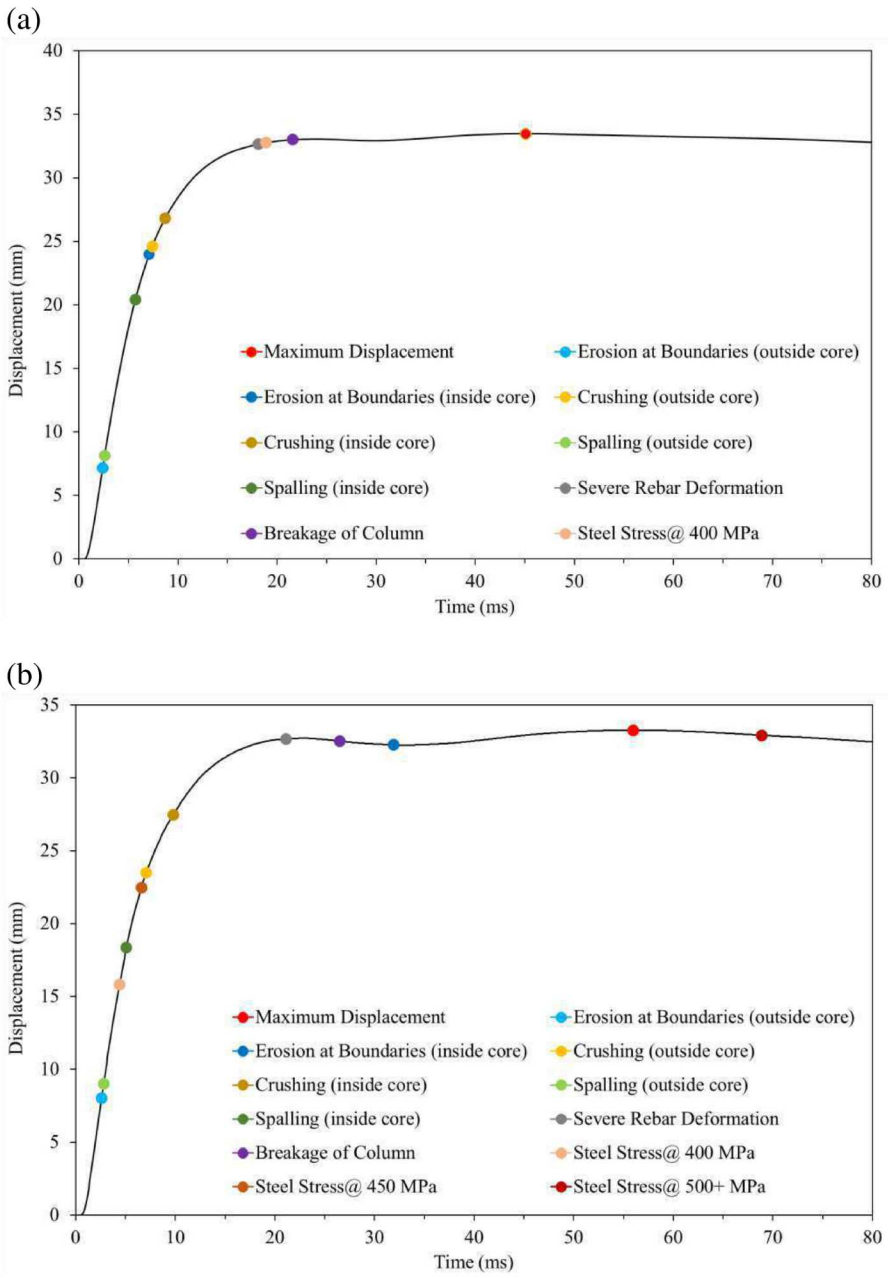

Figure 6.26 Displacement curves for Toronto columns, Case III, X2: (a) tied column, (b) spiral column.

It can be seen in Fig. 6.26 that both the tied and spiral column are able to reach peak maximum displacement within the 80 ms simulation time and experience a very minor form of rebounding, which was not observed for Cases I and II. In addition, the spiral column experiences a rebounding pattern that is more noticeable than the tied column. It is interesting to point out that the reinforcement of both tied and spiral columns experience yielding stress and deformation before breakage, which reduced concrete erosion.

6.2.3.2 Vancouver columns

Concrete failure mechanisms

The greatest improvements in blast resistance for Case III are for the two Vancouver columns. It can be seen in Fig. 6.27 that there is no crushing of concrete that penetrates the core for both the tied and spiral column, which occurred in Cases I and II. Moreover, this is the only case for charge height X2 where the Vancouver tied and spiral columns do not experience breakage.

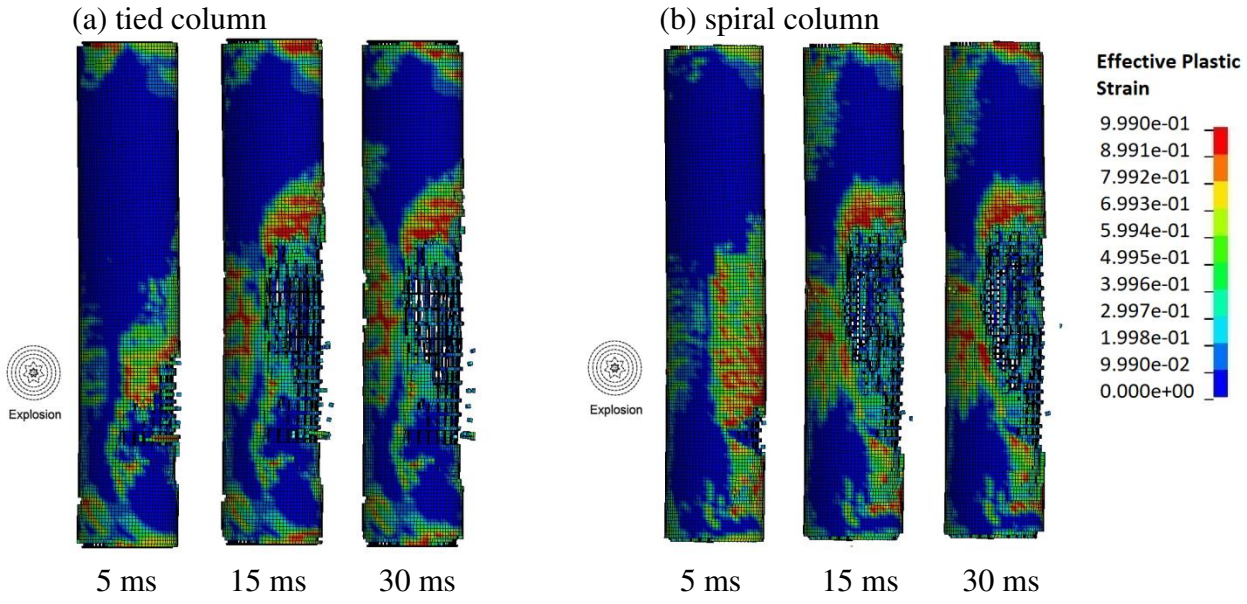

Figure 6. 27: Contour of the effective plastic strain in Vancouver columns, Case III, X2.

As illustrated in Fig. 6.28, the spiral column of Case III does not experience the 45 degree shear crack inside the bottom plastic hinge region. Most of the eroded concrete is around mid-height, which suggests that the erosion was due more from flexure rather than shear. The spiral column slightly outperforms the tied column, and this did not occur in Cases I and II. From the results of all three cases for charge height X2, it is concluded that as the blast gets more severe, the inefficiencies of the spiral column, due to insufficient spacing of transverse reinforcement in the plastic hinge region, becomes more apparent.

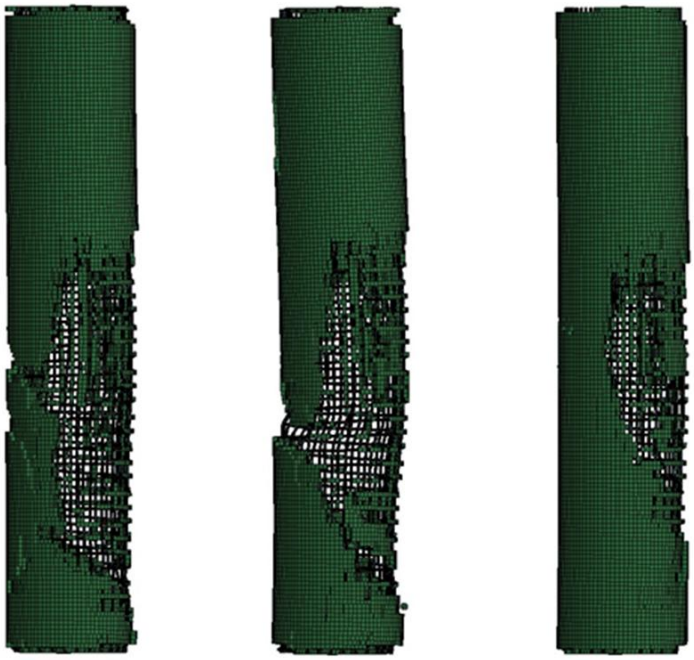

Case I Case II Case III

Figure 6.28 Side view of the Vancouver spiral columns at the end of simulations, X2.

Reinforcement stress and behaviour

Similar to the first two cases, stress in the reinforcement of the tied column started at charge height and shifted towards mid-height and accumulated in that area. The accumulated stress at mid-height dissipated as time went on. Severe deformation of longitudinal reinforcement did occur as shown in Fig. 6.4, but fewer bars were affected as compared to the

first two cases. The behavior of the longitudinal reinforcement of the spiral column is different than the first two cases. In Case I and Case II, stress started at charge height and shifted to the top of the column. In this case, the stress accumulates at mid-height and gradually dissipates as time went on. Moreover, this is the only case for charge height X2 where the longitudinal reinforcement of the spiral column did not experience severe deformation. When comparing the behavior of reinforcement for both columns, the spiral column slightly better than the tied column.

Displacement curves

The shape of the displacement curve for the tied column (Fig. 6.29a) is similar to the previous two cases. More specifically, crushing only occurs outside the core after the occurrence of maximum displacement, which implies that it is a result of rebounding and not from the positive pressure phase. The spiral column experiences crushing outside the core and boundary erosion inside the core after maximum displacement, which is due to rebounding. For concrete erosion, the spiral column performs better resisted the blast during the positive pressure phase. With respect to the reinforcement, the spiral column is able to dissipate greater energy and experience no severe deformation of longitudinal reinforcement. The shape of the displacement curve (Fig. 6.29b) demonstrates that the spiral column experienced more rebounding cycles and was able to dissipate more energy. In conclusion, the spiral column presents a better performance than the tied column for the major qualitative observations.

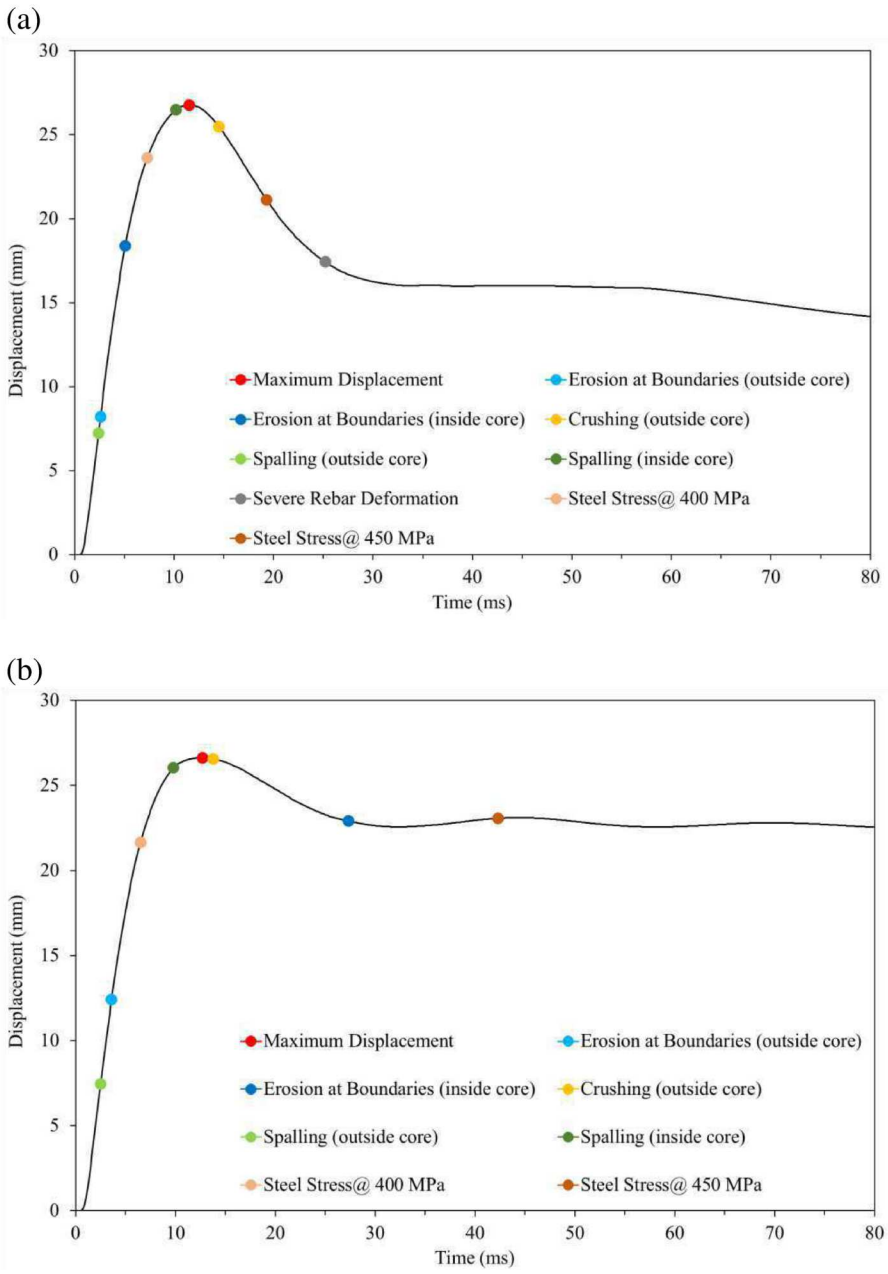

Figure 6.29 Displacement curves for Vancouver columns, Case III, X2: (a) tied column, (b) spiral column.

6.2.3.3 Victoria columns

Concrete failure mechanisms

The results Figs. 6.30 and 6.31 show the Victoria columns perform well and experience no major concrete failures. The blast pressure is low enough that none of the columns experience

noticeable crushing on the front face before the occurrence of maximum displacement. When crushing does occur, it is outside the core and it is a result of rebounding. Erosion inside the core concrete also occurs as a result of rebounding after maximum displacement.

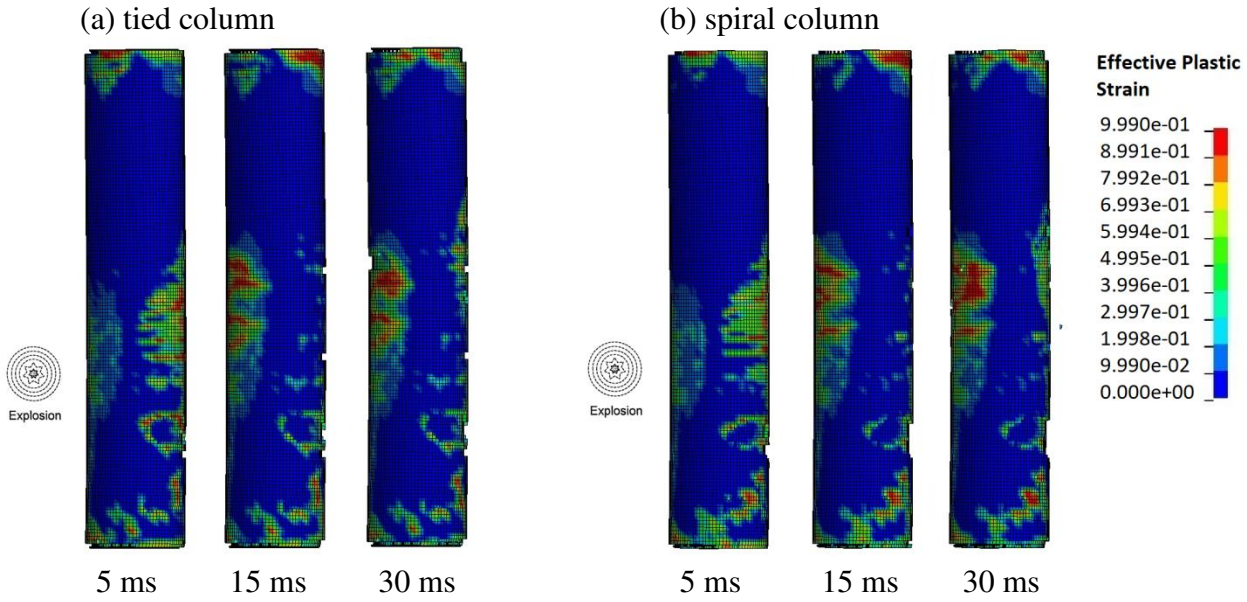

Figure 6.30 Contour of the effective plastic strain in Victoria columns, Set 1 design, Case III, X2.

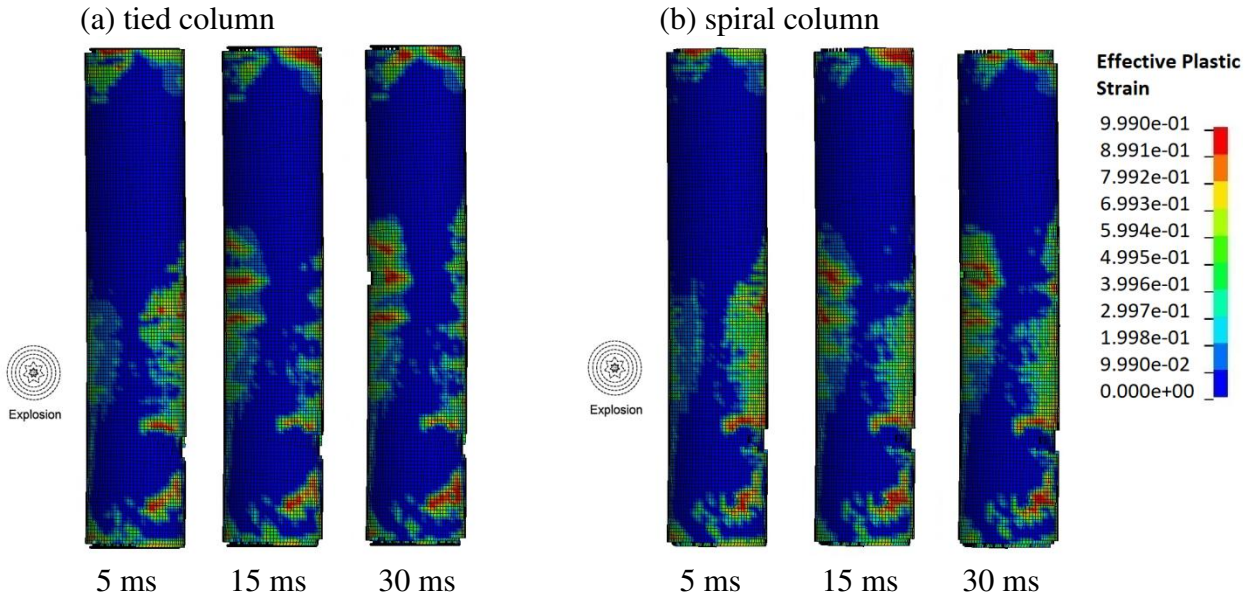

Figure 6.31 Contour of the effective plastic strain in Victoria columns, Set 2 design, Case III, X2.

It is difficult to make a distinction regarding the performance of the Victoria columns. Generally speaking, when the blast load is severe, inefficiencies in column design (e.g., insufficient transverse reinforcement) become apparent, which is what happened to the Vancouver spiral column. However, because the pressure of the Case III blast is low, the Victoria columns perform extremely similarly with regards to concrete erosion. By comparing the concrete erosion, it is found out that the tied columns of Set 2 and spiral columns of Set 1 perform better. Moreover, the spiral column for Set 2 is the only Victoria column to experience spalling inside the core, which is a minor indication that it is inferior to the Set 1 spiral column.

Reinforcement stress and behaviour

The transverse reinforcement of all four Victoria columns reach yield stress before the occurrence of maximum displacement, but the longitudinal reinforcement of all four columns does not reach yield stress, which is different from Case I and Case II. The relatively low level of the blast was not sufficient to generate enough flexural pressure on the column for the longitudinal reinforcement to sustain significantly high levels of stress. On the contrary, when the transverse reinforcement of the Victoria columns experience stresses above 450 MPa, it occurs at the time when the rebounding peak arrives after maximum displacement. This is due to the shift in stress from the back to the front of the column as it is rebounding back and forth.

Displacement curves

The displacement curve of the Set 1 tied column (Fig. 6.32a) illustrates that the column sustains all major mechanisms after the occurrence of maximum displacement such as crushing outside the core, reinforcement stress above 450 MPa, and erosion at boundaries inside the core, occur at the peaks of rebounding cycles. This occurs for all four of the Victoria columns, as several failure mechanisms occur at the peaks of rebounding cycles. The Set 2 spiral column is

the only column to experience spalling inside the core, and this is observed before the occurrence of maximum displacement and within the positive pressure phase. With respect to the yielding of reinforcement, the Set 2 tied column yields faster and is considered superior to the Set 1 column, which is opposite to the observation for the spiral columns, i.e., Set 1 design yields slightly faster than Set 2.

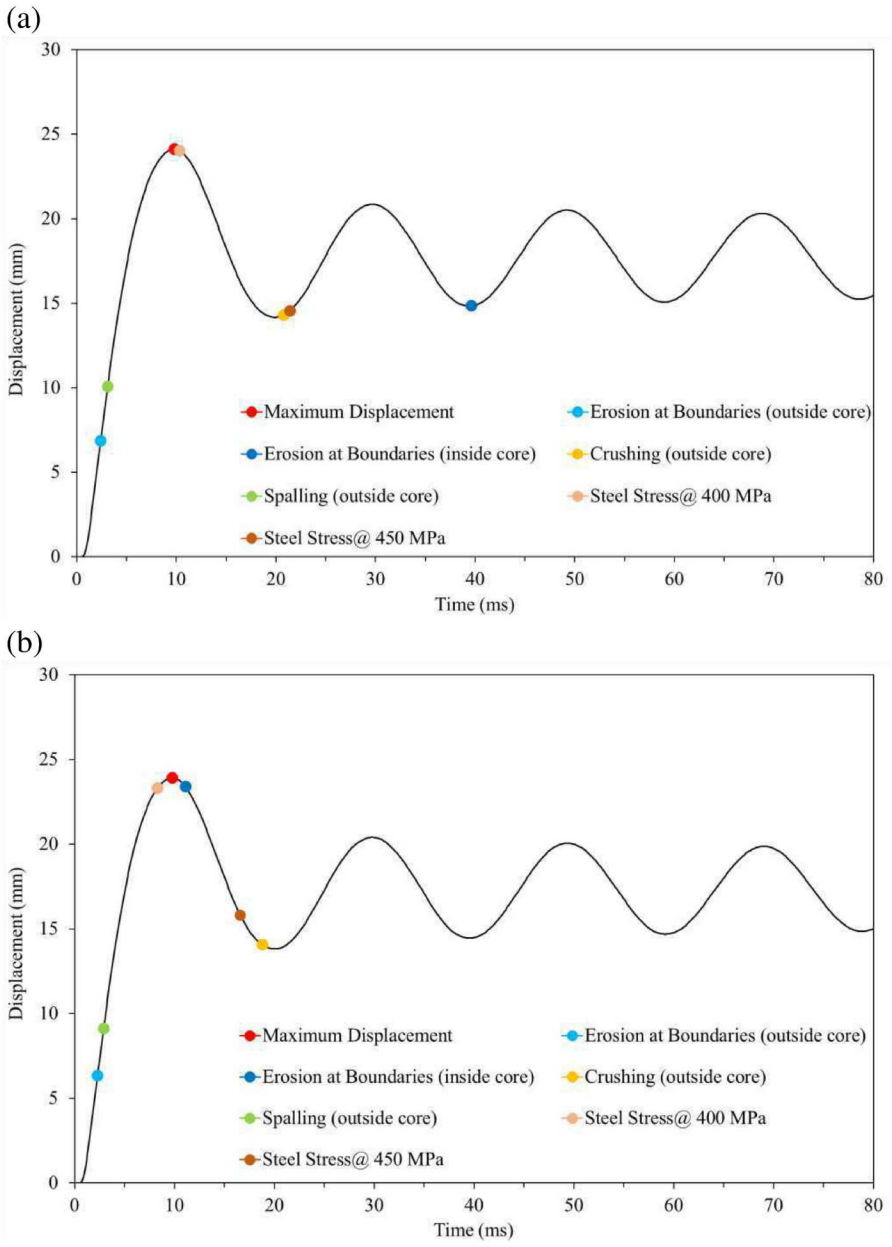

Figure 6.32 Displacement curves for Victoria columns, Set 1 design, Case III, X2: (a) tied column, (b) spiral column.

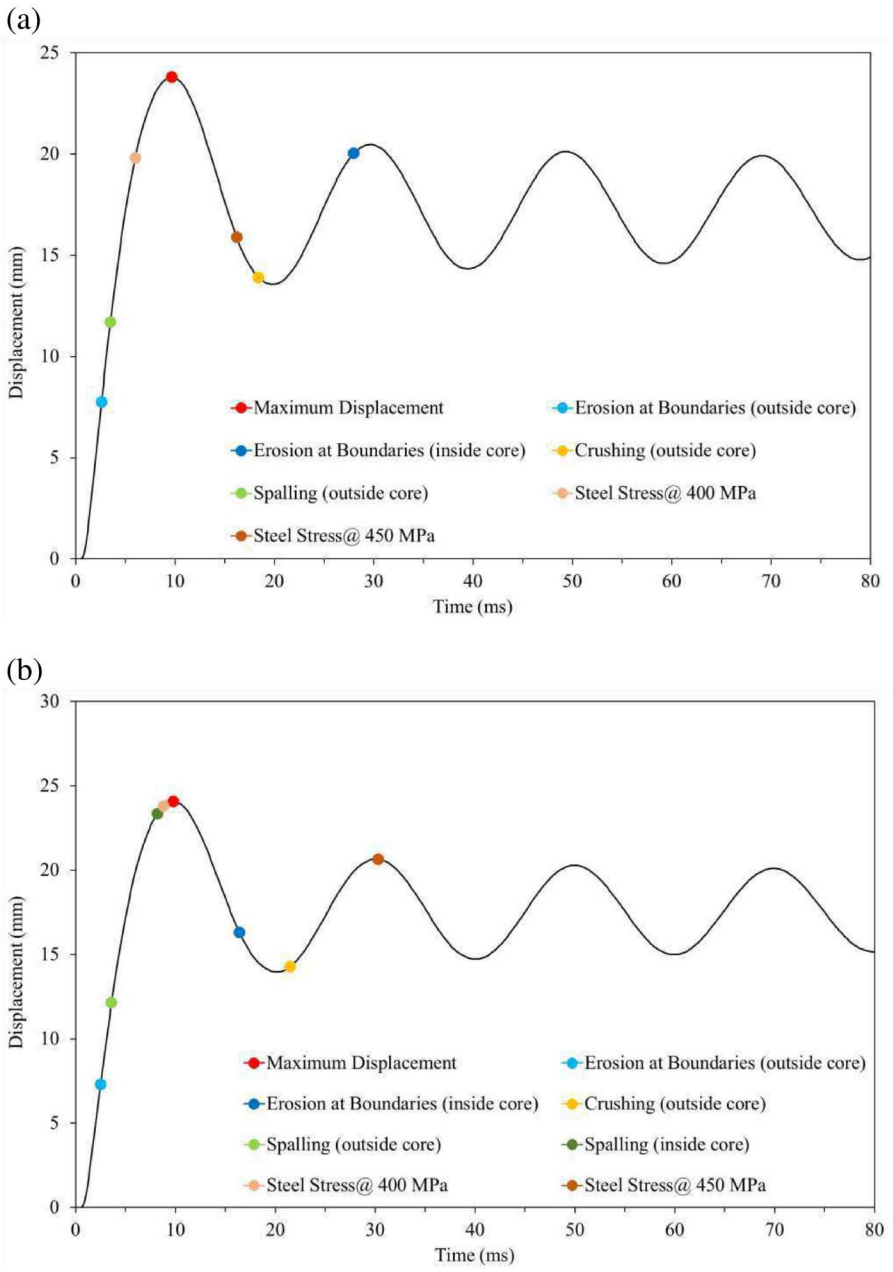

Figure 6.33 Displacement curves for Victoria columns, Set 2 design, Case III, X2: (a) tied column, (b) spiral column.

6.2.3.4 Comparison of results for all Columns of Case III

Qualitative comparison

The results from the comparison of the qualitative failure mechanisms (Table 6.5) show that all columns experienced lower levels of failure compared to Case I and Case II. The

Vancouver spiral column represents a drastic improvement in its ability to resist the blast load, even though it still experiences high levels of spalling inside the concrete core. The Victoria columns are the only columns to have successfully resisted the blast, but the Vancouver columns performed well enough to be a starting baseline for adequate transverse reinforcement design. This conclusion is based on overall erosion of concrete, reaction of reinforcement, and displacement curve shape with regards to rebounding, as discussed above.

Table 6.5 Summary of failure mechanisms for all columns, Case III, X2.

Failure mechanism		Toronto		Vancouver		Victoria			
		Tied	Spiral	Tied	Spiral	Set 1,Tied	Set 2, Tied	Set 1, Spiral	Set 2, Spiral
Erosion at boundaries	outside core	Yes	Yes	Yes	Yes	Yes	Yes	Yes	Yes
	inside core	High	Medium	Low	Low	Low	Low	Low	Low
Crushing	outside core	Yes	Yes	Yes	Yes	Yes	Yes	Yes	Yes
	inside core	High	Medium	No	No	No	No	No	No
Spalling	outside core	Yes	Yes	Yes	Yes	Yes	Yes	Yes	Yes
	inside core	High	High	High	High	No	No	No	Low
Severe rebar deformation		Yes	Yes	Yes	No	No	No	No	No
Breakage of column		Yes	Yes	No	No	No	No	No	No
Steel Stress	400 Mpa	Before	Before	Before	Before	Before	Before	Before	Before
	450 Mpa	No	Before	After	After	After	After	After	After
	500 Mpa	No	After	No	No	No	No	No	No

Comparison of maximum displacements

The columns for Case III experience an average reduction of about 31% for maximum displacement when compared to Case I. Moreover, this is the only case for charge height X2 where all columns were able to obtain peak maximum displacement in the 80 ms simulation. As shown in Table 6.6, the greatest improvements are for the Toronto tied and Vancouver spiral columns. Specifically, the Toronto and Vancouver columns experienced a reduction of about 48% in maximum displacement when compared to Case II, i.e., the worst case scenario. On the other hand, the Victoria columns experienced a reduction of about 39% when compared to Case

II. Therefore, the maximum displacement of the Toronto and Vancouver columns is more dependent on the severity of the blast as compared to the Victoria columns, which do not experience drastic increases in maximum displacement with different blast loads.

Table 6.6 Maximum displacement for all columns, Case III, X2.

Location	Column	Maximum displacement (mm)	Percent difference from Case I
Toronto	tied	33.5	-36.6%
	spiral	33.3	-24.8%
Vancouver	tied	26.8	-33.3%
	spiral	26.6	-35.8%
Victoria	Set 1, tied	24.1	-30.0%
	Set 2, tied	23.8	-29.6%
	Set 1, spiral	23.9	-30.1%
	Set 2, spiral	24.1	-30.6%

Comparison of displacement curves

The results of the displacement curves (Fig. 6.34) reveal that the Toronto tied and spiral columns follow almost identical curves, which indicates that they have similar performance. Such a result is not surprising. The conclusion from the analysis in all previous cases suggest that as the blast load becomes more severe, the spiral column performs significantly better than the tied column. However, if the blast load is relatively low (i.e., not severe), the advantage of spirals becomes hidden.

The displacement curves of the Vancouver columns (Fig. 6.34) show that the spiral column performs better than the tied column. Although the tied column has smaller spacing of transverse reinforcement in the plastic hinge regions, this does not reveal a strong advantage for this case, and the type of reinforcement (i.e., ties or spirals) is more important. In summary, for the Vancouver columns, when the blast is relatively severe, such as in Cases I and II, the spacing of transverse reinforcement has more effect on the resistance than the type of reinforcement.

When the blast is relatively low, such as in Case III, the type of transverse reinforcement is more important than spacing of reinforcement, and spirals perform better for blast resistance.

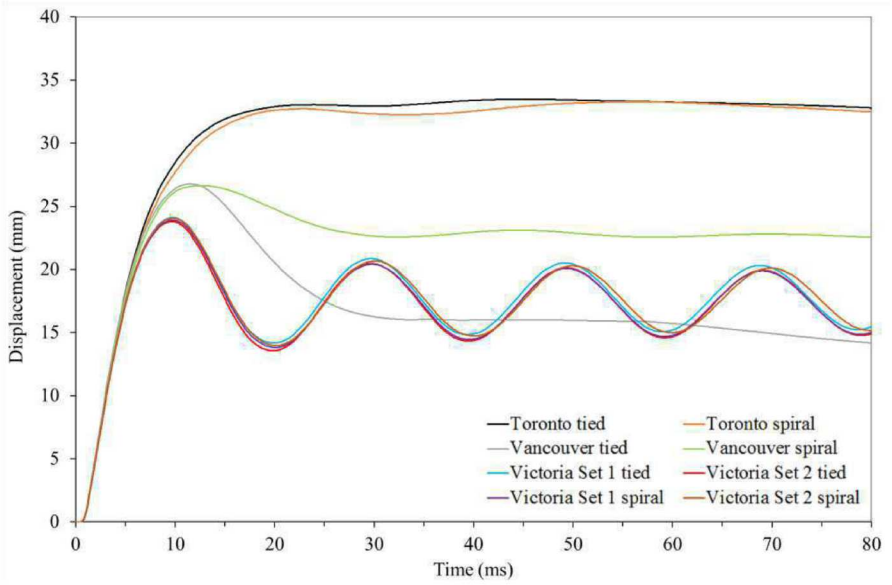

Figure 6.34 Displacement curves for all columns, Case III, X2.

6.3 Comparison of Results for Charge Height X1 and Charge Height X2

6.3.1 Comparison of Concrete Failure Mechanisms

The results of the 48 simulations reveal that charge height X2 (closer to the base) is much more critical than charge height X1 (at mid-height). All forms of concrete failure mechanisms, including crushing, spalling, and erosion at the boundaries are noticeably more severe for charge height X2. The major difference between charge height X1 and charge height X2 is breakage of the columns. There are two breakage patterns observed in this study. The first pattern is when the column breaks along a horizontal line in the top half of the column (e.g., Fig. 6.25, Case III). The columns have a pinned boundary condition at the top which allows for rotation and this pattern of column breakage will lead to flexure failure. The second breakage pattern is a failure surface

along a 45 degree line that penetrated the bottom plastic hinge region (e.g., Fig. 6.25, Case I and Case II), which is an indication of shear failure and is not desired. In this study, it is found that there are more columns that experience shear breakage for charge height X2 (42%) than charge height X1 (29%). In addition, the breakage line is dependent on the amount of transverse reinforcement in the plastic hinge region.

It is also noticed in this study that there is strong correlation between concrete erosion and transverse reinforcement in the column, such as the spacing, bar size, and type of reinforcement (i.e., ties or spirals). The impact of these parameters depends on the severity of the blast and charge height. As an example, the Toronto columns fail in all three cases (Cases I, II, and III) of both charge heights (X1 and X2), which indicates that spacing of reinforcement, bar size, and type of reinforcement need to be improved regardless of the severity of blast and charge height. To the contrary, the performance of the Vancouver columns depends on severity of the blast and charge height rather than spacing, bar size, and type of reinforcement. As illustrated in Fig. 6.35, the performance of the Vancouver spiral column is significantly different for the Case II blast at different charge heights X1 and X2. More specifically, for height X1, the column successfully resists the blast, while for height X2, the column breaks due to shear. The two sets of Victoria columns were designed to measure the difference between the three reinforcement parameters, namely bar size, spacing, and type of transverse reinforcement. The results show that because both sets of designs have high reinforcement ratios in the column, small changes in spacing and bar size, as well as type of reinforcement, do not have significant impact on blast resistance. The severity of the blast and charge height did not have significant impact on the performance of the Victoria columns. Generally speaking, smaller spacing of transverse reinforcement, bigger bar size, and spirals will reduce concrete erosion and improve blast

resistance of columns, but in certain cases their impact can be minimal based on severity of the blast and charge height. For columns that are adequately designed (i.e., Victoria columns) and can resist different severities and locations of blast, cost-benefit analysis and ease of construction should govern design rather than spacing, bar size, and type of reinforcement.

Figure 6.35 Side view of the Vancouver spiral column at the end of simulations, Case II.

6.3.2 Comparison of Reinforcement Stress and Behaviour

Results from this study show that, for charge height X2, the transverse reinforcement of columns yielded faster and maintained yield stress for longer periods of time as compared to columns for charge height X1. Specifically, yield stress of ties and spirals in the plastic hinge regions remained for longer periods of time for charge height X2. There were also more instances of tie pullout and severe deformation of both ties and spirals for charge height X2.

The longitudinal reinforcement experienced similar stress distribution patterns for both charge height X1 and X2. Stress on longitudinal bars of columns that did not successfully resist blast shifted towards the top of the columns. The longitudinal reinforcement of columns that successfully resisted the blasts experienced accumulation of stress on the tension side around mid-height and the stress then shifts back and forth due to rebounding.

There is a difference in the failure pattern of longitudinal reinforcement for the two charge heights. For charge height X1, deformation of longitudinal reinforcement occurs along a horizontal line in the top half of the column. For charge height X2, deformation occurs along a 45 degree line that penetrates the bottom plastic hinge region. In summary, it was observed that 29% of columns experienced severe deformation of longitudinal reinforcement for charge height X1 and 46% for charge height X2.

6.3.3 Comparison of Maximum Displacement

Table 6.7 illustrates the total maximum displacements that were obtained for the three examined cases (Cases I, II, and III) and two charge heights (X1 and X2). The total maximum displacement is calculated by adding the maximum displacement values of all eight columns for each case and respective charge height. It can be seen in the table that for Cases I and II, the columns of charge height X2 have bigger maximum displacements, but the difference between the two charge heights is exactly the same at 13%. To the contrary, columns of Case III experienced a 19% difference for maximum displacement between charge height X1 and X2. This result indicates that for severe blasts (i.e., Cases I and II), some columns have such little resistance to blast that adequate reinforcement will not reduce their displacement. For relatively

lower blast levels, such as Case III, the reinforcement has greater impact in reducing displacement.

Table 6.7 Summary of total maximum displacement for all cases.

Cases	Charge height X1	Charge height X2	Difference
Case I	260 mm	297 mm	13%
Case II	296 mm	338 mm	13%
Case III	178 mm	216 mm	19%

6.3.4 Comparison of Displacement Curves

The difference in the various types of displacement curves of the columns for charge heights X1 and X2 is well noticeable with the Vancouver spiral column. As seen in Figure 6.36, the displacement curve of this column is desirable for X1 cases because it experiences many

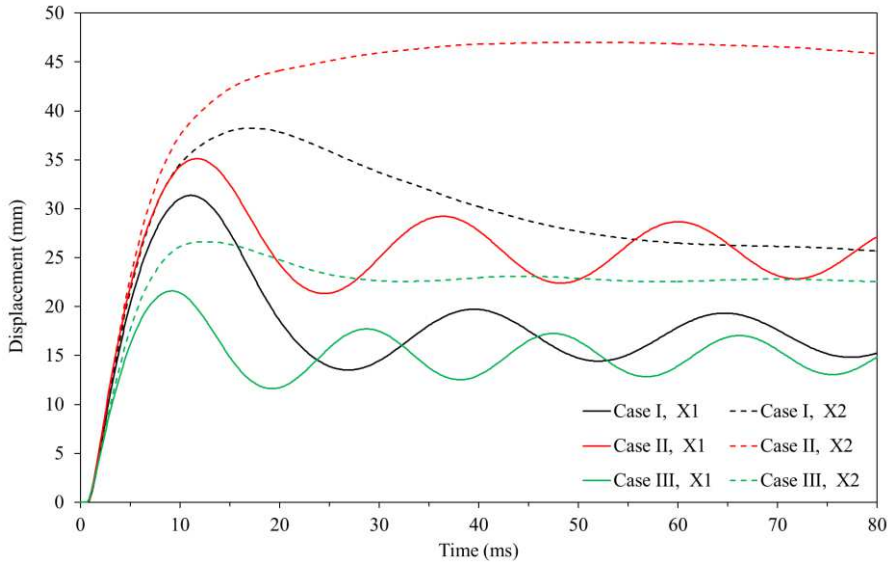

Figure 6.36 Displacement curves for all Vancouver spiral columns.

rebounding cycles, but it does not experience notable rebounding for X2 cases. Specifically, the shape of the displacement curve of this column for Case II at charge height X2 is not desirable as

it is similar to the poorly performing Toronto columns. Generally speaking, the shape of the displacement curves for the Toronto and Victoria columns remained the same for the different cases and charge heights. The Vancouver columns, especially the spiral column, experienced many different displacement curve shapes based on severity of blast and charge height.

Chapter 7: Conclusion

7.1 Conclusion

The main objective of this research was to examine the impact of transverse reinforcement, such as type of the transverse reinforcement (tie and spiral), diameter, and the spacing, on the ability of reinforced concrete bridge columns to resist blast loads. Three cities with different seismic hazard were chosen: Toronto (low seismic hazard), Vancouver (high seismic hazard), and Victoria (extremely high seismic hazard). A hypothetical two-span continuous highway bridge was designed according to 2006 CHBDC. Blast load analyses on the columns were carried out for three cases using the advanced finite element software LS-DYNA. Among the three cases, the scaled standoffs were kept the same while the charge weight and the scaled distance were treated as variables in order to assess the impact of each on blast load resistance. In each case, simulations were run for two scenarios for the charge height, i.e., one is at mid-height of the column while the other is closer to the base of the column. Based on the simulation results, qualitative observations and quantitative recordings were made in order to assess the effect of transverse reinforcement on blast load resistance.

The major conclusions of this study are summarized as follows:

- The columns located in high (Vancouver) and extremely high (Victoria) seismic zones would be able to resist the blast loads while the columns located in the low seismic zone (Toronto) would fail. This indicates that satisfying the requirements for seismic design will not assure that a column survives in a blast attack. More specifically, attention should be given to those columns located in low seismic zones if a potential attack becomes a concern.

- For columns that perform poorly under blast loads, the type of the transverse reinforcement has no noticeable effect on the behaviour, i.e., both tied and spiral columns make no difference.
- For columns having satisfactory performance, the effects of the transverse reinforcement on blast load resistance depend on charge height. For the charge at mid-height of the column, using spirals as transverse reinforcement could be a better choice while ties are preferred if the charge is close to the ground.
- For the design of the transverse reinforcement, it is better to consider smaller bar size and smaller spacing if possible in order to achieve acceptable performance of columns against blast loads.

7.2 Recommendations

Due to limitations of this study, the following recommendations are made for future studies:

- The current study examined the performance of columns at only two charge heights. Therefore, more charge heights should be considered, including a broad range of hand-placed bombs, in order to define the most critical bomb location.
- Detailed studies should be conducted to develop a methodology for incorporating seismic design into blast load design. This will protect columns located in low seismic hazard zones (e.g., Toronto, Montreal, etc.) and stable zones (e.g., Edmonton, Winnipeg, etc.) from failure due to blasts.
- Research on optimization of the diameter and the spacing of transverse reinforcement might bring some interesting findings.

- Considering the development of guidelines for blast load design are still at the early stages, a critical blast load for the bridge design should be defined, which can be examined in the future studies.

References

American Association of State Highway and Transportation Officials (AASHTO). (2007). *LRFD Bridge Design Specifications*, 4th Ed., Washington, DC.

American Society of Civil Engineers (ASCE). (1997). *Design of Blast Resistant Buildings in Petrochemical Facilities. Task Committee on Blast-Resistant Design*, New York, New York.

American Society of Civil Engineers (ASCE). (2010). *Design of blast-resistant buildings in petrochemical facilities*. ASCE Publications.

Aviram, A., Mackie, K. R., & Stojadinovic, B. (2008). *Effect of abutment modeling on the seismic response of bridge structures*. Earthquake engineering and engineering vibration, *7*(4), 395-402.

Bae, S., & Bayrak, O. (2008). *Seismic performance of full-scale reinforced concrete columns*. ACI Structural Journal, 105(2), 123.

Baker, W. E. (1973). *Explosions in air*. Austin, Texas: University of Texas Press.

Baylot, J., Ray, J., & Hall, R. (2003). *Prediction method for response of steel bridge beams and girders to blast and fragment loads*. Transportation Research Record: Journal of the Transportation Research Board, (1827), 69-74.

Biggs. John, M. (1964). *Introduction to structural dynamics*. Volume 3. McGrew-Hill, Inc., New York, New York.

Bounds, W. (1998). *Concrete and Blast Effects*. American Concrete Institute. Farmington Hills, MI.

Brannon, R. M., & Leelavanichkul, S. (2009). *Survey of four damage models for concrete*. Sandia National Laboratories Report SAND2008-xxxx (in press), Albuquerque, NM.

Britt, J. R., D. E. Ranta, and A. P. Ohrt. *A User's Manual for the BlastX Code*, *Version 4.0*. U.S. Army Engineer Waterways Experiment Station, Vicksburg, Miss., 1998.

Caltrans, S. D. C. (2004). *Caltrans Seismic Design Criteria version 1.3*. California Department of Transportation, Sacramento, California.

Canadian Standard Association (CSA). (2006). *Canadian Highway Bridge Design Code, CHBDC 2006*. 10th Edition, Ontario, Canada

Computers and Structures Inc (CSI). (2015a). CSI Bridge 2015 v17.3.0

Computers and Structures Inc (CSI). (2015b). SAP 2000 17 v17.3.0

Conrath, E.J., Krauthammer, T., Marchand, K.A. and Mlakar, P.F. (1999). *Structural Design for Physical Security: State of the Practice*. American Society of Civil Engineers. Reston, VA.

Crepeau, J. *SHAMRC Second-Order Hydrodynamic Automatic Mesh Refinement Code, Volume 2: User's Manual*. Applied Research Associates, Inc., Albuquerque, N.Mex., 2001.

Department of the Army. (1990). *Structures to Resist the Effects of Accidental Explosions. TM 5-1300*, Washington, D.C.

Department of Defense. (2002). *DoD minimum antiterrorism standards for buildings*. Unified Facilities Criteria. Washington, DC.

Department of Defense. (2008). *Structures to resist the effects of accidental explosions*. Unified Facilities Criteria. Washington, DC.

Dusenberry, D. O. (2010). *Handbook for Blast Resistant Design of Buildings*. John Wiley & Sons Inc. Canada. 486pp.

Erhart, T. (2011). *Review of solid element formulations in LS-DYNA: Properties, limits, advantages, disadvantages*. In Proceedings of the LS-DYNA Developers' Forum, Stuttgart, Germany (pp. 12-13).

Euro-International Committee for Concrete. (1990). *CEB-FIP Model Code 1990*. Trowbridge, Wiltshire, UK

Fajfar, P. (2000). *A nonlinear analysis method for performance-based seismic design*. Earthquake spectra, 16(3), 573-592.

Federal Emergency Management Agency (FEMA). (2003). *Risk Management Series:* Reference Manual to Mitigate Potential Terrorist Attacks against Buildings, Washington, DC.

Federal Emergency Management Agency (FEMA). (2011). *Risk Management Series:* Reference Manual to Mitigate Potential Terrorist Attacks against Buildings, Washington, DC.

Federal Highway Administration (FHWA). (2007a). *User's manual for LS_DYNA concrete material model 159*. Publication No. FHWA-HRT-05-062

Federal Highway Administration (FHWA). (2007b). *Evaluation of LS-DYNA concrete material model 159.* Publication No. FHWA-HRT-05-063.

Federal Transit Administration (FTA). (2001). *Surface Transportation Security: Vulnerabilities and Developing Solutions*. Washington, DC.

Fujikura, S., Bruneau, M., & Lopez-Garcia, D. (2008). *Experimental investigation of multihazard resistant bridge piers having concrete-filled steel tube under blast loading*. Journal of Bridge Engineering, 13(6), 586-594.

Fujikura, S., & Bruneau, M. (2010). *Experimental investigation of seismically resistant bridge piers under blast loading*. Journal of Bridge Engineering, 16(1), 63-71.

General Services Administration (GSA). (2003). *Progressive collapse analysis and design guidelines for new federal office buildings and major modernization projects*. Washington, DC.

Grote, D. L., Park, S. W., & Zhou, M. (2001). *Dynamic behavior of concrete at high strain rates and pressures: I. experimental characterization*. International Journal of Impact Engineering, 25(9), 869-886.

Han, Y., & Liu, H. (2015). *Finite Element simulation of medium-range blast loading using LS-DYNA*. Shock and Vibration, 2015.

Islam, A. A., & Yazdani, N. (2008). *Performance of AASHTO girder bridges under blast loading*. Engineering Structures, *30*(7), 1922-1937.

Jacques, E., Lloyd, A., & Saatcioglu, M. (2012). *Predicting reinforced concrete response to blast loads*. Canadian Journal of Civil Engineering, 40(5), 427-444.

Jacques, E., 2014, *RCBLAST* (Version. 0.5.1)

Jenkins, B. M., and Gersten, L. N. (2001). *Protecting public surface transportation against terrorism and serious crime*. MTI Report 01-14, Mineta Transportation Institute, San Jose, CA.

Karlos, V., & Solomos, G. (2013). *Calculation of blast loads for application to structural components*. Luxembourg: Publications Office of the European Union.

Kyei, C. (2014). Effects of blast loading on seismically detailed reinforced concrete columns. Doctoral dissertation. Carleton University Ottawa.

Liu, H., Torres, D. M., Agrawal, A. K., Yi, Z., & Liu, G. (2015). *Simplified Blast-Load Effects on the Column and Bent Beam of Highway Bridges*. Journal of Bridge Engineering, 20(10), 06015001.

Livermore Software Technology Corporation (LSTC). (2006). *LS-DYNA Theory Manual.* Livermore, California.

Livermore Software Technology Corporation (LSTC). (2016a). LS-DYNA v971_r9.0.1.

Livermore Software Technology Corporation (LSTC). (2016b). *LS-DYNA Keword User's Manual, Volume II: Material Models, Version 971.* Livermore, California.

Mahoney, E. E. (2007). *Analyzing the effects of blast loads on bridges using probability, structural analysis, and performance criteria*. University of Maryland, College Park.

Marburg, S. (2002). *Six boundary elements per wavelength: is that enough?*. Journal of Computational Acoustics, 10(01), 25-51.

Murray, Y., Abu-Odeh, A., and Bligh, R. (2007). *Evaluation of LS-DYNA Concrete Material Model 159*. Federal Highway Administration, Georgetown Pike, USA.

National Research Council. (1995). *Protecting buildings from bomb damage: Transfer of blast-effects mitigation technologies from military to civilian applications*. National Academies Press.

National Research Council Canada. (2005). National Building Code of Canada 2005. Ottawa, Ont.

Ngo, T., Mendis, P., Gupta, A., & Ramsay, J. (2007). *Blast loading and blast effects on structures–an overview*. Electronic Journal of Structural Engineering, 7, 76-91.

Pan, Y., Chan, B. Y., & Cheung, M. M. (2012). *Blast loading effects on an RC slab-on-girder bridge superstructure using the multi-Euler domain method*. Journal of Bridge Engineering, 18(11), 1152-1163.

Ray, J., Armstrong, B., & Slawson, T. (2003). *Airblast environment beneath a bridge overpass*. Transportation Research Record: Journal of the Transportation Research Board, (1827), 63-68.

Schwer, L. (2010). *A brief introduction to coupling load blast enhanced with Multi-Material ALE: the best of both worlds for air blast simulation*. LS-DYNA Forum. Bamberg.

Schwer, L. (2014). *Modeling rebar: the forgotten sister in reinforced concrete modeling*. In 13th International LS-DYNA Users Conference.

Shi, Y., Hao, H., & Li, Z. X. (2007). *Numerical simulation of blast wave interaction with structure columns*. Shock Waves, 17(1), 113-133.

Slavik, T. P. (2010). *A coupling of empirical explosive blast loads to ALE air domains in LS-DYNA*. IOP Conference Series: Materials Science and Engineering (Vol. 10, No. 1, p. 012146). IOP Publishing.

Tavarez, F. A. (2001). *Simulation of behavior of composite grid reinforced concrete beams using explicit finite element methods*. University of Wisconsin--Madison.

Tedesco, J., McDougal, W. G., & Ross, C. A. (1999). *Structural dynamics: Theory and approach*. Addison Wesley Longman. Menlo Park, CA.

U.S. Army Corps of Engineers. (2001). ConWep, Version 2.0.6.0. U.S. Army Engineer Research and Development Center. Vicksburg, MS.

Wang, H., Wu, C., Zhang, F., Fang, Q., Xiang, H., Li, P., ... & Li, J. (2017). *Experimental study of large-sized concrete filled steel tube columns under blast load*. Construction and Building Materials, 134, 131-141.

Williams, G. D. (2009). *Analysis and response mechanisms of blast-loaded reinforced concrete columns* (Doctoral dissertation). The University of Texas: Austin, Texas.

Williams, G. D., & Williamson, E. B. (2011). *Procedure for predicting blast loads acting on bridge columns*. Journal of Bridge Engineering, 17(3), 490-499.

Williamson, E. B. (2010). *Blast-resistant highway bridges: Design and detailing guidelines* (Vol. 645). Transportation Research Board.

Williamson, E. B., Bayrak, O., Davis, C., & Williams, G. D. (2011a). *Performance of bridge columns subjected to blast loads. I: Experimental program*. Journal of Bridge Engineering, 16(6), 693-702.

Williamson, E. B., Bayrak, O., Davis, C., & Daniel Williams, G. (2011b). *Performance of bridge columns subjected to blast loads. II: Results and recommendations*. Journal of Bridge Engineering, 16(6), 703-710.

Winget, David Gerrell. (2003). *Design of Critical Bridges for Security against Terrorist Attacks*.

Winget, D. G., Marchand, K. A., & Williamson, E. B. (2005a). *Analysis and design of critical bridges subjected to blast loads*. Journal of Structural Engineering, 131(8), 1243-1255.

Winget, D., Williamson, E., Marchand, K., & Gannon, J. (2005b). *Recommendations for blast design and retrofit of typical highway bridges*. Transportation Research Record: Journal of the Transportation Research Board, (11s), 1-8.

Wu, Y., Crawford, J. E., & Magallanes, J. M. (2012). *Performance of LS-DYNA concrete constitutive models*. 12th International LS-DYNA users conference (pp. 1-14).

Yi, Z., Agrawal, A. K., Ettouney, M., & Alampalli, S. (2013a). *Blast load effects on highway bridges. II: Failure modes and multihazard correlations*. Journal of Bridge Engineering, 19(4), 04013024.

Yi, Z., Agrawal, A. K., Ettouney, M., & Alampalli, S. (2013b). *Blast load effects on highway bridges. I: Modeling and blast load effects*. Journal of Bridge Engineering, *19*(4), 04013023.

APPENDIX A: Column Reinforcement Design

Preliminary Information for Column Design

1) In the design, concrete compressive strength is fc' = 30 MPa, and the yield strength of steel reinforcement is fy = 400 MPa.

2) From *Table 4.1: Site coefficient*, site class I (very dense soil and soft rock) will be used.

3) From *Table 4.1: Seismic performance zones*, the Peak Horizontal Acceleration (PHA) associated with lifeline bridges is used.

4) From National Resources Canada (NBCC, 2005), hazard values of 10% probability of exceedance in 50 years give the following results:

- Toronto: PHA= 0.081g, making it Seismic Performance Zone 3.
- Vancouver: PHA= 0.242g, making it Seismic Performance Zone 4.
- Victoria: PHA= 0.337g, making it Seismic Performance Zone 4.

5) All three locations are in Seismic Performance Zone 3 or Seismic Performance Zone 4. Therefore, design will follow *Clause 4.7.4: Seismic Performance Zones 3 and 4*. As a result, the Response Modification Factor, R, is used to reduce elastic loads. From *Table 4.5: Response modification factor*, $R = 5.0$ for the category of "Multiple-column bents, Ductile reinforced concrete". The loads acting on the columns of the bridge model in CSI Bridge 2015 are modified as follows:

- Axial load: From *Clause 4.7.4*, there is no reduction for axial load; therefore, $R = 1.0$.

- Shear load: From *Clause 4.7.4*, there is no reduction for shear load; therefore, $R = 1.0$.
- Moment load: From *Clause 4.7.4*, the elastic moment is reduced with $R = 5.0$.

With the adjustments of the Response Modification Factor, the following loads are used in the design of the columns for each bridge:

Table A1 Summary of design forces.

Design forces	Toronto	Vancouver	Victoria
P_f (kN)	9717	9717	9717
V_f (kN)	808	3222	6463
M_f (kN·m)	551	1992	4406

Longitudinal Reinforcement Design

Clause 4.7.4.1: General

1) The clear height of the column is 6.5 m and the diameter of the column is 1.3 m. The ratio of clear height to maximum dimension is 5.0, which is greater than 2.5 and classifies the structure as a column.

2) Gross cross sectional area of the column is: $A_g = 1{,}327{,}323\ mm^2$

Clause 4.7.4.2.2: Longitudinal reinforcement

1) Longitudinal reinforcement in the column has to be between 0.8% and 6% of gross cross sectional area. Maximum center-to-center spacing of longitudinal rebar cannot be more than 200 mm.

2) In reference to *Clause 8.8.5.6: Reinforcement limitations*, for circular arrangements, the minimum number of longitudinal reinforcement bars is 6 bars. The maximum spacing of

longitudinal reinforcement from *Clause 8.8.5.6* is 300 mm. Furthermore, the minimum available bar size is 15M.

3) The requirement for minimum longitudinal reinforcement in the column is as follows:

- $\frac{A_s}{A_g} \leq 0.06$; therefore, $A_s \leq 79{,}639\ mm^2$ (governs as maximum)
- $\frac{A_s}{A_g} \geq 0.008$; therefore, $A_s \geq 10{,}619\ mm^2$
- $\frac{A_s f_y}{A_g f'_c} \geq 0.135$; therefore, $A_s \geq 13{,}439\ mm^2$ (governs as minimum)
- From the requirements for A_s , the reinforcement ratio is $\rho_t \geq \frac{A_s}{A_g} = 0.0101$

4) Based on the criteria of *Clause 4.7.4.2.2* and *Clause 8.8.5.6*, the following results are obtained:

- The design will use 25M longitudinal rebar. The governing minimum reinforcement is $A_{s,required} \geq 13{,}439\ mm^2$. From *Clause 8.8.5.6,* at least 27-25M bars have to be provided.
- From *Table 8.5: Minimum concrete cover and tolerances*, for "environmental exposure of no de-icing chemicals and no marine spray" with "components (7) to (9)" and "cast-in-place concrete with reinforcing steel", at least 60 mm of clear cover has to be provided. In the design, 60 mm of clear cover is provided.
- From *Clause 8.14.3: Transverse reinforcement for flexural components*, stirrups are 10M when longitudinal bars are 30M or smaller. This design will uses 25M longitudinal rebar; therefore, preliminary stirrups need to be at least 10M and the final size will be determined during shear design. Based on these requirements, after placement of longitudinal bars, it is noticed that it in order to provide a

maximum of 200 mm spacing, there need to be at least 18-25M bars, which is less than the requirement of *Clause 8.8.5.6*

- From the governing minimum reinforcement ratio, 25M longitudinal rebar, 10M stirrups, and a 60 mm clear cover, and the spacing of longitudinal bars is calculated to be 132 mm:

$$S = \frac{\pi D'}{N} = \frac{\pi * (1300\ mm - 2(60\ mm) - 2(11\ mm) - 25\ mm)}{27} = 132\ mm$$

Clause 4.7.4.2.3: Flexural resistance

1) To validate resistance of longitudinal reinforcement, the combined effects of axial and flexure loads are accounted for on CSA interaction diagrams. On the CSA interaction diagrams, the material resistance factors are $\emptyset_c = 0.65$ and $\emptyset_s = 0.85$. In CHBDC, *Table 8.1: Material resistance factors*, these values are given as $\emptyset_c = 0.75$ and $\emptyset_s = 0.90$. To get an accurate assessment of the columns moment-axial capacity, custom interaction diagrams are created using SAP 2000's *Section Designer* (CSI, 2015b). The interaction curves will have unique values for γ, $\emptyset_c$, $\emptyset_s$, f'_c, f_y, and ρ_t:

2) For 25M longitudinal bars and 10M stirrups, the following factors are calculated:

- $\gamma h = d_{column} - 2cover - 2d_t - d_b = 1300\ mm - 2(60\ mm) - 2(11\ mm) - 25\ mm = 1{,}133\ mm$

  Therefore, $\gamma = \frac{\gamma h}{h} = \frac{1133\ mm}{1300\ mm} = 0.87$

- For the interaction diagrams, $\frac{P_f}{h^2} = \frac{9{,}717\ kN}{(1300\ mm)^2} = 5.75\ MPa$ for the columns of all three cities. The following factors apply to each individual city:
  - Toronto: $\frac{M_f}{h^3} = \frac{551\ kN*m}{(1300\ mm)^3} = 0.25\ MPa$
  - Vancouver: $\frac{M_f}{h^3} = \frac{1{,}992\ kN*m}{(1300\ mm)^3} = 0.91\ MPa$
  - Victoria: $\frac{M_f}{h^3} = \frac{4{,}406\ kN*m}{(1300\ mm)^3} = 2.01\ MPa$

The resulting column interaction diagrams are illustrated in below in Figure A1:

Figure A1 Interaction curves for columns.

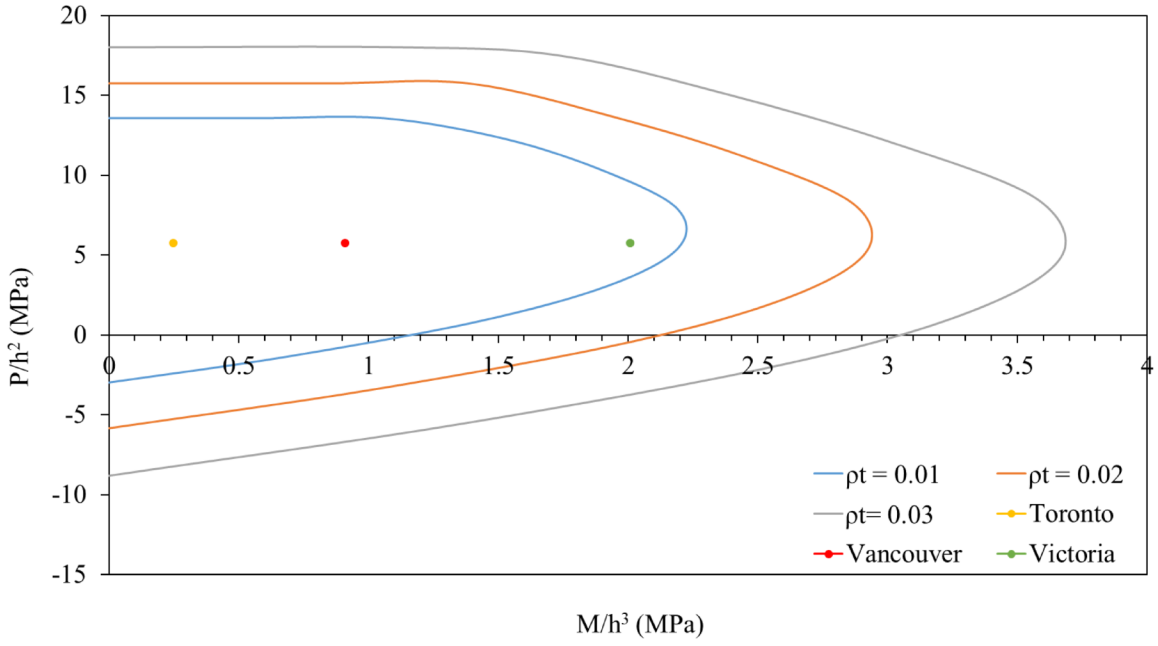

3) The following observations and conclusions are made from Figure A1:

- Toronto: $\rho_t < 0.01$; therefore, minimum reinforcement ratio governs and 27-25M longitudinal bars are provided with a spacing of 132 mm.

- Vancouver: $\rho_t < 0.01$; therefore, minimum reinforcement ratio governs and 27-25M longitudinal bars are provided with a spacing of 132 mm.
- Victoria: $\rho_t < 0.01$; therefore, minimum reinforcement ratio governs and 27-25M longitudinal bars are provided with a spacing of 132 mm.

Transverse Reinforcement Design

Clause 8.8.5.4: Maximum factored axial resistance

For tie reinforcement $P_r \leq 0.75P_o$ and for spiral reinforcement $P_r \leq 0.80P_o$

The following calculations are made for the requirements of *Clause 8.8.5.4*:

$$P_o = \alpha_1 f'_c\left(A_g - A_s\right) + f_y A_s = 0.805(30MPa)(1{,}327{,}323\ mm^2 - 13{,}500\ mm^2) + (400MPa * 13{,}500\ mm^2) = 37{,}129\ kN$$

$$P_r = \emptyset_c \alpha_1 f'_c\left(A_g - A_s\right) + \emptyset_s f_y A_s = (0.75)(0.805)(30MPa)(1{,}327{,}323\ mm^2 - 13{,}500\ mm^2) + (0.90)(400MPa * 13{,}500\ mm^2) = 28{,}657\ kN$$

Therefore, for ties: $P_r = 28{,}657\ kN \leq 0.75(37{,}129\ kN) = 27{,}847\ kN$

Finally, for spirals: $P_r = 28{,}657\ kN \leq 0.80(37{,}129\ kN) = 29{,}703\ kN$

The spiral reinforcement fulfills the requirement, and the difference in error for ties is 2.87% and as such it will be neglected.

Clause 4.7.4.2.4: Column shear and transverse reinforcement

The length of the plastic hinge region for transverse reinforcement is the greatest of the following three requirements:

i. $d_{column} = 1300\ mm$

ii. $\frac{l_u}{6} = 1083\ mm$

iii. $450\ mm$

Therefore, the governing length of the plastic hinge region at the top and bottom of the columns is 1300 mm.

Clause 4.7.4.2.4: Column shear and transverse reinforcement* and *Clause 8.9.3: Sectional design model

1) From *Clause 4.7.4.2.4*, the amount of transverse reinforcement provided in the plastic hinge region will not be less than the minimum amount provided by *Clause 8.9.3*.

2) In the Plastic hinge regions, if $P_{f,min} \geq 0.10f'_cA_g$, then V_c is specified in *Clause 8.9.3*.

$$P_{f,min} = 9{,}180\ kN \geq 0.10(30\ MPa)(1{,}327{,}323\ mm^2) = 3{,}982\ kN$$

Therefore, $P_{f,min} > 0.10f'_cA_g$

As a result, the value of V_c is the same for the plastic and non-plastic hinge regions. The design for V_c is determine from *Clause 8.9.3* for both plastic and non-plastic hinge zones.

Clause 8.9.3.2: Required shear resistance states that $V_r \geq V_f$. Moreover, *Clause 8.9.3.3: Factored shear resistance* states states that $V_r = V_c + V_s$

Clause 8.9.1.2: Regions requiring transverse reinforcement

Transverse reinforcement is provided where $V_f \geq 0.20\emptyset_c f_{cr} b_v d_v$

The following calculations are made to determine the requirements of *Clause 8.9.1.2*:

- *Clause 8.9.3.4* requires that $f_{cr} \leq 3.2\ MPa$:

  $$f_{cr} = 0.6\sqrt{f'_c} = 0.6\sqrt{30\ MPa} = 3.29\ MPa$$

  Therefore, $f_{cr} = 3.2\ MPa$ in the design

- From *Clause 8.9.1.5: Effective shear depth*, d_v is taken as the greatest of 0.72h or 0.9d.

  Assuming 10M transverse reinforcement for preliminary design, the following apply:

  i. $0.72h = 0.72(1300\ mm) = 936\ mm$

  ii. $0.9d = 0.9(1300\ mm - 60\ mm - 11\ mm - 25\ mm) = 1084\ mm$

  Therefore, 1084 mm governs for d_v

- From *Clause 8.9.1.6: Effective web width*, $b_v = diameter$ for solid circular sections

  Therefore, $b_v = 1300\ mm$

- From *Clause 8.9.1.2*, the following calculation is made:

  $$0.20\emptyset_c f_{cr} b_v d_v = 0.20(0.75)(3.2\ MPa)(1300\ mm)(1084\ mm) = 676\ kN$$

  In summary, $V_f \geq 0.20\emptyset_c f_{cr} b_v d_v = 676\ kN$

- From Table A1, the following conclusions are drawn:

  - Toronto: $V_f = 808\ kN$, which is greater the $V_f = 676\ kN$
  - Vancouver: $V_f = 3{,}222\ kN$, which is greater the $V_f = 676\ kN$

- Toronto: $V_f = 6{,}463\ kN$, which is greater the $V_f = 676\ kN$

Therefore, for all three cities, transverse reinforcement is required and will be provided.

Clause 8.9.3.4: Determination of Vc

The requirements for *Clause 8.9.3.4* are:

$$V_c = 2.5\beta\emptyset_c f_{cr} b_v d_v \text{ , where } f_{cr} \leq 3.2\ MPa$$

- β and θ are given in *Clause 8.9.3.6: Determination of β and θ for non-prestressed components (simplified method)*. Columns in this design are not prestressed and not subjected to axial tension. Moreover, $f_y \leq 400\ MPa$, and $f'_c \leq 60\ MPa$

  Therefore, $\theta = 42°$ from the requirements of *Clause 8.9.3.6*

  Assuming that minimum transverse reinforcement, $\beta = 0.18$

  The following calculation is made:

$$V_c = 2.5\beta\emptyset_c f_{cr} b_v d_v = 2.5(0.18)(0.75)(3.2\ MPa)(1300\ mm)(1084\ mm)$$
$$= 1{,}522\ kN$$

Clause 8.9.3.5: Determination of V_s for ties:

$$V_s = \frac{\emptyset_s f_y A_v d_v cot\theta}{s}$$

For transverse reinforcement, V_s , based on optimization of design, some Vancouver and Victoria columns will use 25M transverse reinforcement bars and others will use 30M bars. The Toronto columns will use 15M bars.

The requirement for shear reinforcement will be applied such that minimum transverse reinforcement is provided based on $V_f \leq V_c + V_s$. The minimum spacing of transverse reinforcement, , is determine for each city:

- Toronto: $V_f = 808\ kN < V_c = 1{,}522\ kN$
  Calculation of V_s is not required as $V_c > V_f$, and reinforcement will be provided based on governing spacing requirements and not minimum transverse reinforcement for plastic and non-plastic hinge regions.

- Vancouver: $V_f = 3{,}222\ kN > V_c = 1{,}522\ kN$
  V_s is required and needs to be calculated:

  $V_c = 1{,}522\ kN + V_s \geq V_f = 3{,}222\ kN$; therefore, $V_s \geq 1{,}700\ kN$

  i. Using 25M bars:

$$s \leq \frac{\emptyset_s f_y A_v d_v cot\theta}{V_s} = \frac{(0.90)(400\ MPa)(1000\ mm^2)(1084\ mm)\cot(42°)}{1{,}700\ kN}$$
$$= 255\ mm$$

  Therefore, the spacing of ties in both the plastic and non-plastic hinge regions for 25M bars needs to be less than 255 mm.

ii. Using 30M bars:

$$s \leq \frac{\emptyset_s f_y A_v d_v cot\theta}{V_s} = \frac{(0.90)(400\ MPa)(1400\ mm^2)(1084\ mm)\cot(42°)}{1{,}700\ kN}$$
$$= 357\ mm$$

Therefore, the spacing of ties in both the plastic and non-plastic hinge regions for 30M bars needs to be less than 357 mm.

- Victoria: $V_f = 6{,}463\ kN > V_c = 1{,}522\ kN$
  V_s is required and will have to be determined

  $V_c = 1{,}522\ kN + V_s \geq V_f = 6{,}463\ kN$; therefore, $V_s \geq 4{,}941\ kN$

  i. Using 25M bars:

$$s \leq \frac{\emptyset_s f_y A_v d_v cot\theta}{V_s} = \frac{(0.90)(400\ MPa)(1000\ mm^2)(1084\ mm)\cot(42°)}{4{,}941\ kN}$$

$$= 87\ mm$$

Therefore, the spacing of ties in both the plastic and non-plastic hinge regions for 25M bars needs to be less than 87 mm.

ii. Using 30M bars:

$$s \leq \frac{\emptyset_s f_y A_v d_v cot\theta}{V_s} = \frac{(0.90)(400\ MPa)(1400\ mm^2)(1084\ mm)\cot(42°)}{4{,}941\ kN}$$

$$= 123\ mm$$

Therefore, the spacing of ties in both the plastic and non-plastic hinge regions for 30M bars needs to be less than 123 mm.

Clause 8.9.3.5: Determination of V_s for spirals:

Determination of transverse reinforcement, V_s , for a circular column will not follow the CHBDC formula used for ties. The formula used in ACI 318 and CALTRANS (Caltrans, 2004) is more appropriate:

$$V_s = \frac{A_v f_y h_c}{s}$$

Where $A_v = 2d_{bar}$

$h_c = D - 2cover = 1300\ mm - 2(60\ mm) = 1180\ mm$

Based on optimization of design, some Vancouver and Victoria columns will use 25M transverse reinforcement bars and others will use 30M bars. The Toronto columns will use 20M bars. The minimum spacing of transverse reinforcement, , is determine for each city:

- Toronto: $V_f = 808\ kN < V_c = 1{,}522\ kN$

  Calculation of V_s is not required as $V_c > V_f$, and reinforcement will be provided based on governing spacing requirements and not minimum transverse reinforcement for plastic and non-plastic hinge regions

- Vancouver: $V_f = 3{,}222\ kN > V_c = 1{,}522\ kN$

  V_s is required and will have to be determined

  $V_c = 1{,}522\ kN + V_s \geq V_f = 3{,}222\ kN$, therefore $V_s \geq 1{,}700\ kN$

  i. Using 25M bars:

$$s \leq \frac{A_v f_y h_c}{V_s} = \frac{(2 * 500\ mm^2)(400\ MPa)(1180\ mm)}{1{,}700\ kN} = 278\ mm$$

Therefore, the spacing of spirals in both the plastic and non-plastic hinge regions for 25M bars needs to be less than 278 mm.

ii. Using 30M bars:

$$s \leq \frac{A_v f_y h_c}{V_s} = \frac{(2 * 700\ mm^2)(400\ MPa)(1180\ mm)}{1{,}700\ kN} = 389\ mm$$

Therefore, the spacing of spirals in both the plastic and non-plastic hinge regions for 30M bars needs to be less than 389 mm.

- Victoria: $V_f = 6{,}463\ kN > V_c = 1{,}522\ kN$
  V_s is required and will have to be determined

  $V_c = 1{,}522\ kN + V_s \geq V_f = 6{,}463\ kN$, therefore $V_s \geq 4{,}941\ kN$

  i. Using 25M bars:

$$s \leq \frac{A_v f_y h_c}{V_s} = \frac{(2 * 500\ mm^2)(400\ MPa)(1180\ mm)}{4{,}941\ kN} = 96\ mm$$

Therefore, the spacing of spirals in both the plastic and non-plastic hinge regions for 25M bars needs to be less than 96 mm.

ii. Using 30M bars:

$$s \leq \frac{A_v f_y h_c}{V_s} = \frac{(2 * 700\ mm^2)(400\ MPa)(1180\ mm)}{4{,}941\ kN} = 134\ mm$$

Therefore, the spacing of spirals in both the plastic and non-plastic hinge regions for 30M bars needs to be less than 134 mm.

Clause 4.7.4.2.5: Transverse reinforcement for confinement at plastic hinge regions

1) For tied transverse reinforcement in plastic hinge zones, the total cross-sectional area of required reinforcement, A_{sh} , will not be less than the greater of:

$A_{sh} = 0.30sh_c \frac{f'_c}{f_y}\left[\frac{A_g}{A_c} - 1\right]$ AND $A_{sh} = 0.12sh_c \frac{f'_c}{f_y}[0.5 + \frac{1.25P_f}{\emptyset_c f'_c A_g}]$

where $[0.5 + \frac{1.25P_f}{\emptyset_c f'_c A_g}] \geq 1$

In this design: $\left[0.5 + \frac{1.25P_f}{\emptyset_c f'_c A_g}\right] = 0.91 \leq 1$; therefore, it will be assumed to be 1

Furthermore, $h_c = D - 2cover = 1300\ mm - 2(60\ mm) = 1180\ mm$

$$A_c = \frac{\pi}{4} {h_c}^2 = \frac{\pi}{4}(1180\ mm)^2 = 1{,}093{,}588\ mm^2$$

Therefore, the minimum tied transverse reinforcement requirement is calculated as:

$$A_{sh} \geq 0.30sh_c \frac{f'_c}{f_y}\left[\frac{A_g}{A_c} - 1\right] = 0.30s(1180\ mm)\frac{30\ MPa}{400\ MPa}\left[\frac{1{,}327{,}323\ mm^2}{1{,}093{,}588\ mm^2} - 1\right] = 5.67s$$

$$A_{sh} \geq 0.12sh_c \frac{f'_c}{f_y}\left[0.5 + \frac{1.25P_f}{\emptyset_c f'_c A_g}\right] = 0.12s(1180\ mm)\frac{30\ MPa}{400\ MPa}[1] = 10.62s$$

Therefore, $A_{sh} \geq 10.62s$ governs

Based on the assumption of providing minimum reinforcement in *Clause 8.9.3.4*, the maximum spacing of transverse reinforcement, , is given by:

i. Using 25 M bars: $s \leq \frac{A_{sh}}{10.62} = \frac{1000\ mm^2}{10.62} = 94\ mm$

   Therefore, the spacing of ties in the plastic hinge regions for 25M bars needs to be less than 94 mm.

ii. Using 30M bars: $s \leq \frac{A_{sh}}{10.62} = \frac{1400\ mm^2}{10.62} = 132\ mm$

Therefore, the spacing of ties in the plastic hinge regions for 30M bars needs to be less than 132 mm.

2) For spiral transverse reinforcement in plastic hinge zones, the total cross-sectional area of required reinforcement, ρ_s , will not be less than the greater of the requirement of *Clause 8.14.4.2* and the ρ_s calculated below:

$$\rho_s = 0.12\frac{f'_c}{f_y}\left[0.5 + \frac{1.25P_f}{\emptyset_c f'_c A_g}\right]$$

where $[0.5 + \frac{1.25P_f}{\emptyset_c f'_c A_g}] \geq 1$

In this design: $\left[0.5 + \frac{1.25P_f}{\emptyset_c f'_c A_g}\right] = 0.91 \leq 1$; therefore, it will be assumed to be 1

$$\rho_s = 0.12\frac{f'_c}{f_y}\left[0.5 + \frac{1.25P_f}{\emptyset_c f'_c A_g}\right] = 0.12\frac{30\ MPa}{400\ MPa}[1] = 0.009$$

Based on the calculation, the maximum spacing of transverse reinforcement, given by the h , is:

i. Using 25 M bars: $Pitch \leq \frac{4A_{sp}}{\rho_s D_c} = \frac{4(500\ mm^2)}{(0.009)(1180\ mm)} = 188\ mm$

Therefore, the spacing of spirals in the plastic hinge regions for 25M bars needs to be less than 188 mm.

ii. Using 30M bars: $Pitch \leq \frac{4A_{sp}}{\rho_s D_c} = \frac{4(700\ mm^2)}{(0.009)(1180\ mm)} = 263\ mm$

Therefore, the spacing of spirals in the plastic hinge regions for 30M bars needs to be less than 263 mm.

Clause 4.7.4.2.6: Spacing of transverse reinforcement for confinement region

There center to center spacing of transverse reinforcement in plastic hinge regions should not exceed the following criteria:

i. $0.25 * least\ dimension\ of\ component = 325\ mm$
ii. $6d_b = 150\ mm\ for\ 25M\ bars\ and\ 180\ mm\ for\ 30M\ bars$
iii. 150 mm

Therefore, the governing requirement for maximum spacing of ties (both 25M and 30M bars) and spirals (both 25M and 30M bars) is 150 mm in plastic hinge zones

Clause 8.9.1.3: Minimum amount of transverse reinforcement:

This clause applies to the Toronto columns, which use 15M and 20M bars, to ensure minimum reinforcement. Unlike the Vancouver and Victoria columns, the design of transverse reinforcement for the Toronto columns is governed by spacing and not minimum reinforcement. The minimum transverse reinforcement, A_v , is given by:

$$A_v \geq 0.15 f_{cr}(b_v s / f_y)$$

Maximum spacing of transverse reinforcement, , is calculated as:

i. Using 15M bars: $s \leq \frac{A_v f_y}{0.15 f_{cr} b_v} = \frac{(400\ mm^2)(400\ MPa)}{0.15(3.2\ MPa)(1300\ mm)} = 256\ mm$
ii. Using 20M bars: $s \leq \frac{A_v f_y}{0.15 f_{cr} b_v} = \frac{(600\ mm^2)(400\ MPa)}{0.15(3.2\ MPa)(1300\ mm)} = 385\ mm$

Therefore, the governing requirement for maximum spacing of the Toronto tied column is 256 mm for 15M ties. The governing requirement for maximum spacing of the Toronto spiral column is 385 mm for 20M spirals.

Clause 8.14.3: Transverse reinforcement for flexural components

The spacing of transverse reinforcement for flexure components will not exceed the following three criteria:

i. $16d_{longitudinal\ bar} = 480\ mm$
ii. $least\ dimension\ of\ the\ component = 1300\ mm$
iii. 300 mm

Therefore, the governing requirement for maximum spacing is 300 mm in non-plastic hinge zones.

Clause 8.14.4: Transverse reinforcement for compression components

- Clause 8.14.4.3: Ties

For tied transverse reinforcement, the spacing requirement needs to meet the requirements of *Clause 8.14.3*; therefore, the governing requirement for maximum spacing of ties is 300 mm in non-plastic hinge zones

- Clause 8.14.4.2: Spirals

1) For spiral transverse reinforcement, the maximum center-to-center of spacing in non-plastic hinge zones will not exceed the following two criteria:

   i. $6d_{longitudinal\ bar} = 180\ mm$
   ii. 150 mm

   Therefore, the governing requirement for maximum spacing of spirals is 150 mm in non-plastic hinge zones (applies to *Clause 4.7.4.2.5 for plastic hinge zones*)

2) For spirals, the minimum clear spacing in non-plastic hinge zones will not exceed the following criteria:

   i. 25 mm
   ii. $1.33a_{aggregate}$ = 27 mm (assuming 20 mm aggregate)

Therefore, the governing requirement for minimum spacing of spirals is 25 mm in non-plastic hinge zones (applies to *Clause 4.7.4.2.5 for plastic hinge zones)*

3) For spirals, the ratio of spiral reinforcement is not to be less than the following:

$$\rho_s \geq 0.45\left[\frac{A_g}{A_c} - 1\right]\frac{f'_c}{f_y}\left[0.5 + 1.25\frac{P_f}{\emptyset_c f'_c A_g}\right]$$

$$= 0.45\left[\frac{1{,}327{,}323\ mm^2}{1{,}093{,}588\ mm^2} - 1\right]\frac{30\ MPa}{400\ MPa}\left[0.5 + 1.25\frac{(9{,}717\ kN)}{0.75(30\ MPa)(1{,}327{,}323\ mm^2)}\right] = 0.0065$$

Based on this, the maximum clear spacing, given by the h , will not be greater than the following:

i. Using 30M bars: $Pitch \leq \frac{4A_{sp}}{\rho_s D_c} = \frac{4(700\ mm^2)}{(0.0065)(1180\ mm)} = 365\ mm$

Therefore, the governing requirement for maximum spacing of spirals is 365 mm for 30M bars in non-plastic hinge zones

ii. Using 25M bars: $Pitch \leq \frac{4A_{sp}}{\rho_s D_c} = \frac{4(500\ mm^2)}{(0.0065)(1180\ mm)} = 261\ mm$

Therefore, the governing requirement for maximum spacing of spirals is 261 mm for 25M bars in non-plastic hinge zones

iii. Using 20M bars: $Pitch \leq \frac{4A_{sp}}{\rho_s D_c} = \frac{4(300\ mm^2)}{(0.0065)(1180\ mm)} = 156\ mm$

Therefore, the governing requirement for maximum spacing of spirals is 156 mm for 20M bars in non-plastic hinge zones

$$Pitch \leq \frac{4A_{sp}}{\rho_s D_c} = \frac{4(700\ mm^2)}{(0.0065)(1180\ mm)} = 365\ mm$$

$$Pitch \leq \frac{4A_{sp}}{\rho_s D_c} = \frac{4(500\ mm^2)}{(0.0065)(1180\ mm)} = 261\ mm\ for\ 25M\ spirals$$

$$Pitch \leq \frac{4A_{sp}}{\rho_s D_c} = \frac{4(300\ mm^2)}{(0.0065)(1180\ mm)} = 156\ mm\ for\ 20M\ spirals$$

Final Column Design

From governing clauses of flexural and shear design of longitudinal and shear reinforcement, Table A2 illustrates a summary of the reinforcement design in each column.

Table A2 Summary of reinforcement design for columns.

Location	Column	Longitudinal reinforcement	Transverse reinforcement	
			Plastic hinge	Non-plastic hinge
Toronto	tied	27 - 25M @ 132 mm	15M @ 150 mm	15M @ 200 mm
	spiral	27 - 25M @ 132 mm	20M @ 150 mm	20M @ 150 mm
Vancouver	tied	27 - 25M @ 132 mm	25M @ 100 mm	25M @ 200mm
	spiral	27 - 25M @ 132 mm	25M @ 150 mm	25M @ 150 mm
Victoria	Set 1, tied	27 - 25M @ 132 mm	25M @ 80 mm	25M @ 80 mm
	Set 1, spiral	27 - 25M @ 132 mm	25M @ 80 mm	25M @ 80 mm
	Set 2, tied	27 - 25M @ 132 mm	30M @ 100 mm	30M @ 100 mm
	Set 2, spiral	27 - 25M @ 132 mm	30M @ 125 mm	30M @ 125 mm